DSE Fall 2014 - Group 01

2014 - 2015 AIAA Foundation Undergraduate Aircraft Design Competition Proposal

Design of Next Generation Airlift Military Support Aircraft

Name	Student #	Name	Student #
D.O. Berckmoes	4146565	K.J.W. Kwakman	4091817
J.-S. Fischer	4152638	D.M.N. Milewski	4079981
M.W. Hayat	4102045	N. van Oene	1521802
R.R.A. Hoefsloot	4065158	F.H.A. van Tilborg	4187156
		S.J.J. Zuurendonk	4006461

Final Report

Design Synthesis Exercise

TU Delft Delft University of Technology

Faculty of Aerospace Engineering

January 27, 2015

THIS PAGE IS INTENTIONALLY LEFT BLANK

Delft University of Technology Undergraduate Team

From left to right: Waqas Hayat, Koen Kwakman, Richard Hoefsloot, Frank van Tilborg, Damian Milewski, Jan Fischer, Bas Zuurendonk, Dennis Berckmoes, Nick van Oene

Name	AIAA Member #	Role	Signature
D.O. Berckmoes	530649	Structural Design	
J.-S. Fischer	518028	Propulsion & Performance	
M.W. Hayat	530602	Flight Dynamics	
R.R.A. Hoefsloot	513419	Systems	
K.J.W. Kwakman	530323	Team Leader & Aerodynamics	
D.M.N. Milewski	530628	Stability & Control	
N. van Oene	530322	Landing Gear	
F.H.A. van Tilborg	530630	Stability & Control	
S.J.J Zuurendonk	530629	Structural Design	
Dr. Ir. R. Vos	254874	Faculty Advisor	

Preface

This is the final report of the Fall 2014 DSE Group 01. The goal is to present a class II aircraft design that will meet the requirements set for the design of the Next-Generation Airlift Military Support Aircraft. At the start of the project, three different concepts have been created and designed to a class I estimation. A trade-off was performed to select the final concept: the Wide Hull Airlifter for Long Endurance (W.H.A.L.E.). This report presents the class II design of this concept. The design will compete in the AIAA Undergraduate Design Competition.

In writing this report a basic knowledge of engineering, physics and aircraft design is assumed. Readers who are interested in more information on the estimation methods used are referred to the cited books.

The group would like to express their gratitude to Dr. Ir. R.Vos, Dr. Ir. S. Hartjes, Dr. Ir. D.Pool, Prof. Dr. C. Kassapoglou and Prof. Dr. Ir. E. Torenbeek for their help, guidance and insights during this project.

Contents

List of Figures

List of Tables

Nomenclature

Acronyms	Description
A/C	AirCraft
AIAA	American Institute of Aeronautics and Astronautics
AMPR	Aeronautical Manufacturers Planning Report
APU	Auxiliary Power Unit
BFL	Balance Field Length
CBWB	Canard Blended Wing Body
CRPF	Counter Rotating Prop Fan
DSE	Design Synthesis Exercise
EIS	Entry Into Service
FB	Functional Breakdown
FFD	Functional Flow Diagram
FOB	Forward Operating Base
FSL	Forward Supply Location
GD	General Dynamics
HLD	High-Lift Device
IWB	Integrated Wing Body
ISA	International Standard Atmosphere
LCC	Life Cycle Cost
LEMAC	Leading Edge Mean Aerodynamic Chord
MTOW	Maximum Take-Off Weight
MTR	Mid-Term Review
OBS	Organizational Breakdown Structure
OEW	Operating Empty Weight
PAX	Persons ApproXimately
PL	PayLoad
PSP	Primary Supply Point
RDTE	Research, Development, Test and Engineering
SLS	Sea Level Static
STOL	Short Take-Off and Landing
TO	Take-Off
TOC	Top Of Climb
USAF	United States AirForce
USD	United Stated Dollars
WBS	Work Breakdown Structure
WFD	Work Flow Diagram
W.H.A.L.E.	Wide Hull Airlift for Long Endurance

Subscripts	Description
ac	Aerodynamic center
cr	Critical
dd	Drag divergence
e	Engines
f	Flap
h	Horizontal
i	Inboard
$land$	Landing
LE	Leading Edge
max	Maximum
min	Minimum
o	Outboard
$prop$	Propeller
r	Root
ref	Reference
t	Tip
tot	Total
TO	Take-Off
ult	Ultimate
v	Vertical
w	Wing

Symbols	Description	Imperial Units	SI Units	Value (Imperial (SI))
a	Speed of sound	[ft/s]	[m/s]	
A	Aspect ratio	[-]	[-]	
b	Span	[ft]	[m]	
BPR	Bypass ratio	[-]	[-]	
c	Chord / Climb rate	[ft] / [ft/s]	[m] / [m/s]	
C_{acq}	Acquisition cost	[USD]	[USD]	
C_{disp}	Program total disposal cost	[USD]	[USD]	
C_D	Drag coefficient	[-]	[-]	
C_{D_0}	Zero lift drag coefficient	[-]	[-]	
C_{fol}	Fuel, oil and lubricant cost	[USD]	[USD]	
C_L	Lift coefficient	[-]	[-]	
C_{man}	Program manufacturing cost	[USD]	[USD]	
C_{ops}	Program operating cost	[USD]	[USD]	
$C_{ops/hr}$	Operating cost per flight hr	[USD]	[USD]	
$C_{pro_{man}}$	Manufacturing phase profit	[USD]	[USD]	
$C_{pro_{RDTE}}$	RDTE phase profit	[USD]	[USD]	
d	Distance	[ft]	[m]	
D	Diameter / Drag	[ft] / [lbf]	[m] / [N]	
e	Oswald efficiency	[-]	[-]	
EW	Empty Weight	[lbs]	[kg]	
E	Endurance / Young's Modulus	[min] / [ksi]	[min] / [Pa]	
ff	Fuel fraction	[-]	[-]	
g	Gravitational acceleration	[ft/s^2]	[m/s^2]	32.174 (9.80665)
h	Height	[ft]	[m]	
i	Incidence angle	[deg]	[deg]	
l	Length	[ft]	[m]	
I	Area moment of inertia	[ft^4]	[m^4]	
L	Lift	[lbf]	[N]	
$MTOW$	Maximum take-off weight	[lbs]	[kg]	
n	Load factor	[-]	[-]	
N	Number	[-]	[-]	
OEW	Operational Empty Weight	[lbs]	[N]	
P	Pressure / Power	[psi] / [hp]	[Pa] / [W]	
$P_{ac_{est}}$	Estimated price per aircraft	[USD]	[USD]	
R	Range	[nm]	[m]	
S	Surface area	[ft^2]	[m^2]	
SFC	Specific fuel consumption	[lb/h/shp] / [lb/h/lbf]	[g/s/kW] / [g/s/kN]	
t	Thickness	[ft]	[m]	
T	Temperature / Thrust	[K] / [lbf]	[K] / [kg]	
v	Velocity	[kts]	[m/s]	
V	Volume	[ft^3]	[m^3]	
w	Width	[ft]	[m]	
W	Weight	[lbs]	[kg]	
α	Angle of attack	[deg]	[deg]	
δ	Deflection angle	[deg]	[deg]	
γ	Air heat capacity ratio	[-]	[-]	1.4 (1.4)
Γ	Dihedral	[deg]	[deg]	
ε	Twist angle	[deg]	[deg]	
η	Spanwise station	[-]	[-]	
λ	Taper ratio	[-]	[-]	
Λ	Sweep angle	[deg]	[deg]	
μ	Kinematic viscosity	[lbs*s/ft^2]	[kg*s/m^2]	
ρ	Density	[slug/ft^3]	[kg/m^3]	

Executive Summary

In the context of ongoing modernisation of the USAF, a new generation strategic transport aircraft for EIS 2030 has been developed. It is supposed to transport a warload of 120,000 lbs over a range of 6300 nautical miles and have a maximum payload capacity of 300,000 lbs. It should accommodate 44 463L master pallets or one M104 Wolverine Heavy Assault Bridge. The take-off and landing field length should be 9,000 ft, climb to cruise should take no more than 20 minutes and cruise speed should be at least Mach 0.6.

Three class I concepts were worked out and a trade off resulted in a concept to be worked out to a class II standard. The Wide Hull Airlift for Long Endurance, the W.H.A.L.E., is a 231 ft long, 262.5 ft span ultra wide body aircraft with slender, 12° sweep, straight trailing edge strut-braced wing featuring winglets and a V-tail. Six counter-rotating open-rotor prop-fans are mounted on the wing. The MTOW is 988,000 lbs, OEW is 483,000 lbs, the maximum payload weight is 300,000 lbs and the design payload is 120,000 lbs. The harmonic range is 1,870 nmi. The wing area is 7,640 ft^2 with adapted dropped-hinge flaps along 59% of the span and outboard ailerons along 23% span, the V-tail area is 3,440 ft^2 with a 37.5°dihedral and full span ruddervators for control. The front and rear cargo doors allow for rapid loading and unloading of various types of cargo. It is able to accommodate 72 passengers alongside any cargo and has a maximum passenger capacity of 440. The landing gear consist of a 4-wheel single strut nose gear and a 4 bogey, 16 wheel main gear stored inside the fuselage. The ride-height is 7.2 ft and can be kneeled during loading to 4.2 ft. It has a pitch- and yaw damper to ensure sufficient damping of the eigenmotions.

The main material used is Al 7075-T6, because of its high material properties, good manufacturability and recyclability. A cradle-to-cradle philosophy has been adopted throughout the design process, ensuring a sustainable solution. The unit cost was estimated at $191 M.

1. Introduction

In the context of the ongoing modernization of the US armed forces, a new generation strategic transport aircraft needs to be developed. The anticipated Entry Into Service (EIS) is the year 2030. For this purpose the fall 2014 DSE Group 01, consisting of nine Bachelor students from the faculty of Aerospace Engineering at Delft University of Technology, is tasked to submit a concept proposal for the AIAA Undergraduate Aircraft Design Competition. Having moved from mission analysis and concept finding to the detailed design this report is the final milestone of the project, following the previous Baseline and Mid-Term reports.

In the Mid-Term report the concept generation and selection process was documented. The winning concept, from now on called the Wide Hull Airlift for Long Endurance (W.H.A.L.E.), has been slightly modified by implementing open rotor engines, replacing the Π-tail by a V-tail and adding winglets. This report contains the detailed design of the W.H.A.L.E. and contains analysis on its structural, aerodynamic, operational and other characteristics. It shows the technical and operational feasibility of the proposed concept and explains the philosophy behind it.

The report starts with the general description of the W.H.A.L.E., containing the mission specification, system description, the concept design, the general layout and the sizing in Chapters 2 to 4. The aerodynamic and structural wing design is shown in Chapter 5. The fuselage design follows in Chapter 6. The weight and flight dynamics are analyzed in Chapter 8, which includes the design of the empennage and the control surfaces. Chapter 9 contains the design of the following subsystems: The propulsion system, the fuel system, the landing gear, the flight deck, the avionics, the hydraulic system, the electric system, the furnishing, the defense system and the environmental control. The performance characteristics for runway, climb and descent, maneuver and range of the aircraft are presented in Chapter 10. Additionally, Chapter 11 contains information on the realization of the aircraft, discussing operations and logistics, production, costs, sustainability, compliance and risks. Finally, conclusions and recommendations are included in the report.

2. Mission Specification

As a starting point for the design process of the aircraft the mission has to be specified. The mission is defined by the following four sections and contains requirements, a system description and a mission profile.

2.1 Requirements

The requirements for the aircraft are listed below. They contain requirements that have been provided to the team via the RFP[1] from the AIAA as well as requirements that have been set by the team itself, because it is believed they increase the feasibility of the solution.

Req1 The aircraft shall have a 6,300 nm (11,668 km) unrefueled range with a wartime planned load of 120,000 lbs (54,431 kg).

Req2 The maximum warload shall be no less than 300,000 lbs (136,078 kg).

Req3 The unrefueled warload range shall be no less than 1200 nm (2222 km).

Req4 The cruise Mach number of the aircraft shall be no less than 0.6.

Req5 The time to top of climb/climb to initial cruise altitude shall be no more than 20 minutes with a payload of 205,000 lbs (92,986 kg).

Req6 The take-off field length and balanced field length with maximum payload as well as the landing field length with maximum landing weight shall be no greater than 9,000 ft (2,743 m).

Req7 The take-off, landing and climb requirements shall be met at sea level on an ISA +30 K day. Take-off and landing performance should also be shown at ISA +10 K at 10,000 ftd above MSL.

Req8 The aircraft shall be able to perform a take-off, climb to pattern altitude, conduct pattern flight, and return to base with one or more engines out immediately after decision speed. Aircraft with an even number N engines shall meet this requirement with any $N/2$ engine inoperative; if N is odd then assume $(N+1)/2$ engines inoperative. This requirement has to be met in ISA +10 K, 10,000 ft (3048 m) conditions.

[1] URL: http://www.aiaa.org/uploadedFiles/Events/Other/Student_Competitions/2014-2015_UndergradTeamAircraft_Update_9Sept.pdf, [cited 21 Jan 2015]

Req9 The aircraft shall be able to perform a tactical approach for arrivals to bases embedded in combat environments.

Req10 The internal cargo volume, and corresponding cargo weight capacity, shall be no less than 44 463L master pallets, or one M104 Wolverine Heavy Assault Bridge.

Req11 The aircraft shall be able to loiter for 30 minutes at destination.

Req12 The fuel reserves shall be enough for a change of airport in a 200 nm (370.4 km) radius from the original.

Req13 The aircraft shall be able to climb at a speed no higher than 250 kts (128.6 m/s) below 10,000 ft (3048 m).

Req14 The aircraft shall be able to transport at least 70 people.

Req15 The aircraft shall be able to perform high- velocity airdrops for cargo and personnel.

Req16 The aircraft shall be able to land on unpaved runways.

Req17 The aircraft shall be able to land on Class 4-F airports according to the ICAO Aerodrome Reference Code as well as on airports that support Code VI aircraft according to the FAA Airplane Design Group.

Req18 The aircraft shall be able to be refueled aerially.

Req19 The aircraft shall have a decoy flare system to counter infrared homing air missiles.

Req20 The time for loading 44 463L Master pallets shall be no more than 90 minutes.

Req21 The maximum operational altitude shall at least be 25,000 ft.

Next to the requirements the team was provided with design objectives. The objectives that need to be pursued during the design process are listed below. They are split into primary and secondary objectives, depending on their priority.

- **Primary design objectives:**
  - The fuel consumption for all missions shall be minimized.
  - The harmonic range shall be maximized.
  - The operating and flyaway cost shall be minimized. This includes, but is not limited to: refueling, cargo operations, servicing and maintenance.
  - The time and ground track distance below 10,000 ft (3048 m) for optional tactical approach and landing shall be minimized.
- **Secondary design objectives:**
  - The cargo capacity in terms of number of units, without mixing, of the following (with consideration for weight and volume) shall be maximized: M1A Abrams main battle tanks, M2/M3 Bradley Infantry Vehicles, Apache helicopters.
  - The reliability of the overall aircraft shall be maximized.

2.2 System Description

This section contains the functional flow diagram and the functional breakdown of the next-generation military airlift. It explains operations that the aircraft should perform on a typical mission.

2.2.1 Functional Flow Diagram

This section contains the functional flow diagram (FFD) for the aircraft. It contains all the operations performed by the aircraft in a chronological order. Operations start from starting of the engines and taxi to the runway followed by the take off. After that, aircraft climb to cruise altitude and then cruise to destination, followed by the aircraft descent and landing. In the unlikely event where aircraft can not land at the base, it can loiter for maximum 30 minutes, again climb to reference altitude, cruise to alternate airport followed by descent and then landing and taxi.
After landing at the base, operations like unloading of cargo, loading of new cargo, refueling and take-off takes place in order to fly to the next destination. A functional flow diagram for the aircraft can be found in Figure 2.1.

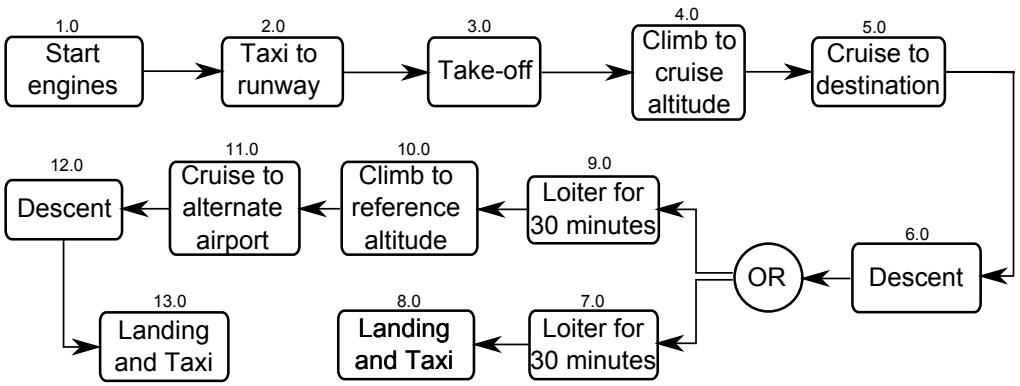

Figure 2.1: *Functional flow diagram of a typical military transport aircraft.*

2.2.2 Functional Breakdown

This section contains the overview description of all the operations that are mentioned in the functional flow diagram. It can be divided into two categories, namely ground operations and airborne operations. Ground operations contain all the activities that are performed by the aircraft on ground level. The airborne operations consist of the operations performed by the aircraft during flight. The functional breakdown diagram (FBD) can be found in Figure 2.2.

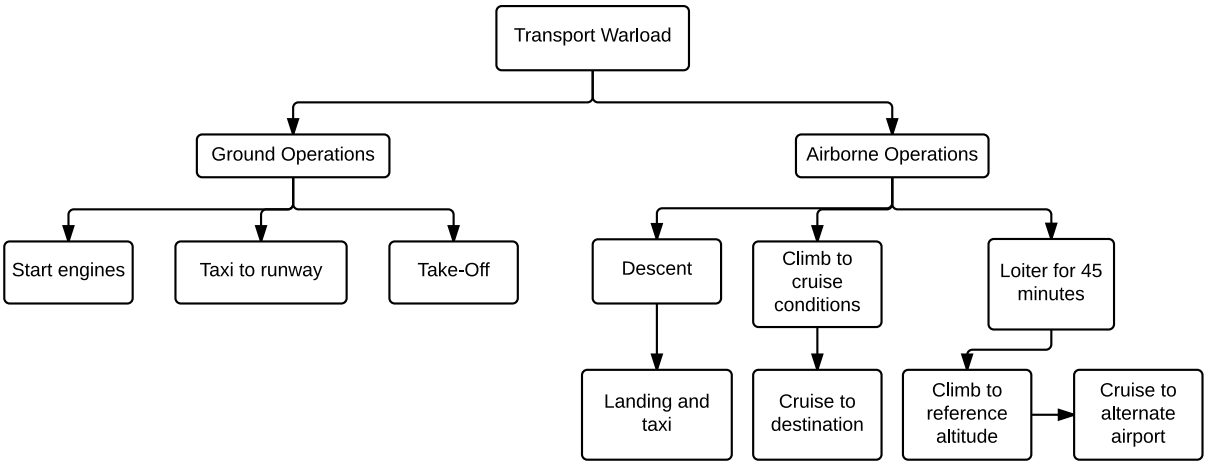

Figure 2.2: *Functional breakdown diagram of a typical military transport aircraft.*

2.3 Mission Profile

From the requirements a mission profile has been derived (see Figure 2.3). It shows the design mission for which the aircraft is sized and contains the most important flight phases from the start of the engines at the airport of departure until their shut down at the destination or alternative airport.

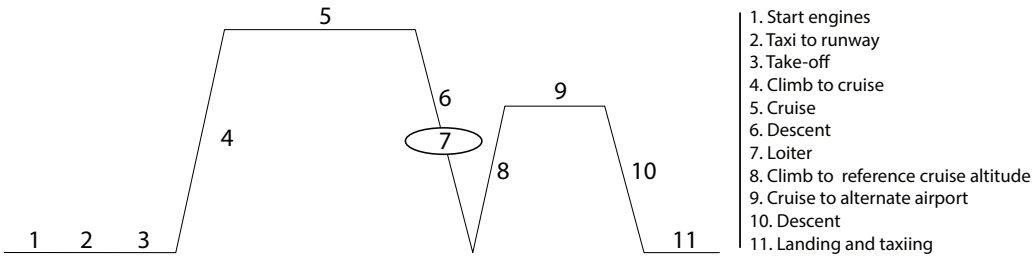

Figure 2.3: *Mission profile*

2.4 Design Philosophy and Technical Approach

The concept shall follow a certain design philosophy that the team tried to incorporate during the whole design process. This philosophy is based on the requirements and design objectives that have been analyzed previously. It aims at accelerating the turn-around process, minimizing the fuel consumption and achieving high versatility.

For the design process many methods have been implemented in to small MATLAB [2] tools. These tools were used to estimate the relevant aircraft characteristics, e.g. class I & II weight estimation, aircraft sizing, drag estimation, structural design, landing gear design and flight dynamics. These tools were integrated in an aircraft analysis program that iterates the design until a coherent design is found. Next to this program the established Advanced Aircraft Analysis tool [3] from DAR Corporation was used to cross-check the results.

3. Concept Design

3.1 Reference Aircraft

It is important for the design process to get an idea of general aircraft data. These may include relations of Maximum Take-Off Weight (MTOW) to PayLoad (PL) as a function of design range, engine count or flight speed. Therefore, existing aircraft with comparable missions have been collected and are shown in Table 3.1.

Table 3.1: *Reference aircraft*

Aircraft	MTOW [10^3 lb] ([t])	max. PL [10^3 lb] ([t])	Cruise Mach [-]	max. Range [nm] (10^3 [km])	max. PL Range [nm] (10^3 [km])	Eng. #	Engine Type
Jets							
C-5M Galaxy[2]	840 (381)	285 (129)	0.77	6985 (12.9)	2960 (5.5)	4	CF-80C2
An-124 100M-150[3]	893 (405)	330 (150)	0.75	6425 (11.9)	1728 (3.2)	4	D-18T
KC-10 Extender[4]	590 (268)	170 (77)	0.76	10000 (18.5)	3800 (7.0)	3	CF6-50C22
C-141B Starlifter[5]	323 (147)	74 (34)	0.74	2501 (4.6)	6390 (10.3)	4	TF-33-P
747 400F[6]	875 (397)	248 (112)	0.85	5100 (9.4)	4445 (8.2)	4	CF6-80C2
C17 Globemas. III[7]	585 (265)	170 (77)	0.77	5610 (10.4)	2420 (4.5)	4	PW2040
UAC/HAL Il-214[8]	149 (68)	44 (20)	0.76	3942 (7.3)	1755 (3.3)	2	PD-14M
A330 MRTT[9]	514 (233)	99 (45)	0.86	8000 (14.8)	3800 (7.0)	2	CF6-80E1
747-8F[10]	987 (448)	295 (134)	0.85	7092 (13.1)	4390 (8.1)	4	GEnx-2B67
A380-800F[11]	1300 (590)	336 (152)	0.85	8000 (14.8)	5620 (10.4)	4	Trent 900
Xian Y-20[12]	485 (220)	145 (66)	0.75	5400 (10.0)	2430 (4.5)	4	D-30
IL-76MD-90A[13]	463 (210)	115 (52)	0.82	4590 (8.5)	2700 (5)	4	PS-90A-76
Propeller							
An-22[14]	551 (250)	176 (80)	0,67	2700 (5.0)	5940 (11)	4	NK-12MA
A400M Atlas[15]	141 (64)	81 (37)	0,7	5412 (10.0)	2049 (3.8)	4	TP400-D6
C-130 Hercules[16]	155 (70)	72 (33)	0,59	4522 (8.3)	2050 (3.8)	4	T-56 A-15
Short Belfast[17]	230 (104)	75 (34)	0,47	4605 (8.5)	850 (1.6)	4	Tyne
C-133[18]	286 (122)	110 (50)	0,46	3788 (7.0)	1943 (3.6)	4	T34-P-9W
AN-70[19]	287 (130)	104 (47)	0.7	4320 (8)	1620 (3)	4	Pro. D-27

3.2 Concept Creation

The creation of concepts was done in two brainstorm sessions in groups of three students with changing team compositions. This way it was tried to generate concepts with different focus and approach. After these sessions each group presented its concept to the rest of the team. By discussing the concepts and asking critical questions the designs were altered until assumed feasible or, if that did not happen, the concept was rejected. In the end three concepts were left which were analyzed in more detail with a class I analysis.

3.2.1 Concept 1: The Canard Blended Wing Body (CBWB)

The first concept to be discussed in this report is a Canard Blended Wing-Body aircraft. The design is focused on a short turn-around time, efficiency and reliability. It features four turbofan engines mounted on top of the leading edge of the wing. The design has a front part that represents a conventional widebody fuselage which is pressurized. The pressurized part continues to the aft of the aircraft where a ramp-door can open. It features a canard and double vertical fins which are also located at the front of the aircraft. At approximately 45 percent of the fuselage length the wings start and blends with the tubular section. In the aft part, next to the tubular section, is an unpressurized cargo-hold in the wings on either side of the center part that can fit a maximum of six 463L pallets each. These side-cargo areas each have a ramp door. The remaining volume of the wing can be used for fuel storage, accommodate control surfaces, flaps, slats and storage for the landing gear. An illustration of the concept can be seen in Figure 3.1.

[2]URL: http://www.globalsecurity.org/military/systems/aircraft/c-5-specs.htm [cited 10 Nov 2014]
[3]URL: http://www.antonov.com/aircraft/transport-aircraft/an-124-100-ruslan [cited 10 Nov 2014]
[4]URL: http://www.theaviationzone.com/factsheets/kc10_specs.asp [cited 10 Nov 2014]
[5]URL: http://simviation.com//rinfolocc141.htm [cited 10 Nov 2014]
[6]URL: http://www.boeing.com/boeing/commercial/747family/pf/pf_400f_prod.page? [cited 10 Nov 2014]
[7]URL: http://www.globalsecurity.org/military/systems/aircraft/c-17-specs.htm [cited 10 Nov 2014]
[8]URL: http://www.globalsecurity.org/military/world/russia/il-214-specs.htm [cited 10 Nov 2014]
[9]URL: http://militaryaircraft-airbusds.com/Aircraft/A330MRTT/A330MRTTSpec.aspx [cited 10 Nov 2014]
[10]URL: http://www.boeing.com/boeing/commercial/747family/747-8_fact_sheet.page [cited 10 Nov 2014]
[11]URL: http://www.aerospace-technology.com/projects/airbus_a380/ [cited 10 Nov 2014]
[12]URL: http://www.flugzeuginfo.net/acdata_php/acdata_an22_en.php [cited 10 Nov 2014]
[13]URL: http://www.ilyushin.org/en/aircrafts/transport/1188/ [cited 24 Nov 2014]
[14]URL: http://www.globalsecurity.org/military/systems/aircraft/c-22-specs.htm [cited 10 Nov 2014]
[15]URL: http://militaryaircraft-airbusds.com/Aircraft/A400M/A400MSpec.aspx [cited 10 Nov 2014]
[16]URL: http://www.globalsecurity.org/military/systems/aircraft/c-130.htm [cited 10 Nov 2014]
[17]URL: http://www.airliners.net/aircraft-data/stats.main?id=355 [cited 10 Nov 2014]
[18]URL: http://www.angelfire.com/wa2/c133bcargomaster/c133btechdata.html [cited 10 Nov 2014]
[19]URL: http://www.globalsecurity.org/military/world/russia/an-70-specs.htm [cited 24 Nov 2014]

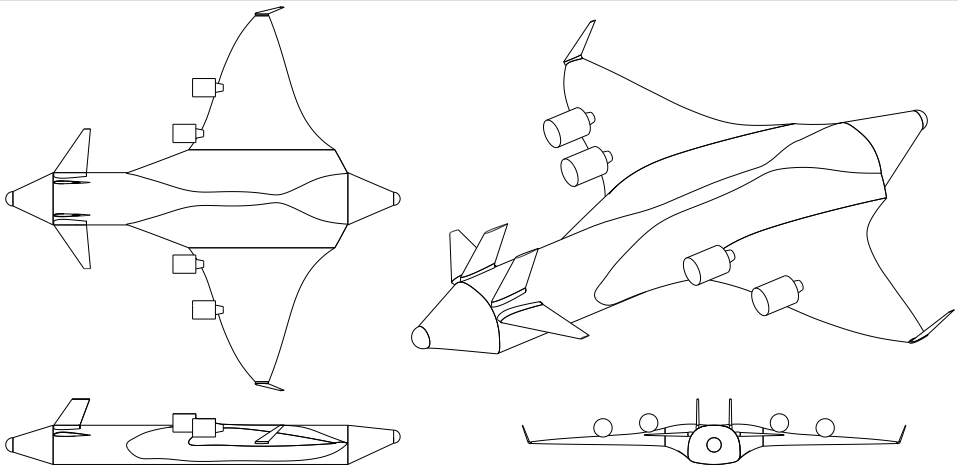

Figure 3.1: *3-view sketches of the canard blended wing body concept.*

3.2.2 Concept 2: The Modular Integrated Wing Body (MIWB)

The second concept proposes a modular design. An integrated wing body carries a module that can be exchanged for different missions. This design focuses on a fast turn-around process, high aerodynamic efficiency and versatility. It features four counter-rotating open rotors and a V-tail configuration. On the sides of the module and the pressurized section pallets can be placed in unpressurized cargo areas with doors in the front of the aircraft. The choice of the integrating wing configuration results from the fact that this concept allows a module to be placed in the aircraft and still have a possibility to place the landing gears easily next to it, which is not possible for a conventional configuration. Additionally, the promising prediction for aerodynamic efficiency by recent literature led to the selection of the integrated wing. The front area of the aircraft is pressurized and contains the cockpit and a passenger compartment. An illustration of the concept is shown in Figure 3.2.

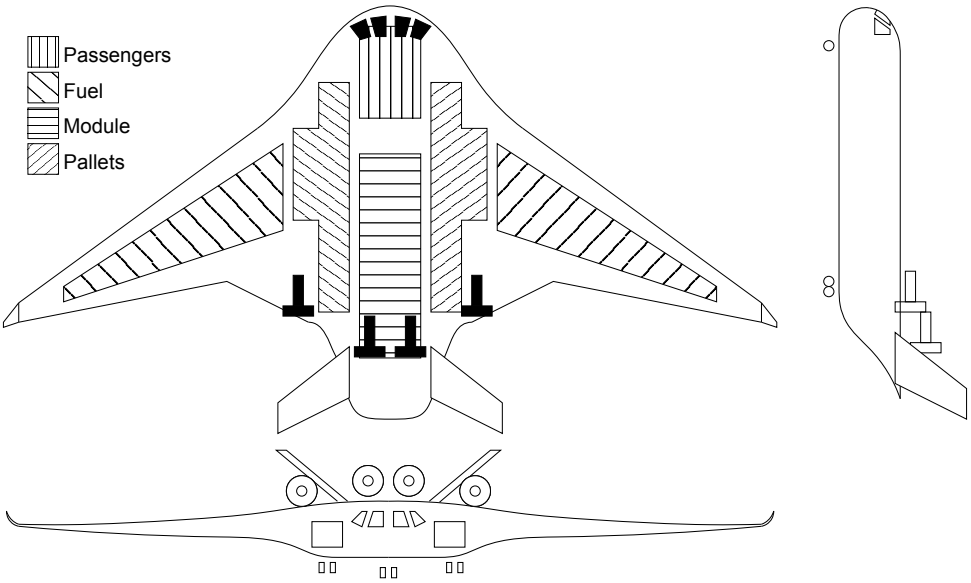

Figure 3.2: *3-view sketches of the modular flying wing concept.*

3.2.3 Concept 3: The Ultra Wide Body (UWB)

The third concept that is proposed is an Ultra Wide Body aircraft. This aircraft will rely on a conventional tube and wing configuration similar to the C-5 with a high wing and a V-tail, that is propelled by four turbofan engines. Main design goals were lowering the turn-around time and increasing aerodynamic efficiency by focusing on a reduction of wetted area and increasing the aspect ratio of the wing. Main design aspects of the UWB are a wider cargo bay and door that help to reduce the turn-around time, a lifting nose surface and integration of the main landing gear in the fuselage body. The whole fuselage is pressurized, ensuring that any type of cargo and passengers can be carried. The use of struts to support the wings allows for a slender wing design with a large span without a high penalty in structural weight. An illustration of this concept can be found in Figure 3.3.

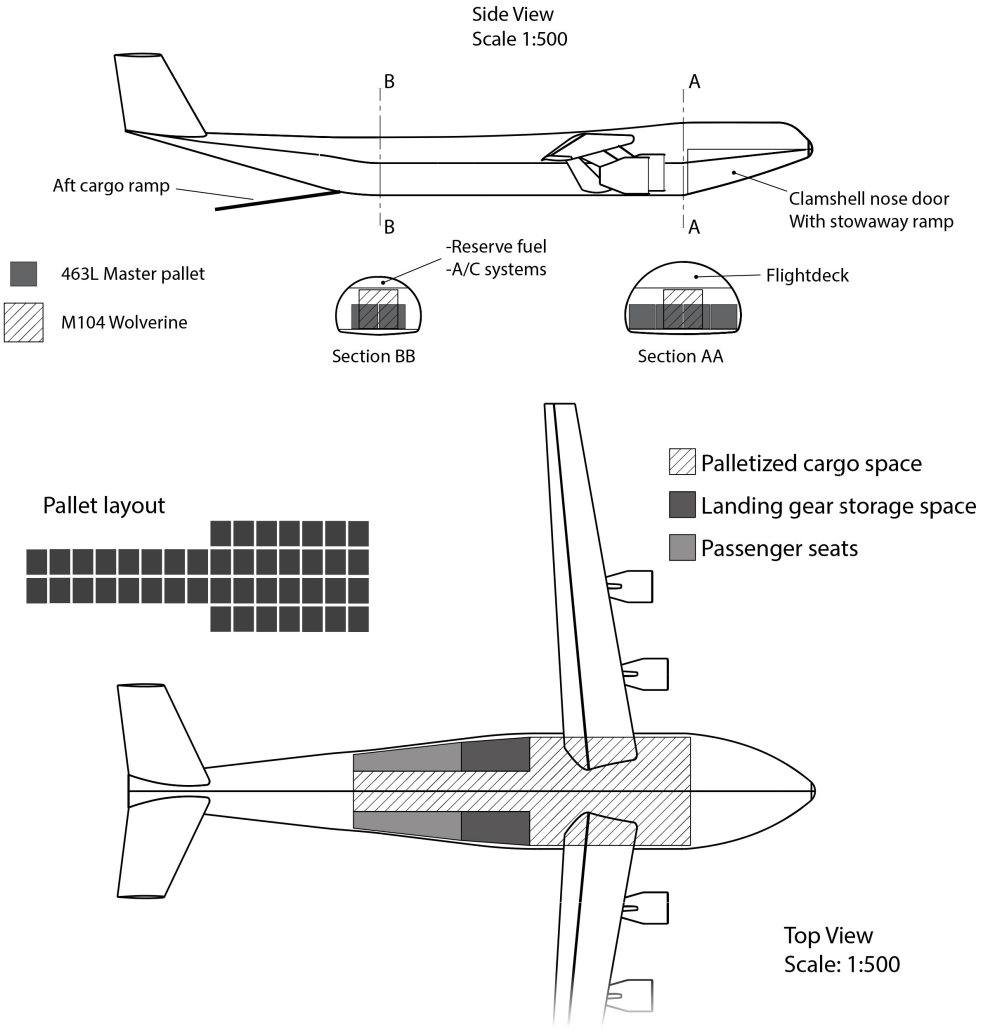

Figure 3.3: *3-view sketches of the ultra wide body concept.*

3.2.4 Concept Analysis

The previously described concepts were analyzed with class I methods to determine their main characteristics and being able to compare them in a trade-off. The most important assumptions and results of the class I analysis are summarized in Table 3.2.

Table 3.2: *Concept analysis results*

Parameter	Concept 1	Concept 2	Concept 3	Units
$MTOW$	756 (343)	746 (339)	806 (365)	[10^3 lbs] (10^3 [kg])
OEW	334 (152)	326 (148)	368 (167)	[10^3 lbs] (10^3 [kg])
W_{fuel}	298 (135)	233 (106)	338 (152)	[10^3 lbs] (10^3 [kg])
M_{cruise}	0.82	0.75	0.8	[-]
h_{cruise}	35,000 (10,668)	40,000 (12,192)	35,000 (10,668)	[ft] ([m])
W/S	89.81 (4,300)	90 (4,310)	174 (8,334)	[lbf/ft^2] ([N/m^2])
T/W	0.245	0.263	0.2618	[-]
T_{total}	185 (822)	193 (858)	211 (939)	[10^3 lbf] ([kN])
S_{ref}	8417 (782)	8,293 (770)	4758 (442)	[ft^2] ([m^2])
b_{ref}	208.6 (63.6)	257.2 (78.4)	261.5 (79.7)	[ft] ([m])
A	5.22	7	14.4	[-]
λ	0.0424	0.04	0.4	[-]
Λ_{LE}	35	25	20	[deg]
S_h	421 (39.1)	1,332 (123)	(969 (89.3))	[ft^2] ([m^2])
$S_{v,each}$	462 (43)	406 (38)	861 (80)	[ft^2] ([m^2])
e	0.85	0.85	0.8	[-]
SFC_{cruise}	0.48 (14.16)	0.44 (12.5)	0.5 (14.2)	[lbs/hr/lbf] ([g/s/kN])
$(L/D)_{max}$	22	24	21	[-]
$(L/D)_{trimmed}$	18.7	20.6	19	[-]
$C_{L_{max,clean}}$	1.0	1.5	1.5	[-]
$C_{L_{max,land}}$	1.5	1.7	2.7	[-]
$C_{L_{max,TO}}$	1.3	1.36	2.1	[-]
C_{D_0}	0.0072	0.00948	0.0145	[-]
S_{wet}/S_{ref}	3.5	2.2	5.5	[-]
$C_{L_{design}}$	0.323	0.474	0.897	[-]
$R_{300,000lb}$				[nm] ([km])
PAX	110	70	110	[-]

3.3 Concept Trade-Off

As a first step a method has to be set up which is used to select a concept to be taken into the class II design phase. The team decided to organize a down-selection workshop during which the students, together with their tutors, estimate the performance of all concepts with respect to predefined criteria. These criteria are given different weighting factors to take into account their relevance for the overall design feasibility.

Table 3.3: *Assessment scale*

-3	-1	0	+1	+3
very poor	poor	neutral	strong	very strong

Next to that a maturity assessment is part of the selection process. It assesses the likelihood of success (i.e. the feasibility of the proposed technologies) and the effort for realization of a concept (i.e. the effort to get the proposed technologies to

the Technology Readiness Level (TRL) 9).

Table 3.4: *Maturity assessment*

high	5	10	15	20	25
	4	8	12	16	20
Likelihood of Success	3	6	9	12	15
	2	4	6	8	10
low	1	2	3	4	5
	high		**Effort**		low

The following paragraphs contain the criteria that the group found to be important for the decision.

Complexity The complexity of a concept has a significant impact on the design, production, operation and maintenance of the aircraft in later stages. Complexity is divided into mechanical complexity and design complexity. Mechanical complexity increases the amount of maintenance, part count and costs. Design complexity increases the resources needed to design the system and is characterized by large interactions between the subsystems and new technologies. Therefore, concepts with lower complexity are ranked higher than those with high complexity but with below average weighting.

Efficiency The efficiency of the aircraft should be high. Sub-categories are structural, propulsion system and aerodynamic efficiency. A high structural efficiency means that the structural weight is comparatively low, e.g. due to integrated structures. The propulsion system efficiency is highly depended on the choice of the engine type and should be maximized. The aerodynamic efficiency describes the ability of the aircraft to generate lift with as little drag as possible. Efficiency has a medium weighting.

Mission Performance & Versatility Important for a military transport aircraft is its performance for the specified mission, but also its versatility to allow the application of the aircraft in the diverse and yet unknown challenges of the coming decades. The first thing to be considered in this category is the aircraft's performance for ground operations. This includes turn-around time (to be minimized) and supported airports on which the plane can operate. Further, a high cruise speed is beneficial to get faster to the destination. A higher ferry range is also favorable. A reduction of needed crew members to operate the vehicle reduces personnel costs and the needed space and weight that is allocated for the crew. The more possibilities exist to configure the cargo (e.g. only passengers, only pallets, mixed cargo, ...) the more versatile the aircraft is. Finally, the performance related to special capabilities should be as high as possible. For this aircraft this means that the aircraft has a good ability to do air-drops and that it can perform tactical approaches as steep as possible. This category is given the highest weight, because it determines what the aircraft can be used for and how well it can adapt to different missions.

Maintainability The maintenance effort for an aircraft should be as low as possible. Maintenance causes time during which the aircraft cannot be operated and produces costs for parts and labor. The needed maintenance effort is dependent on material selection, complexity and other factors. Maintainability is given an average weight, because it is important to

keep the down-times and maintenance costs low.

Costs Costs should of course be kept as low as possible. This is valid for both the production costs and the operational costs. This measure is one of the most important for the costumer and often exceeds previously defined limits. Still, the costs are not given a high weight, because the number of built aircraft is limited and the military does not put the same pressure on this topic as the market does for civil transport aircraft.

Originality The originality of the design should be high. This proves that the team thinks out of the box and looks for innovative solutions for the problems of the next generation military airlift support aircraft. Originality has an average weight, because it should be considered, but is not crucial for the success of the design.

The results of the selection process are shown in the trade summary in Table 3.5. With the help of this table the final concept was determined during a concept selection session with the tutors. This may be one of the concepts or a combination of favorable attributes from different concepts.

Table 3.5: *Selection matrix*

Criteria	Weight	Concept 1	Concept 2	Concept 3
Complexity	**0.15**	**-2.5**	**-1.5**	**0.25**
Mechanical Complexity	0.25	-1	-3	1
Design Complexity	0.75	-3	-1	0
Efficiency	**0.20**	**0**	**-0.05**	**0**
Aerodynamic Efficiency	0.35	-1	-1	1
Propulsion System Efficiency	0.30	0	1	0
Weight	0.35	1	0	-1
Mission Performance/Versatility	**0.30**	**0.8**	**0**	**1.8**
Ground Operations (turn-around, airports)	0.3	1	0	1
Cruise Speed	0.10	0	0	-1
Harmonic Range	0.10	0	0	1
Max. Tank/Helicopter/Passenger number	0.25	1	0	3
Versatility in Cargo Composition	0.25	1	0	3
Costs	**0.15**	**0.5**	**0**	**0**
Production Costs	0.50	0	0	1
Operational Costs	0.50	1	0	-1
Innovation/Originality	**0.2**	**3**	**1**	**0**
Novelties compared to other aircraft	1.00	3	1	0
Score		**0.54**	**-0.04**	**0.58**
Maturity Assessment		**2**	**9**	**16**
Likelihood of Success		2	3	4
Effort to get the technology ready		1	3	4

Concept 1 performed well at the category originality because it was an unconventional approach with many novelties like the shark-fin rudder and the canard configuration. It also scored on the mission performance because it is able to carry many units in different combinations. Bad scores were obtained in the complexity and the maturity assessment. The very integrated configuration with its complex control system will lead to high complexity and reduces both the likelihood of success as well as the effort to get the needed technologies ready and implemented.

Concept 2 could also score on the originality. Apart from that, however, it did not turn out as well as initially thought. The complexity of the module integration is a draw back. The key characteristic of this concept was found to be not feasible. Its versatility is limited for airports with modules in stock and the appropriate module-service vehicles. Further, the aerodynamic efficiency was not as good as assumed in the beginning because trimming the aircraft introduces a lot of additional drag. The feasibility was rated to be average.

Concept 3 was not able to score in the innovation aspect. It is the most conventional concept of the proposed ones. This, however, also lead to high scores in the maturity assessment, because many proven and well known technologies can be used. Further, the mission performance was rated best for this concept because it can carry the most units with the most variability in its composition. It also had a higher harmonic range than the other proposals and allows for fast ground service with its large doors.

As a result Concept 3 was chosen to be taken to the next design stage. It will, however, be equipped with more advanced open rotor engines of Concept 2 to increase its performance.

4. General Description

This chapter gives a general idea of the aircraft and the philosophy behind it. The mission is defined and requirements are listed. Furthermore, graphics of the concept are presented, including a three view and a rendering and the sizing of the aircraft is shown.

The selected concept, 'The W.H.A.L.E.', follows the design philosophy that the team followed in many aspects. The turn-around time is minimized by implementing two large doors that allow for quick loading and unloading procedures. Additionally, the Ultra Wide Body (UWB) fuselage can be loaded from the front with four pallets at the same time, offering space inside half of the fuselage to store four pallets next to each other.

In order to reduce the fuel consumption highly efficient Counter Rotating Prop Fans (CRPF's) are attached to the wings. Furthermore, a high aspect ratio, strut braced wing with winglets maximizes the aerodynamic efficiency of the aircraft.

Versatility has many facets and the W.H.A.L.E. achieves high performance in many of them. The large, fully pressurized cargo bay can store many different cargo compositions, offers seats for 36 passengers and has a back ramp that is designed to allow air drops. Being a successor of the C-5 Galaxy, the W.H.A.L.E.'s performance is measured against the aircraft from Lockheed Martin. Hence, the team made sure that the new concept can compete with it in every imaginable way.

4.1 Layout

The aircraft features a UWB fuselage that offers a lot of space for the required cargo units, Figure 4.1. It has a lifting nose with a clamshell nose door, a rear door ramp and is fully pressurized. The wings are high-mounted in order to have enough ground clearance for the low landing gear and the large engine rotors. The high aspect ratio, nearly unswept wings with winglets are designed for aerodynamic efficiency and are strut-braced to reduce the high weight of such slender wings. The wing span is maximized to 262.5 ft, a longer span would result in the aircraft not longer fulfilling req17 concerning class 4-F airports. The six engines are mounted on the wings. They are CRPF's that are able to fly at a decent speed and altitude with improved efficiency compared to usual turbofan engines. An upper deck is located above the cargo bay and features a cockpit for a crew of 6 and accommodates 36 more passengers. A V-tail is attached to the tail of the fuselage. The V-tail is structurally a more efficient design than the conventional T-tail, resulting in a lightweight empennage. A

rendered CATIA model [4] is presented in Figure 4.2.

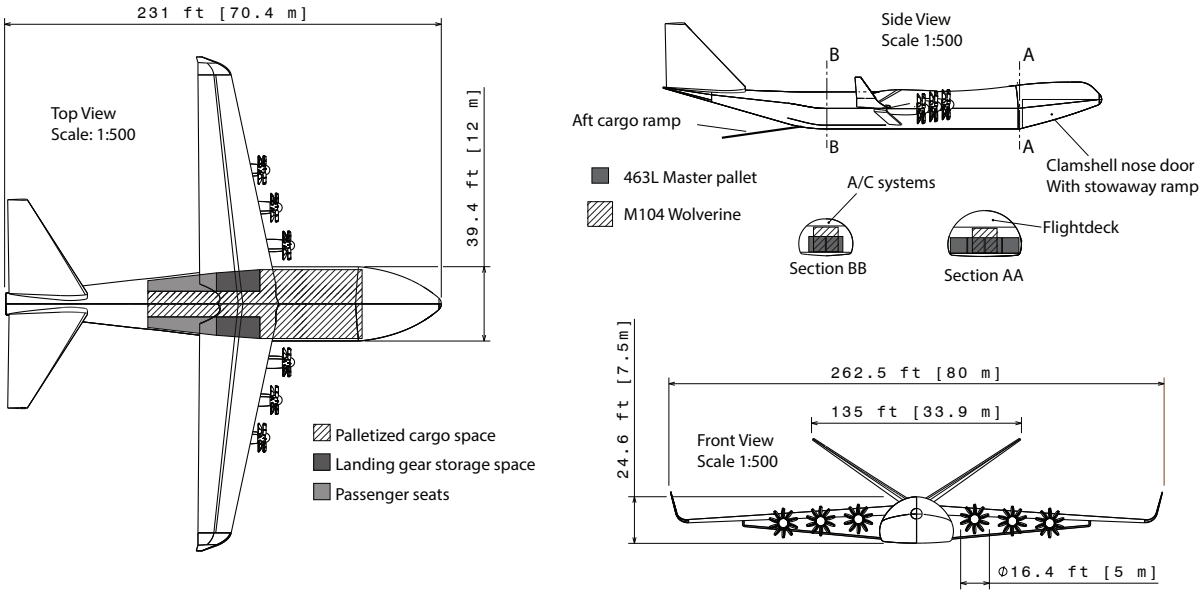

Figure 4.1: *General layout of the W.H.A.L.E.*

Figure 4.2: *CATIA render of the W.H.A.L.E.*

The landing gear was designed in such a way that the main gear is positioned behind the center of gravity and that the turn-over angle is larger than the rotation angle. Also, the loads on the nose gear should be between 8% and 15% of the MTOW of the aircraft. This leads to the nose landing gear being located at 20% of the fuselage length from the nose and the main landing gear at 49% fuselage length from the nose. In figure 4.3 the clearance angles of the aircraft are shown. The sizing of the landing gear will be discussed in section 9.3.

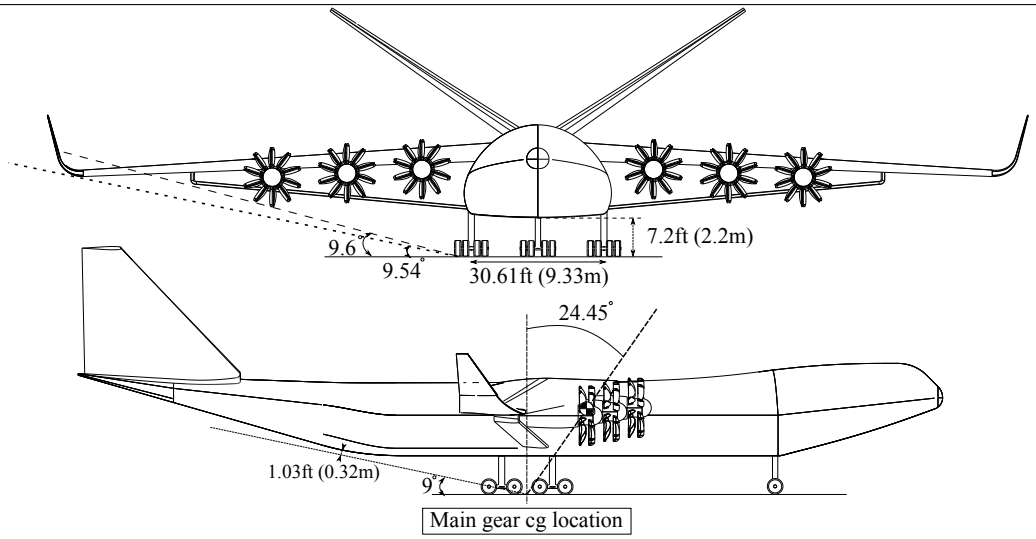

Figure 4.3: *Clearance lines and angles of the aircraft*

4.2 Sizing

For the sizing of the aircraft a class I weight estimation and a wing loading/thrust loading diagram was used. For this procedure, several initial assumptions had to be made that were updated during the design process. The input values are summarized in Table 4.1

Table 4.1: *Design point calculation input*

Parameter	Value	Units	Parameter	Value	Units
e	0.8	[-]	C_f	0.003	[-]
W_{PL}	120,000 (54,431)	[lbs] ([kg])	n_{max}	2	[-]
R	6,300 (11,668)	[nmi] ([km])	M_{cruise}	0.75	[-]
$R_{reserve}$	200 (370)	[nmi] ([km])	h_{cruise}	35,000 (10,668)	[ft] ([m])
SFC_{cruise}	0.44 (12.1)	[lbs/hr/lbf] ([g/s/kN])	$v_{climb_{max}}$	194.38 (100)	[kts] ([m/s])
$(L/D)_{cruise}$	17	[-]	c	39.4 (12)	[ft/s] ([m/s])
$(L/D)_{endurance}$	19	[-]	E	30	[min]
$(C_L)_{max,clean}$	1.8	[-]	W_{land}/W_{TO}	0.9	[-]
$(C_L)_{max,land}$	2.7	[-]	d_{land}	9,000 (2,743)	[ft] ([m])
$(C_L)_{max,TO}$	2.4	[-]	S_{wet}/S_{ref}	5.48	[-]
C_{D_0}	0.0206	[-]			

4.2.1 Weight Estimation

The weight of the aircraft was initially estimated with statistical data of similar aircraft and the fuel fraction method. The weights have then been determined in more detail during the design process and were iterated. The estimated weights are a MTOW of 988,000 lbs (488,000 kg) and a OEW of 483,000 lbs (220,000 kg). Te estimated fuel fractions (acc. to Vos [5]) are summarized in Table 4.2.

Table 4.2: *Fuel fractions*

Mission stage	Value		
Start	0.99	Climb	0.98
Taxi	0.99	Descent	0.99
Take-off	0.995	Landing	0.992

4.2.2 Design Point

The design point has been found by translating the requirements into a thrust loading and wing loading diagram. This diagram is presented in Figure 4.4. It was aimed at getting the highest possible wing loading which is limited by the buffet onset boundary. The thrust loading was subsequently minimized and is limited by the BFL and take-off requirements.

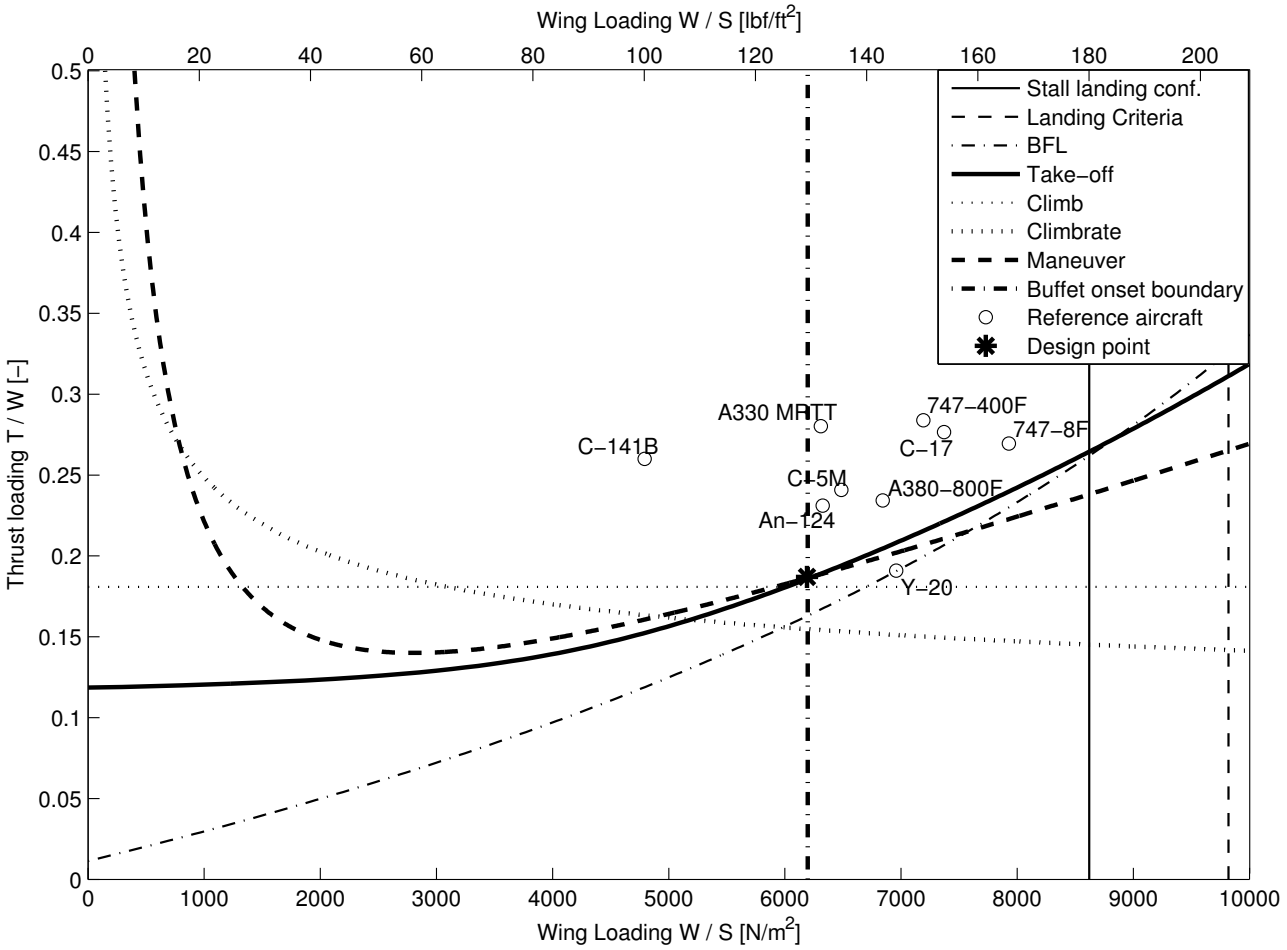

Figure 4.4: *Design point*

As a result, a wing loading of 129.3 lbf/ft^2 (6,190 N/m^2) and a thrust loading of 0.187 were identified as the design point for the aircraft. It was decided to fly at a cruise Mach number of M=0.75. A sensitivity study showed that with a higher flight speed, less fuel would be consumed. The speed was then limited by the decision to minimize the sweep and hence, the drag divergence Mach number of 0.75. Further, the selected engine type performs best at approximately this Mach number. Cruise speed and altitude were based on a sensitivity study and constraints for the selected configuration. The engines perform well at flight speeds around M=0.75 and can reach high altitudes. The sensitivity study showed that a

higher flight speed than the required 0.6 would reduce the fuel consumption for the design mission. Following the design philosophy of maximizing versatility, the cruise altitude should be rather high. Also the drag reduction favored a high altitude. Taking all these effects into account, the cruise condition was set at M=0.75 at 35,000 ft. More sizing results can be found in Table 4.3

Table 4.3: *Sizing results*

Parameter	Value	Units	Parameter	Value	Units
W/S	129.3 (6,190)	[lbf/ft^2] ([N/m^2])	b_h	99.7 (30.4)	[ft] ([m])
T/W	0.187	[-]	Λ_h	28	[deg]
$MTOW$	988,000 (488,000)	[lbs] ([kg])	S_v	1,249 (116)	[ft^2] ([m^2]
W_{fuel}	383,000 (174,000)	[lbs] ([kg])	b_v	52.5 (16)	[ft] ([m])
W_{empty}	483,000 (220,000)	[lbs] ([kg])	Λ_v	20	[deg]
T_{total}	189,400 (842,500)	[lbf] ([N])	$d_{wing-horizontalstab.}$	122 (37.2)	[ft] ([m])
N_e	6	[-]	$l_{fuselage}$	231 (70.4)	[ft] ([m])
S_{ref}	7,642 (710)	[ft^2] ([m^2])	$h_{fuselage}$	22.3 (6.79)	[ft] ([m])
A	9	[-]	$w_{fuselage}$	28.5 (8.7)	[ft] ([m])
b	262.5 (80)	[ft] ([m])	$V_{pressurized}$	104,000 (2900)	[ft^3] ([m^3]
λ	0.37	[-]	$(t/c)_{wingroot}$	0.15	[-]
Λ_{LE}	12	[deg]	R_{max}	8,186 (151,60)	[nmi] ([km])
$C_{L_{design}}$	0.64	[-]	PAX	72	[-]
S_h	1,873 (174)	[ft^2] ([m^2]			

5. Wing Design

This chapter presents the design process of the wing. Firstly, the airfoil is selected. Secondly, the planform is developed and the high-lift devices are chosen. Then some aerodynamics analysis is performed. At last, the structural design of the wing is presented.

5.1 Airfoil Selection

This section will elaborate on the considerations in selection of the wings airfoil.

5.1.1 Design Lift Coefficient

In order to determine what the lift coefficient of the wing airfoil should be, the following equation was used [6]:

$$C_{l,des} = \frac{1.1}{\rho \cdot V_{cruise}^2 \cdot \cos^2(\Lambda_{LE})} \cdot \frac{1}{2} \left(\left(\frac{W}{S} \right)_{start\ cruise} + \left(\frac{W}{S} \right)_{end\ cruise} \right) \tag{5.1}$$

Since the primary operating condition of the aircraft is the cruise phase, equation (5.1) optimizes the design lift coefficient for cruise conditions by using the average wing loading during cruise. Also a correction for leading edge wing sweep is included, since sweep will reduce lift. After filling in the numbers the airfoil design lift coefficient turned out to be $C_{l,des} = 0.73$ and the wing design lift coefficient is $C_{L,des} = 0.64$.

5.1.2 Airfoil Selection

For the airfoil selection, the NASA SC(2) series is chosen because of its high maximum lift coefficient, its drag bucket at high Mach numbers and its high critical Mach numbers. Because of the needed design lift coefficient of 0.73, a NASA SC(2)-07xx airfoil is needed. The selected airfoil is NASA SC(2)-0714, because a thickness of 14% was found to be a good compromise between a lower thickness for a higher critical Mach number and a higher thickness for improved load carrying capability and fuel storage.

The airfoil thickness is varying along the span, gradually reducing from the root to the tip. The root airfoil therefore has a thickness of 15% and the tip airfoil has a thickness of 12%. This action is taken to increase the bending load carrying capability near the root of the wing and to reduce the drag created at the tip of the wing. The mean aerodynamic airfoil

section is shown in Figure 5.1.

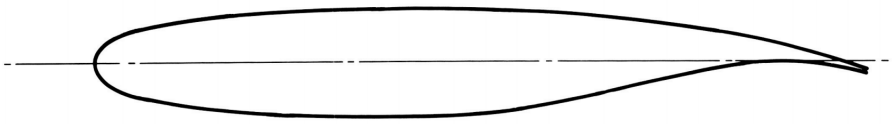

Figure 5.1: *Selected airfoil NASA SC(2)-0714 [7]*

5.1.3 Aerodynamic Characteristics

For the aerodynamic characteristics of the airfoil a lot of experimental data is available [7, 8]. From this data the important airfoil characteristics were gathered and are summarized in Table 5.1. This includes a drag divergence Mach number of 0.75, a zero lift angle of attack of -4.5 degrees, a zero angle of attack lift coefficient of 0.55, a maximum lift coefficient of 2.1 at 18 degrees angle of attack for cruise conditions (Re=$14 \cdot 10^7$), a maximum lift coefficient of 1.8 at 15 degrees angle of attack for take-off and landing conditions (Re=$6 \cdot 10^7$) and a lift gradient of 0.10 per degree.

Additionally, the center of pressure was determined by integrating the pressure over the airfoil. It was found to be located at 24% of the local chord length at low Mach numbers.

Table 5.1: *Airfoil characteristics*

Parameter	Value	Units	Parameter	Value	Units
$C_{L_{\alpha=0}}$	0.55	[-]	$C_{l_{\text{des}}}$	0.73	[-]
α_{0L}	-4.5	[deg]	M_{crit}	0.7	[-]
$C_{l_{\text{max}}}$	2.1	[-]	C_{m_0}	-0.014	[-]
$\alpha_{C_{L_{\text{max,TOL}}}}$	18	[deg]	M_{dd}	0.75	[-]
$\alpha_{C_{L_{\text{max,cruise}}}}$	15	[deg]	$(x/c)_{ac}$	0.24	[-]

5.2 Planform Design

In the following sections the planform of the wing is specified. The incidence angle, sweep angle, taper ratio, anhedral and twist angle are determined.

Wing Incidence Angle

From aerodynamic analysis followed that the chosen airfoil delivers the design lift coefficient when put at an angle of attack of 0 degrees (see Section 5.5). Thus, the incidence angle of the mean aerodynamic chord is set to be 0 degrees, since the wing's performance is then optimal in cruise. For the rest of the span the twist will change the incidence angle.

Sweep Angle

The high critical Mach number of the airfoil, equaling the design Mach number, does not force a sweep angle on the design from an aerodynamic point of view. It was, however, decided to put the leading edge of the wing to a 12 degrees

sweep angle. This has, first of all, the benefit of setting the engines at a longitudinal offset, making the design safer in case of a blade-off event. Secondly, the combination with the taper ratio leads to a zero sweep angle for the trailing edge. This makes the high-lift devices simpler.

Taper Ratio

The taper ratio selection was based on tip stall behavior and induced drag reduction. Corke [9] suggests in his book that the taper ratio would be optimal for induced drag at $\lambda = 0.37$ for a quarter chord sweep angle of 9 degrees. According to Howe [10], the taper ratio should not be lower than 0.35 in order to avoid bad tip stall characteristics (see equation 5.2). For this reason the taper ratio is set at 0.37.

$$\lambda = 0.2 \cdot A^{(1/4)} \cdot cos^2 \Lambda_{1/4} \tag{5.2}$$

Anhedral

The anhedral is set to 3 degrees. This decision is based on a C_{l_β} analysis with the AAA software from DAR Corporation [3]. The angle is introduced to improve the stability characteristics of the aircraft concerning spiral and dutch roll motions. In order to achieve stability an angle of 7 degrees would be required. This, however, is not feasible because of geometrical constraints like the ground clearance. It was therefore decided to set the angle at a typical value of 3 degrees [10] in combination with a yaw-damper (see Section 8.4).

Twist

It is suggested in literature to set the twist angle between 0 and 5 degrees. An optimization for the cruise condition is out of the scope of this project. However, Raymer [11] proposes a twist angle of 3 degrees to be sufficient to achieve a good lift distribution as an initial guess.

Planform Summary

Table 5.2 summarizes the results of the last sections.

Table 5.2: *Planform characteristics*

Parameter	Value	Units	Parameter	Value	Units
S	7642 (710)	[ft^2] ([m^2])			
b	262.5 (80)	[ft] ([m])	c_r	42.7 (13)	[ft] ([m])
b_{eff}	294 (89.6)	[ft] ([m])	c_t	15.7 (4.79)	[ft] ([m])
A	9.0	[-]	$(t/c)_r$	0.15	[-]
A_{eff}	11.3	[-]	$(t/c)_t$	0.11	[-]
Λ_{LE}	12	[deg]	λ	0.37	[-]
$\Lambda_{0.25c}$	9	[deg]	Γ	-3	[deg]
MAC	31.3 (9.53)	[ft] ([m])	ε	3	[deg]
y_{MAC}	55.5 (16.93)	[ft] ([m])	i_w	0	[deg]
cantilever ratio	20.6	[-]			

A visualization of the wing can be found in Figure 5.2.

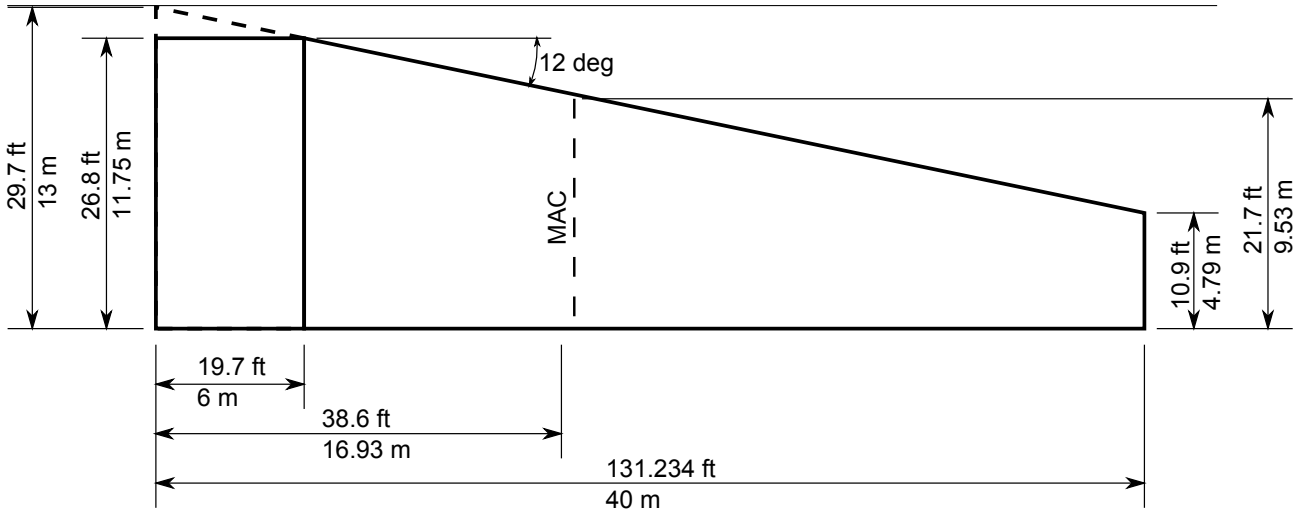

Figure 5.2: *Planform*

5.3 Winglet Design

One of the aims during the design process of this aircraft is to maximize the aspect ratio to decrease the induced drag. The span, however, is limited by the 80m requirement. Hence, it was decided to add winglets to the design that increase the effective aspect ratio by a factor of approximately 1.2 [11]. As a result the physical aspect ratio of 9.0 is treated as 11.3 for the aerodynamic calculations. A drawing of the initial design is shown in Figure 5.3.

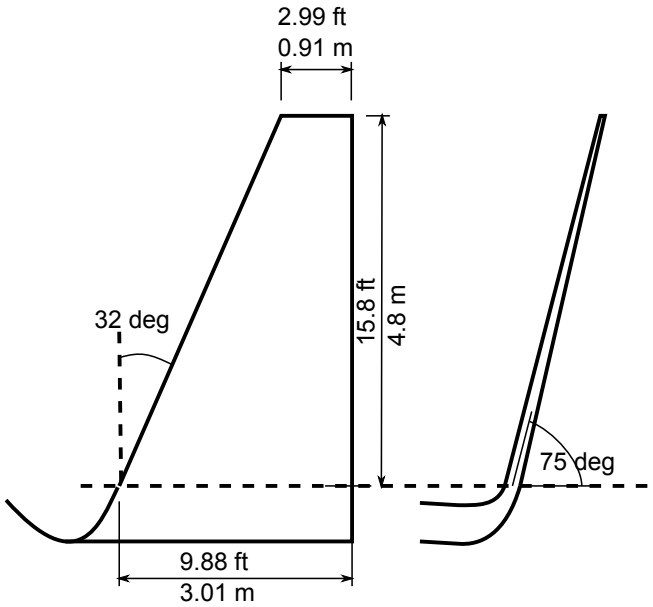

Figure 5.3: *Winglet design*

For the sizing of the winglets guidelines from F. George [12] and Torenbeek [13] are used. George recommends for an initial design to set the thickness of the winglet to 0.08c. In chord-wise direction the winglet shall start at the maximum thickness position and end at the trailing edge of the wing. Additionally, a taper ratio of 0.3, a dihedral of 75 degrees and an incidence angle of -4 degrees are recommended. The height was set at 4.8m and is based on Torenbeek. The data is summarized in Table 5.3.

Table 5.3: *Winglet characteristics*

Parameter	Value	Units	Parameter	Value	Units
Λ_{LE}	32	[deg]	(t/c)	0.08	[-]
h	15.8 (4.8)	[ft] ([m])	λ	0.3	[-]
c_r	9.88 (3.01)	[ft] ([m])	Γ	75	[deg]
c_t	2.99 (0.91)	[ft] ([m])	$i_{winglet}$	-4	[deg]
Γ	75	[deg]			

5.4 High-Lift Devices

This section will cover the design of the high-lift systems on the wing. The driving philosophy behind the high-lift systems is simplicity, while achieving a sufficient lift coefficient increment.

Looking at the planform it can be seen that the fuselage starts at a certain percentage of the wing span. Control surface sizing, see Section 8.3, has shown that the aileron limits the spanwise flap length. This means that the space for flaps is bounded by span stations $0.11 \cdot b/2$ and $0.70 \cdot b/2$.

In the Class I design some lift coefficient values were assumed. However, analysis pointed out, as opposed to what was first assumed, that landing was not sizing. Thus, these values were altered before being used in the sizing of the high lift system. The maximum lift coefficient was now estimated to be $C_{L_{max}} = 1.8$, the maximum landing lift coefficient, $C_{L_{max,land}} = 2.7$ and the maximum take-off lift coefficient was taken to be $C_{L_{max,TO}} = 0.9 \cdot C_{L_{max,land}}$. With these values, a Raymer [11] sizing method was done. Fowler flaps were selected for simplicity and effectiveness and analyzed. For take-off 70% of flap lift increment was assumed. This gave the specifications shown Table 5.4.

Table 5.4: *Fowler flap characteristics*

Parameter	Value	Units	Parameter	Value	Units
$\frac{c_f}{c}$	0.35	[-]	$\delta_{f,TO}$	20	[deg]
$\frac{S_{wf}}{S}$	0.64	[-]	$\Delta C_{L_{max,TO}}$	0.6	[deg]
$\frac{b_f}{b}$	0.59	[-]	$\delta_{f,land}$	45	[deg]
η_i	0.11	[-]	$\Delta C_{L_{max,land}}$	0.9	[deg]
η_o	0.70	[-]			

Figure 5.4 shows a schematic overview of the wing, including some dimensions. Fairings that hinge down with the flaps are installed under the wing to provide space to put the high-lift systems actuators. The fairings are not integrated with the engine nacelles, since then they will get in the way of the exhaust jet. Also, because the engines are close to the wing, some accelerated air from the propfans will flow over the airfoil and create additional lift. This cannot be taken into account for certification, but is present nonetheless.

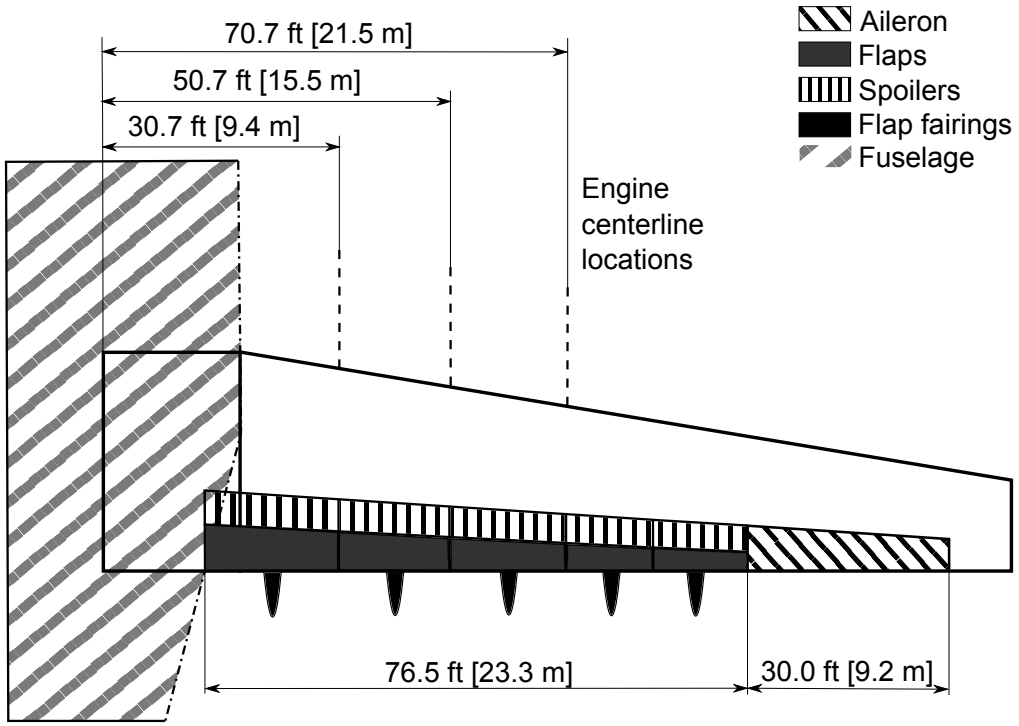

Figure 5.4: *Schematic overview of the wing high-lift system and control surface*

As stated in the Baseline Report [14], use can be made of Adaptive Dropped Hinge Flaps (ADHF). This system uses a dropped hinge flap in combination with a droop spoiler, as shown in Figure 5.5. When the flap is deployed, the independently controlled spoiler is drooped to close the rather large gap between the flap and fixed trailing edge. This requires some system integrated in the flight control computer.

The linear part of the C_L, α-curve outperforms a single slotted flap due to the increase camber. However, performance at high angles of attack is slightly worse, according to Airbus [15] and Figure 5.6. Even so, in the typical operating range of the aircraft, the dropped hinge flap gives an improvement over a single slotted Fowler. Therefore, this system is favorable over the Fowler flap, since complexity - and subsequently weight - is much lower.

For now, it is assumed that the total lift coefficient with HLD's fully deployed does not change with the introduction of ADHF's and that the benefit lies solely in decreased complexity and weight. However, aerodynamic analysis and flight testing will have to verify this assumption.

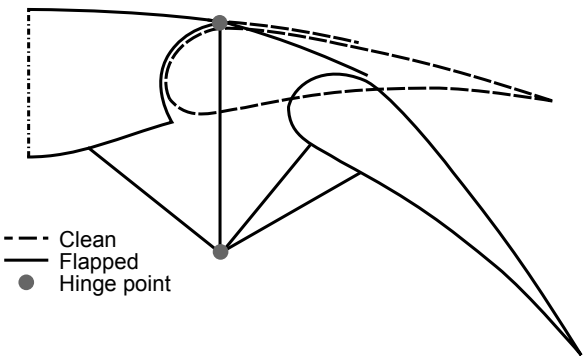

Figure 5.5: *Schematic side view of the dropped hinge flap mechanism*

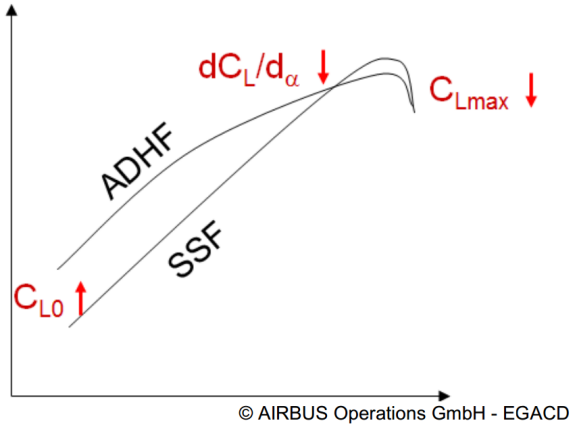

Figure 5.6: *C_L, α-curve comparison of Single Slotted Flap (SSF) and Adaptive Dropped Hinge Flap (ADHF)*

5.5 Aerodynamic Analysis

Having the geometric parameters of the wing and the aerodynamic properties of the airfoil, it is possible to determine the aerodynamic performance of the wing.

The lift curves of the aircraft for clean, landing and take-off configuration are presented in Figure 5.7. They are based on the DATCOM method as presented by La Rocca [6]. The maximum lift coefficient is determined with Equation 5.3.

$$C_{L_{max}} = 0.9 \cdot C_{l_{max}} \cdot cos(\Lambda_{0.25c}) \quad \text{and} \quad C_{L_{max,flapped}} = C_{L_{max,clean}} + 0.9 \cdot \Delta C_{l_{max}} \cdot \frac{S_{wf}}{S} \cdot cos(\Lambda_{hinge-line}) \tag{5.3}$$

The lift curve slope was determined with equation 5.4. Here, β is the compressibility correction factor $\sqrt{1-M^2}$ and the airfoil efficiency μ was assumed to be 0.95 as recommended by La Rocca.

$$C_{L_\alpha} = \frac{2 \cdot \pi \cdot \alpha}{2 + \sqrt{4 + \left(\frac{A \cdot \beta}{\mu}\right)^2 \cdot \left(1 + \frac{tan^2(0.5c)}{\beta^2}\right)}} \quad \text{and} \quad C_{L_{\alpha,flapped}} = C_{L_{\alpha,clean}} \cdot \frac{S_w f}{S} \tag{5.4}$$

The stall angle was calculated with equation 5.5 where $\Delta\alpha_{C_{L_{max}}}$ is the change in stall angle due to the non-linear part of the lift curve. It is a function of quarter chord sweep angle and was estimated using Raymer [11].

$$\alpha_{stall} = \frac{C_{L_{max}}}{C_{L_\alpha}} + \alpha_{0L} + \Delta\alpha_{C_{L_{max}}} \tag{5.5}$$

The zero lift angle of attack was approximated with equation 5.6, where $(\Delta\alpha_{0L})_{airfoil}$ was assumed to be -10 degrees for take-off and -15 degrees for landing as suggested by La Rocca.

$$\alpha_{0L,flapped} = \alpha_{0L} + (\Delta\alpha_{0L})_{airfoil} \cdot \frac{S_{wf}}{S} \cdot cos(\Lambda_{hinge-line}) \tag{5.6}$$

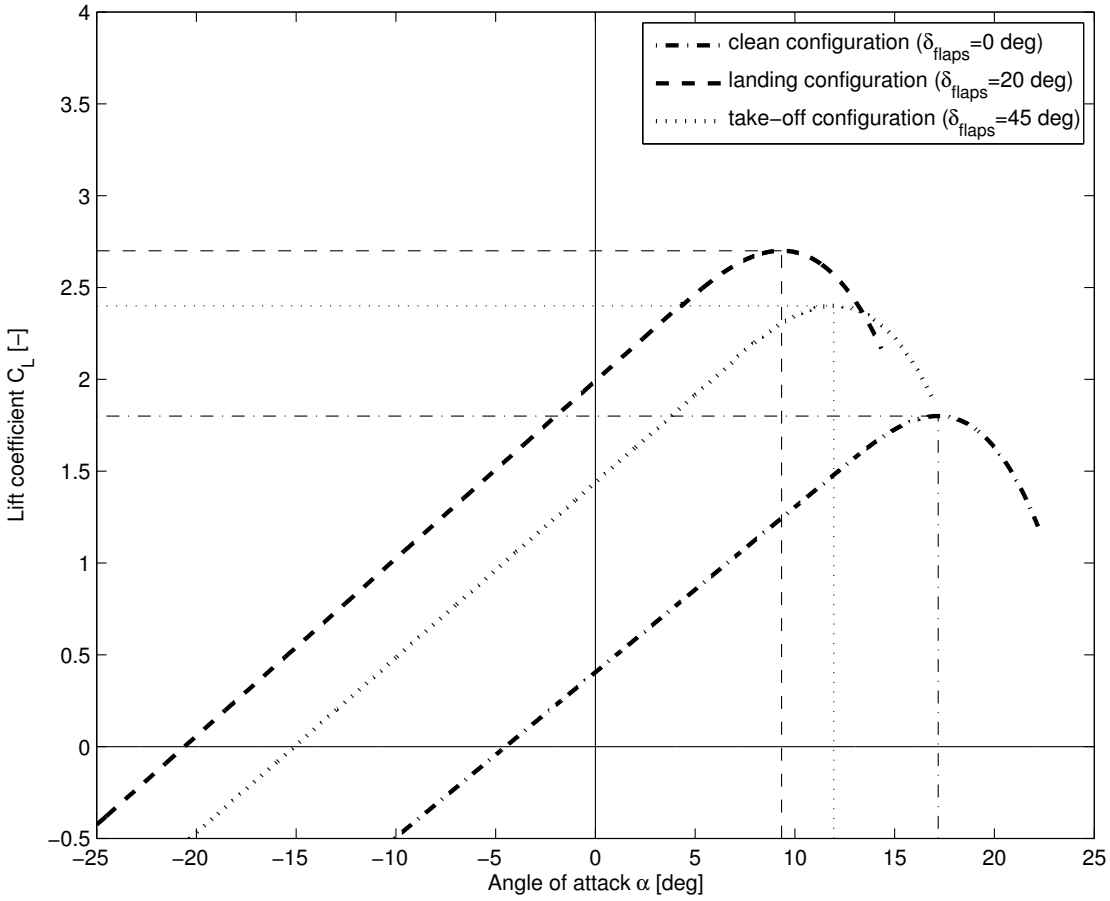

Figure 5.7: *Lift curve (M=0.25, sea-level conditions)*

The drag polar of the entire aircraft during cruise conditions is shown in Figure 5.8. The drag can be split up in a zero lift drag coefficient, a trim drag coefficient and a lift induced drag coefficient. For landing and take-off configurations, the landing gear and flaps add drag as well. The trim and lift drag are computed according to Sadraey [16]. The additional drag for gear and flaps are determined using Roskam [17].

$$C_D = C_{D_0} + C_{D_{trim}} + C_{D_{induced}} + C_{D_{gear}} + C_{D_{flap}} \tag{5.7}$$

The zero lift drag coefficient is based on the method from Gur et al [18]. This method takes into account the friction/form drag, the interference drag and the wave drag. The parts that were included in the friction/form drag analysis are fuselage, wings, empennage, engines and struts. For the interference drag the interference between wings and fuselage, wings and struts, fuselage and struts and fuselage and v-tail are included.

$$C_{D_0} = C_{D_{form/skin-friction}} + C_{D_{interference}} + C_{D_{wave}} \tag{5.8}$$

$$C_{D_{trim}} = \frac{1}{\pi \cdot A \cdot e} \cdot \frac{S_h}{S_{ref}} \left[(C_L - C_{L_w}) \cdot \frac{S_{ref}}{S_h} \right]^2 \tag{5.9}$$

$$C_{D_{induced}} = \frac{{C_L}^2}{\pi \cdot A \cdot e} \tag{5.10}$$

The computed lift-independent drag components are summarized in Table 5.5.

Table 5.5: *Drag components*

Zero lift drag components	Cruise	Take-off	Landing
$C_{D_{form/skin-friction}}$ (fuselage)	0.0035	0.0040	0.0040
$C_{D_{form/skin-friction}}$ (wing)	0.0065	0.0074	0.0074
$C_{D_{form/skin-friction}}$ (empennage)	0.0022	0.0026	0.0026
$C_{D_{form/skin-friction}}$ (engines)	0.0021	0.0024	0.0024
$C_{D_{form/skin-friction}}$ (struts)	0.0006	0.0007	0.0007
$C_{D_{form/skin-friction}}$ (total)	0.0150	0.0170	0.0170
$C_{D_{interference}}$ (fuselage - wing)	0.0030	0.0021	0.0021
$C_{D_{interference}}$ (struts - wing & fuselage)	0.0007	0.0006	0.0006
$C_{D_{interference}}$ (fuselage - empennage)	0.0002	0.0003	0.0001
$C_{D_{interference}}$ (total)	0.0039	0.0030	0.0028
$C_{D_{wave}}$	0.0025	0	0
C_{D_0}	0.0257	0.0401	0.0697
$C_{D_{gear}}$	0	0.0030	0.0030
$C_{D_{flaps}}$	0	0.0095	0.0331

From the above-mentioned drag components a drag polar for the aircraft was constructed (see Figure 5.8). Polars for the most important flight phases, cruise, take-off and landing conditions, are presented. Furthermore, the lift-to-drag ratios are shown for the whole range of positive lift coefficients.

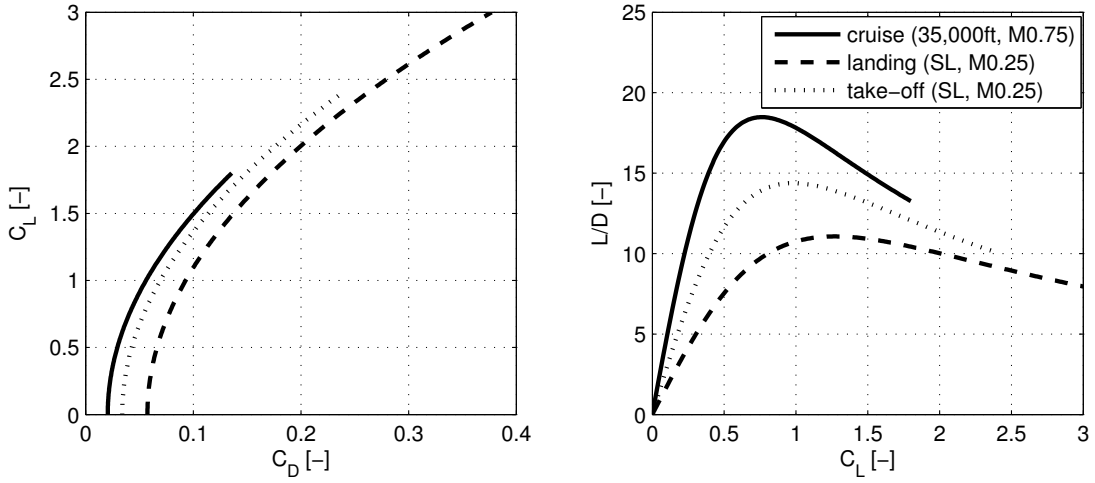

Figure 5.8: *Drag polar and L/D curve*

Important aerodynamic characteristics of the aircraft that have been determined in this section are summarized in Table 5.6

Table 5.6: *Aerodynamic characteristics*

Parameter	Value	Units	Parameter	Value	Units
$\alpha_{stall,landing}$	9	[deg]	$C_{L_{max,landing}}$	3.0	[-]
$\alpha_{stall,TO}$	12	[deg]	$C_{L_{max,TO}}$	2.4	[-]
$\alpha_{stall,clean}$	17	[deg]	$C_{L_{cruise}}$	0.537	[-]
$\alpha_{L=0,landing}$	-21	[deg]	$C_{D_{landing}}$	0.375	[-]
$\alpha_{L=0,TO}$	-15	[deg]	$C_{D_{TO}}$	0.240	[-]
$\alpha_{L=0,clean}$	-4.5	[deg]	$C_{D_{cruise}}$	0.031	[-]
$C_{L_{\alpha,clean}}$	0.0899	[1/deg]	$(L/D)_{max}$	18.5	[-]
$C_{L_{\alpha,TO}}$	0.0953	[1/deg]	$(L/D)_{cruise}$	17.3	[-]
$C_{L_{\alpha,landing}}$	0.0967	[1/deg]	$(L/D)_{TO}$	10	[-]
$C_{L_{\alpha,cruise}}$	0.1211	[-]	$(L/D)_{landing}$	8	[-]

5.6 Structural Design of the Wing

The wing of this aircraft is mainly characterized by its slender design, resulting in a span of 262.5 ft. In general it is quite difficult to realize a light structure that is to support this wing. The weight penalty of having slender wings is reduced significantly by supporting the wing with a strut. The addition of the strut relieves the bending moment in flight, which results in a lighter wing box construction. This chapter presents the structural design of the Strut Braced Wing (SBW) as a result of a strut-wing geometry optimization.

The strut braced wing is in this case an ordinary cantilever high wing supported by a strut, a rod that is suspended between two hinge points located at the belly of the fuselage and somewhere along the span of the wing, Figure 5.9.

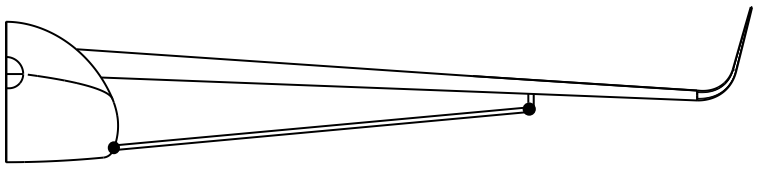

Figure 5.9: *Front view of the left half of the aircraft where the wing is supported by a slender truss. The black dots represent the hinge points of the strut.*

From Figure 5.9 it can be seen that the strut is attached to a point that is slightly below the wing. This is done such that the strut intersects the wing surface perpendicularly. According to Ttrault et al. [19] this results in the lowest drag penalty from the strut-wing interference. It will however introduce an extra moment in the wing box due to the tension in the strut. The wing is sized such that the strut is fully effective when the wing is lifting and only partially effective, or not carrying at all, when the aircraft is on the ground (taxi bump loads, landing loads). Sizing for these landing or taxi loads could be problematic due to column buckling [20].

5.6.1 Materials for the wing structure

The material of choice for the wing box is Al 7075-T6. This material is widely applied on large transport aircraft, mainly because it displays a high specific strength for a metal alloy and it comes at a relatively low price per kg. Production

of aluminium structures is a well understood process in the aerospace industry and a lot of facilities are available, thus reducing the production costs. Additionally, aluminium is fully recyclable, which fits with the cradle to cradle design philosophy for the W.H.A.L.E..
Material properties for Al 7075-T6 that are used for the design of the wing are presented in Table 5.7. For the fatigue strength it is assumed that the wing will have to last 10,000 design cycles, the stress level was then read from an S-N presented in [21].

More weight savings could be achieved using Carbon Fiber Reinforce Polymers (CFRP). A drawback is that CFRP is more notch and impact sensitive. When debris from unpaved runways or enemy fire hits or penetrates the wing the carbon fiber composites cannot yield and can delaminate, significantly reducing the compressive strength of that section of the wing box. Also, inspection for damage on a carbon fiber construction requires ultrasonic equipment and will be hard to perform outside of the home base of the aircraft [22].

The strut is made from a CFRP since it is mainly loaded in one direction and the fibers can therefore be oriented in the direction of the load. Such a highly anisotropic lay-up has a high specific strength and modulus in the direction of the fibers. This yields a lighter strut structure than when an isotropic material such as aluminum is used.
The strut has a length of 100 ft (30.6 m) and it is hinged at both ends. Additionally the strut is mounted close to the engines and is in a highly turbulent flow. Therefore vibrations and thermal stresses will exist in the strut. Designing for these loads is out of the scope of this analysis. Instead, the material properties of the carbon fiber UD laminate were multiplied by an extra knockdown factor, resulting in a more pessimistic tensile strength. The material properties of the carbon/epoxy laminate can be found in table 5.7. The values for the carbon/epoxy were based on data from HexTow® IM7, which is an aerospace certified product [20].

Table 5.7: *Design values for the materials used in the wing structure*

Material	Strength	Shear strength	Young's Modulus	Density
Aluminium 7075-T6	51 ksi (350 MPa)	34 ksi (233 MPa)	10,150 ksi (70 GPa)	5.24 slug/ft^3 (2700 kg/m^3)
Carbon/expoxy UD laminate	145 ksi (1000 Mpa)	-	23,200 ksi (160 GPa)	3.5 slug/ft^3 (1800 kg/m^3)

5.6.2 Design approach for wing structural design

For the structural analysis the wing box is idealized as a multi-section box beam that consists of spar caps, spar webs and wing skins, see Figure 5.10 for a cross-sectional view of the wing box. It is assumed that the spar caps only carry the direct stresses, resulting from bending and compressive or tensile forces on the wing box. The spar webs and wing skins carry the torsional shear stress. It is assumed that only the skins between the spars are load carrying. Finally, the spar webs are also sized to carry the vertical shear forces. The indicated directions of the torque (T) and the force (F) are considered to be positive in this analysis.

[20] URL: `http://www.hexcel.com/resources/datasheets/carbon-fiber-data-sheets/im7.pdf` [cited 24 Jan 2015]

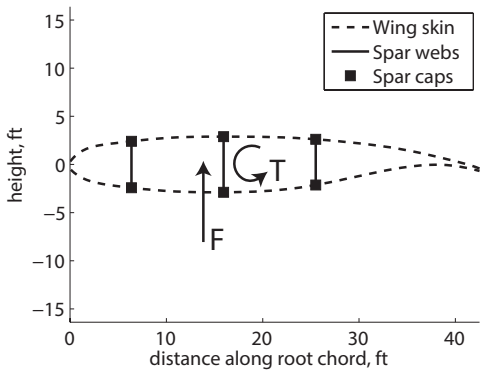

Figure 5.10: *Cross-sectional view of the idealized wing box structure at the root. For the analysis a pure torque (T) and a shear force (F) is applied to each cross-section*

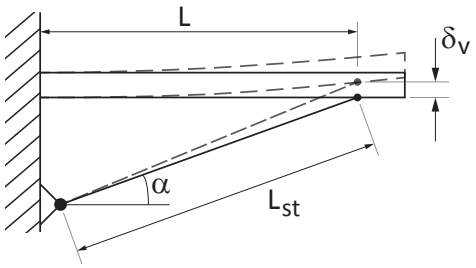

Figure 5.11: *The wing is simplified to a cantilever beam. The dashed lines show how the beam and strut deflect during loading.*

The cross-section shows three spars located at 15%, 37.5% and 60% of the chord length respectively. The middle spar is located near the point of maximum thickness of the airfoil, thus maximizing its effectiveness in taking up the bending load.

The strut braced cantilever wing is a first degree statically indeterminate system. Therefore the amount of force carried by the strut is completely dependent on the flexural stiffness of the wing box and vice versa. This system is solved by assuming that the displacement of the wing at the connection of the strut has to be equal to the strain of the strut itself. Figure 5.11 shows a simplified representation of the system. The system is then solved using Equations 5.11 and 5.12, where δ_v is the vertical deflection at the strut attachment location on the wing.

$$\delta_v = \varepsilon \cdot L_{st} \cdot sin(\alpha) = \frac{\sigma \cdot L_{st}}{E} \cdot sin(\alpha) \tag{5.11}$$

$$\delta_v = \sum_{i=1}^{N} \left[\frac{M_i \cdot \Delta L_i^2}{2E \cdot I_i} + \frac{M_i \cdot \Delta L_i}{E \cdot I_i} \cdot \Delta L_i \right] \tag{5.12}$$

Equation 5.11 represents the strain of the strut, which depends solely on the material and the attachment location of the strut. Equation 5.12 governs the deflection of the cantilever beam (wing). For the latter the wing is subdivided in N sections of equal length ΔL, the total deflection at the attachment point of the strut is the sum of the deflections of each individual beam element. The first term in the equation is the vertical displacement due to the internal moment M in the beam and the second term is displacement due to the rotation of the beam element. The internal moment along the span of the wing can be evaluated, as is explained in section 5.6.2 and is dependent on the force carried by the strut.

Solving Equations 5.11 and 5.12 and solving the equations for static equilibrium will result in a final idealized structural design, resulting in an idealized structural weight of the wing box. Subsequently, using empirical relations, such as those proposed by [23] and [24], the final wing weight is then determined based on this wing box weight estimation.

Load cases

The wing is designed such that it can sustain the ultimate load during any part of its defined operation. It was established that there are two load cases that could be encountered during operation that are critical for the sizing of the wing of this aircraft, namely:

1. Aircraft performs a 2.5g pull-up maneuver at maximum payload weight, wings are fueled up until aircraft is at MTOW.

2. Aircraft encounters -1.7g taxi-bump whilst taxiing at MTOW with full wing tanks

The first requirement is based on the minimum required limit load as dictated by regulations, FAR 25.337. At MTOW the lift produced by the wing is at maximum. Additionally, by taking the maximum payload weight on board, MTOW can be achieved by having less fuel in the wings, thus providing less bending moment relief on the wing. The second requirement was based on Advisory Circular AC 25.491-1 [25] which proposes a taxi-bump load that is to help the designer to comply with FAR 25.491 (concerned with taxi, takeoff and landing roll design loads). The wing is designed for whichever load case is more constraining.

Wing loading diagrams

The wing box is sized by the loads introduced by the lift, fuel weight, wing structural weight, engine weight and strut location. For the lift a parabolic load distribution is assumed and the fuel and wing weight are assumed to vary linearly over the semi span of the wing. The resulting net force distributions over the semi-span are displayed in Figure 5.12. The engines and the strut are treated as point forces at their attachment location, which are not indicated in this figure. All figures presented in this chapter are made for the most ideal strut location for this wing analysis, being at 70% of the semi-span.

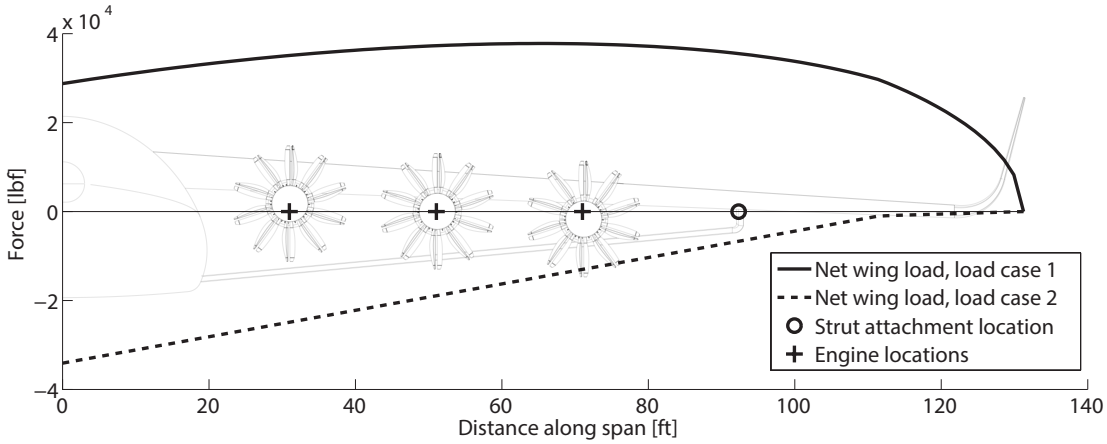

Figure 5.12: *The force distribution over the semi-span of the aircraft.*

The effect of the winglet on the lift distribution is ignored. The lift coefficient is higher at the tip [26], but the chord is also a lot smaller of the winglet. The net effect on the lift distribution by the winglet would therefore be relatively small and

therefore negligible in light of the accuracy of this wing weight analysis. From the force distribution a shear and moment diagram can be developed for each load case, see Figure 5.13. The large step in the shear flow diagram at 92ft is caused by the tension in the strut, the other discontinuities are caused by the weight of the engines.

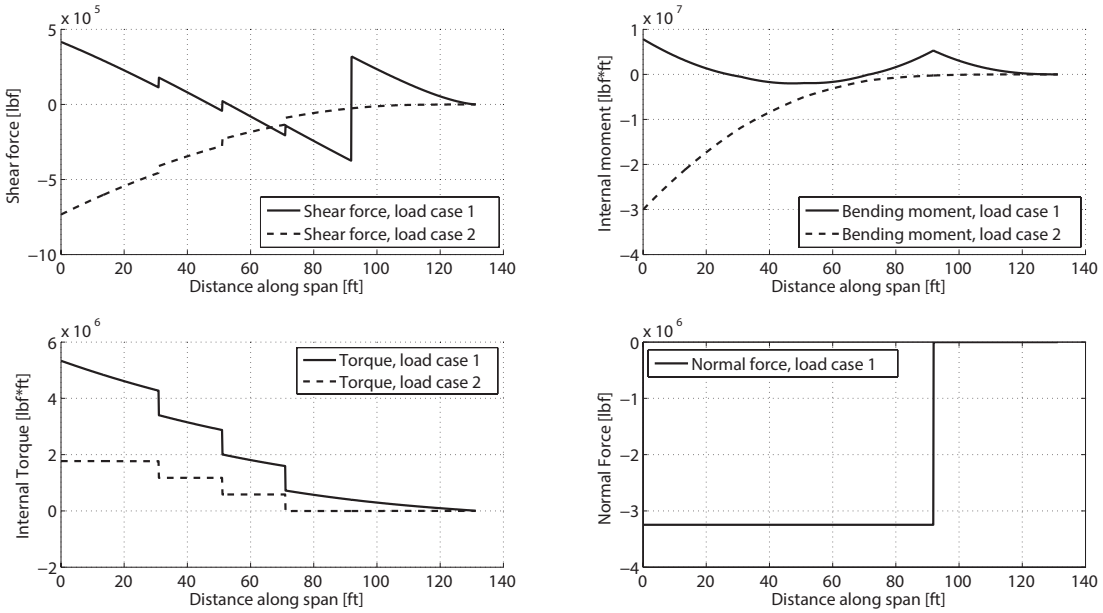

Figure 5.13: *Top left: shear force diagram, top right: bending moment diagram, bottom left: torque diagram, bottom right: normal force diagram.*

The torque was diagram was constructed by adding the torque due to the wing sweep to the aerodynamic torque of the wing. The discontinuities in this plot are a result of the engines, being suspended a certain distance away from the shear center of the wing box. The normal force in the wing is a result of the tensile force in the wing, pulling toward the fuselage, resulting in a compressive force in the wing box. As mentioned earlier, the strut is not load-carrying when the wing is not lifting (deflecting downwards), therefore there exists no normal force for load case 2. The torque and normal force diagrams are displayed in the bottom left and bottom right of Figure 5.13 respectively.

5.6.3 Wing weight estimation

The weight of the idealized box structure is determined using the wing loading diagrams and Equations 5.11 and 5.12. But the outcome of the equations and the loading diagrams will vary for different strut attachment locations along the span of the wing, resulting in varying final weights. Therefore this system was evaluated for different strut locations, the result of this is presented in Figure 5.14. A strut location of 0% represents a pure cantilever wing.

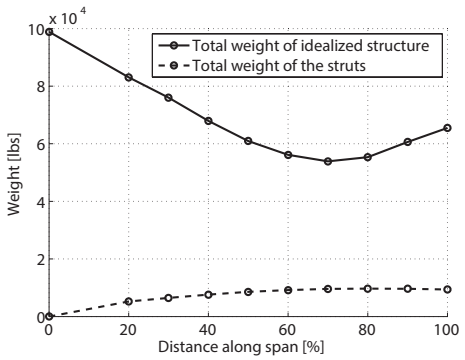

Figure 5.14: *The effect of strut attachment location in % of the semi-span versus the total structural weight of the wing.*

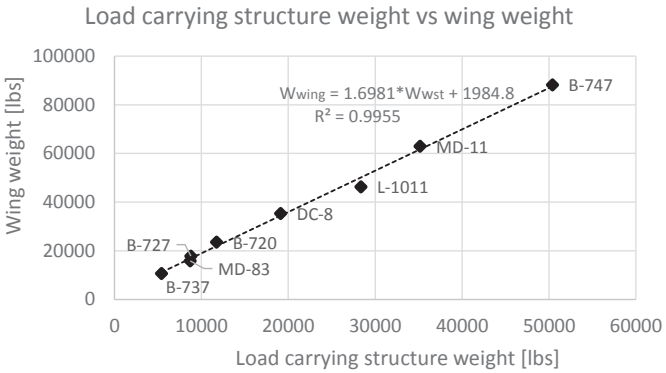

Figure 5.15: *Linear regression for prediction of wing weight based on the weight of the wing box structure.*

From this plot it is concluded that for this aircraft the strut attachment location resulting in the lowest wing weight is at 70% of the semi-span. For this design point the strut has a diameter of 10 inches if a circular cross-section is used.

In order to predict the wing weight an empirical relation between wing box weight and total wing weight is established from actual values of a number of reference aircraft, Figure 5.15. These reference values were take from [24].
The wing box weights for these aircraft include the weight of the ribs. The ribs are not sized for this idealized wing structure, rather the weight is estimated through an empirical relation proposed by E. Torenbeek [13]. After Adding the weight of the ribs to the calculated weight of the wing box, the total wing weight can be determined from Figure 5.15. The final results can be found in Table 5.8.

Table 5.8: *Results of the structural analysis of the wing*

Parameter	Value	Units
Weight of idealized wing structure	53,900 (24450)	[lbs] ([kg])
Weight of one strut	4850 (2200)	[lbs] ([kg])
Weight of all ribs	4775 (2166)	[lbs] ([kg])
Total wing weight	101600 (46100)	[lbs] ([kg])

6. Fuselage Design

6.1 Structural Design of the Fuselage

In this chapter the design procedure of the fuselage will be explained. In the first part the assumptions and calculation methods will be described. In part two the results will be shown, explained and concluded.

6.1.1 Assumptions and Calculation Methods

In order to calculate all the forces acting on the fuselage structure assumptions are made:

- Static, steady, horizontal symmetric flight (All forces are in equilibrium).
- Payload is modeled as a distributed load per square foot.
- Maximum normal force is equal to maximum thrust.

Finally the cross-section parameters are determined in order for the total stress exerted on the cross-section, multiplied by a g-force of 2.5 and then a 1.5 safety factor, not to exceed the yield stress of the material. The Von Mises criteria should be evaluated at every location along the fuselage, but to preserve time and for simplicity the Von Mises criteria is calculated with the maximum occurring stress in each direction. For shearstress this is the crossing of the centroidal y-axis with the arc and for bending stress the maximum occurs farthest away from the centroidal y-axis, at the top of the arc. This results in a structure that is highly conservative with respect to the failure criteria.

Other simplifications are that at first the floor is sized for payload and pressure difference, as shown in Figure 6.1 , after that the skin and floor combination of the fuselage are sized for the highest shear and bending moment that can be found working on the fuselage and the fuselage will at first have a constant thickness, these assumptions simplify the necessary calculations greatly, while maintaining a sufficient level of detail for this design stage. This means that the wing-box carries all torsion by itself and does not relay any torsion into the fuselage. The floor carries all the loads caused by the payload and transfers this load into the wing-box. This creates a case of superposition for all different loads with respect to the fuselage.

To calculate the forces acting on the fuselage in flight all components and their respective weights were plotted as a function of distance from the nose. These forces were then used to generate the shear-force diagram of the side view of the

aircraft. Integrating the shear forces over their respective length that they work on generates another plot; the internal moment diagram. The three diagrams can be found in Figure 6.2. With these plots the maximum loads that are acting on the fuselage are determined and these are then used to size the fuselage. The cross-section of the fuselage determines whether it can cope with the forces acting on the fuselage, for the W.H.A.L.E. the cross-section is modeled as a semi-ellipse at the top and a flat floor plate on the bottom of the cross-section, see Figure 6.1. Knowing the loads working on this cross-section, Figure 6.1, the stresses are calculated as a function of bending moment, shear force, pressure difference and payload. With a preset stringer shape and an alternating stringer thickness the optimal area per floor section is determined and checked with buckling. These stresses are calculated separately and later on inserted into the Von Mises criteria in order to know the maximum occurring stress. Maximum bending stress occurs at the farthest distances both positive and negative from the centroid in z-direction.

The final fuselage design is shown in 6.3.

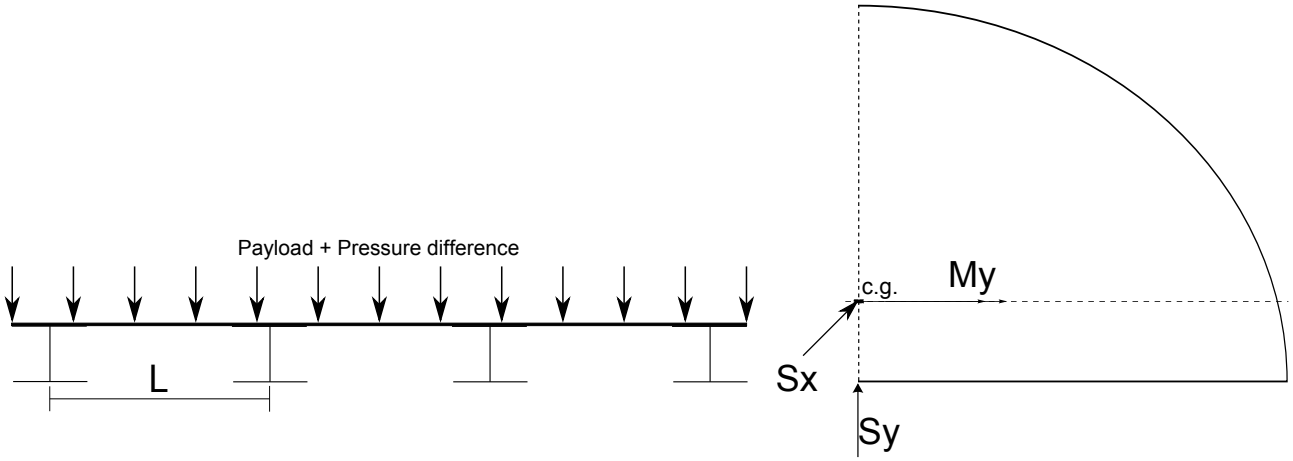

Figure 6.1: *Load case of the floor and fuselage.*

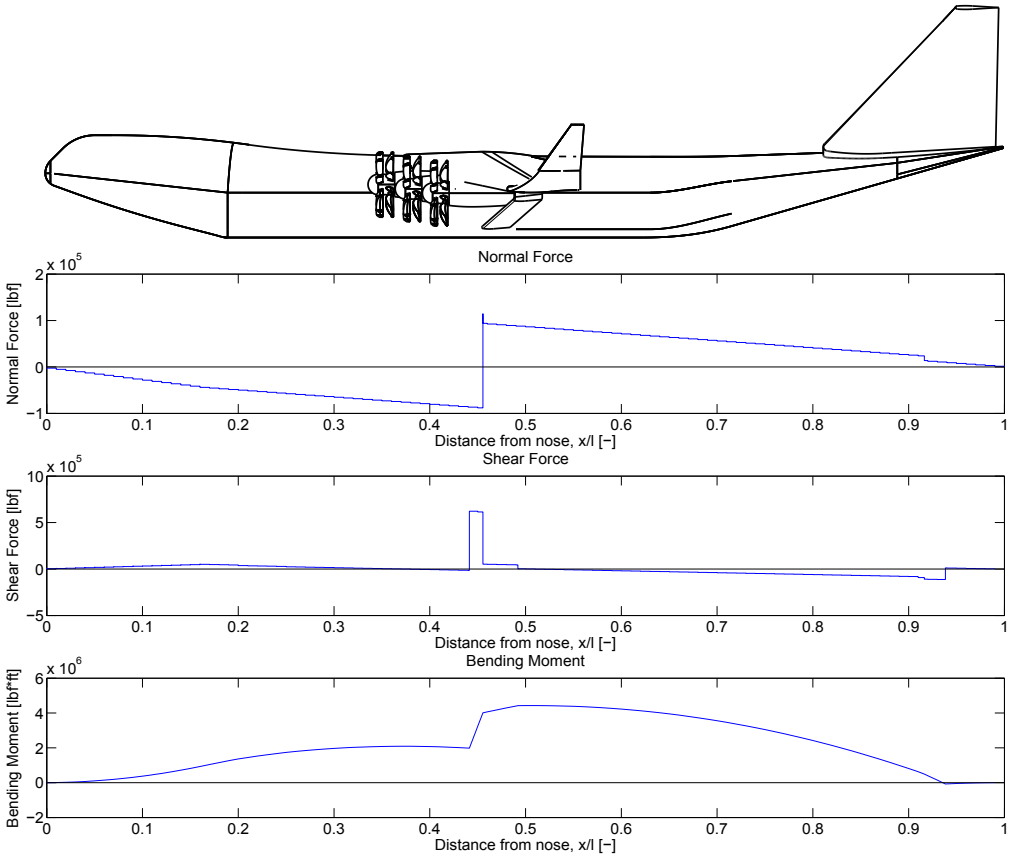

Figure 6.2: *Normal, shear and bending moment diagrams used to find maximum loads in the fuselage.*

6.1.2 Results

The results from the calculations are shown in Table 6.1.

Parameter	Value	Unit
Skin thickness	0.17 (4.3)	[inch] ([mm])
Floor thickness	0.2 (5)	[inch] ([mm])
Fuselage structure mass	86000 (39000)	[lbs] ([kg])
Fuselage mass	165000 (75000)	[lbs] ([kg])
Total material area	1.9 (178000)	[feetˆ2] ([mmˆ2])
Von Mises skin	51000 (349)	[psi] ([MPa])
Von Mises floor	11600(76)	[psi] ([MPa])
Critical buckling length	(3.7)	[ft] ([m])
Beam pitch (both in z- and x- direction)	2.6 (0.78)	[ft] ([m])
Frame pitch	10.2 (3.12)	[ft] ([m])
Number of floor beams in x-direction	17	[-]
Number of floor beams in y-direction	91	[-]

Table 6.1: *Results from structural analysis*

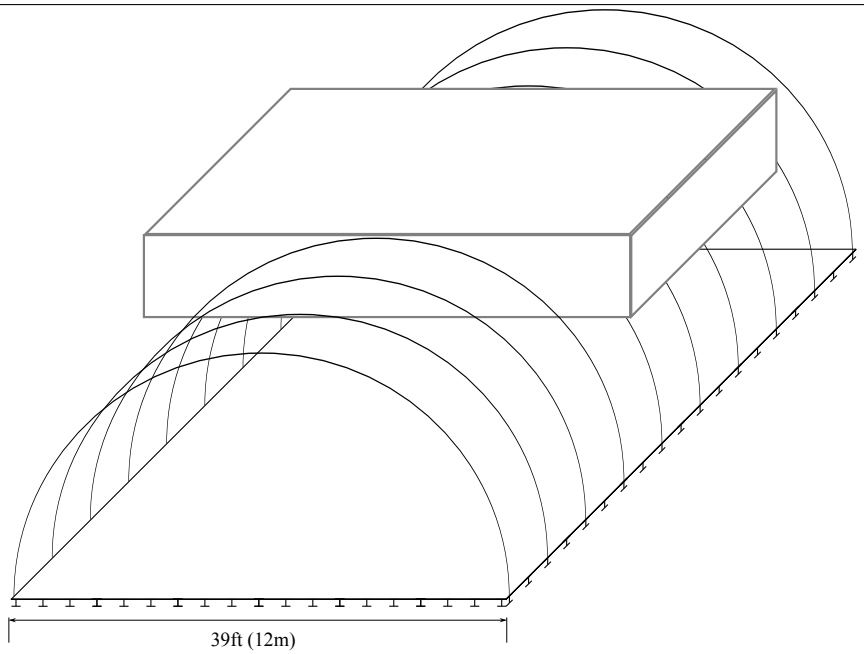

Figure 6.3: *Final fuselage design with interaction of the wingbox.*

The results show that the fuselage needs a thickness for the skin of 0.17 inch to be able to cope with the applied loads, this thickness is a very conservative number because of the method that is used. The skin thickness at the top of the fuselage could have been made smaller since at the top of the fuselage the bending stress is a lot higher than the shear stress, vice versa at the location on the skin that coincides with the z-axis of the centroid. Whereas the Von mises are calculated with the maximum of the found stresses at both locations. The mass that is calculated is based on the assumption that using the length of the aircraft and using the largest cross-section is a good representation of compensation for all additional material that needs to be added for connections and cutouts. The floor is also over-designed with respect to flight loads, as the Von Mises for the floor is smaller than that of the skin.

6.2 Cargo Systems

In this section the cargo holding systems will be discussed. Furthermore, it will be shown that the minimum required cargo fits, and the airdrop mechanism will be described.

6.2.1 Cargo space

The cargo bay of the aircraft is shown in Figure 6.4. The layout for the maximum amount of 44 463L Master Pallets is shown. The M104 Wolverine is also shown in the cutouts, since its height was sizing for the height of the cargo bay. Furthermore, the landing gear storage space is shown, and the space on the side of the cargo bay that is reserved for passengers. The seating configuration of this area is discussed in Section 9.8.

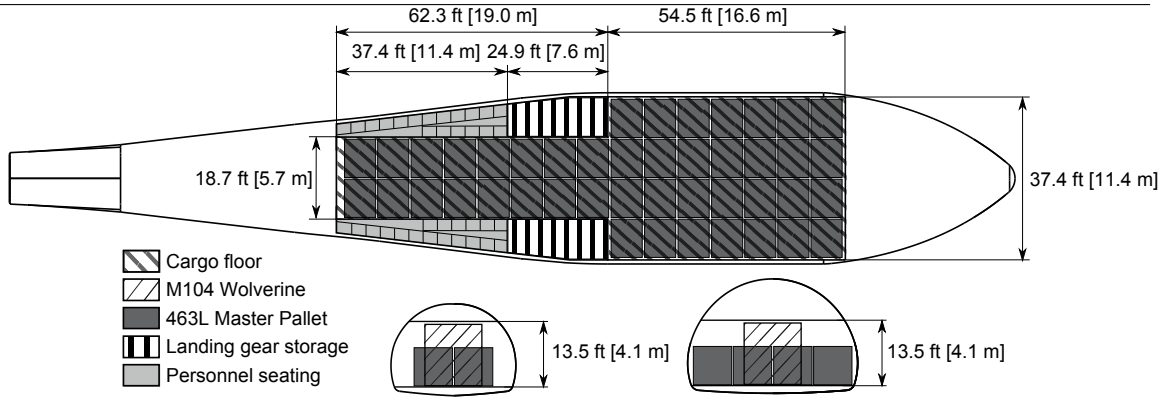

Figure 6.4: *Top view and cutouts of the cargo space.*

Table 6.2 shows how many units of what types of payload can be carried by the aircraft. The number is either constrained by maximum payload weight or by available cargo floor space.

Table 6.2: *Amount and type of payload units that fit in the UWB*

Payload	Number
463L Master Pallet	44
M1A Abrams battle tank	2
M104 Wolverine HAB	2
Fully equipped troops	72 to 442
AH-64 Apache	7[a]
M2 Bradley Infantry Vehicle	4
M3 Bradley Infantry Vehicle	4[b]

[a] Only 4 fully equipped AH-64 Apaches will fit in the fuselage. Carrying 7 units will require removal of the wings and the horizontal tail of the helicopter.

[b] Carrying 5 units of the M2 or M3 IFV will require the maximum payload weight to be increased slightly to 310,000 lbs. One might opt for exchanging some fuel for a little more payload, but it will then have to be taken into consideration for the design.

6.2.2 Cargo floor

The floor of the cargo bay consists of the standard military cargo floor compatible with the 463L Master Pallet system. Rails and rollers can be taken off and stored inside the floor for when (tracked) vehicles need to be transported.

6.2.3 Airdrop

The airdrop system is located in the rear of the aircraft. The rear door will be lowered until is it level with the cargo floor. 463L Master Pallets are certified to be airdropped. Fitted with parachutes, the pallets drawn out of the aircraft. Several methods exist for doing so, a common is to release an extraction parachute that pulls out the pallet by generating drag. Another way is to fly the aircraft at a certain pitch angle to let the payload roll out. Different types of airdrop are optimal for different types of cargo and circumstances. Note that when an airdrop has to be performed, a specially trained crew and special equipment should be taken on board. This reduces the payload weight that can be taken on the airdrop

mission.

6.3 Door Configuration

In this section the door configuration and design philosophy for the cargo doors will be explained. First the front cargo door will be explained and afterwards the design of the rear cargo door will be shown.

The front of the aircraft creates a challenging surface for a cargo door to be implemented, since the nose area of the aircraft has a double taper. The front cargo door has to create a gap large enough in order for a cargo ramp with a width of the floor to come through and high enough for a forklift to place pallets or to fit a M104 Wolverine. The solution to this problem is to use a clamshell door. The door is made up from two parts that swivel away from the mid-point and hinge around the intersection of the flight deck with the fuselage. Even though there is a curvature along the hinge line, if a single hinge is positioned at the bending point of the curvature there should be no complications with rotation. With this method the ground clearance needed to be able to rotate the entire half of the front cargo door is equal to 6 feet, the clearance provided by the landing gear is equal to 10 feet. The ramp is 15 feet long, when the aircraft is kneeled the angle to the ground will be 15 degrees. The ramp is stored by bending it midway into two sections of 7.5 feet and turning it upright into the fuselage.

The rear cargo door of The W.H.A.L.E. has a more general layout. The section is not tapered in two directions like the front of the aircraft. The middle of the cross section is a flat floor, which will be lowered and then function as the cargo ramp. The empennage is sized in such a manner that it can fit an 18 feet wide ramp with a length of 30 feet.

7. Propulsion System

The propulsion system of an aircraft has a big impact on the flight performance. First of all, it has to provide the required thrust in the whole flight envelope. Secondly, the efficiency of the engine has a large effect on the range, operational cost and weight of the aircraft.

7.1 Engine Type Selection

At first, an engine type has to be selected. The combination of high propulsive efficiency and the capability to fly at relatively high Mach numbers and altitudes convinced the team to choose a pulling counter-rotating propfan (CRPF). This type of engine is known to have noise issues. This, however, is not crucial for this type of aircraft because it will mainly not be operating at civil airports with close proximity to cities. Also the number of engines increases with this choice as will be explained in Section 7.2, but this drawback is more than counterbalanced by the reduction in fuel consumption.

The engine will have variable pitch blades to allow a high propulsive efficiency for different Mach numbers. This also reduces the additional drag of the engine in case of a engine out condition. It will be a 3-spool design with a gear that reduces the high rotational speeds from the power turbine. This way, the turbine can run at its high optimum speed and the rotors with their large diameters can rotate at lower rotational speeds in order to reduce the tip speeds. This way, the core engine can be built smaller which compensates for the additional weight of the gear. Figure 7.1 shows a pulling CRPF like it will be installed on the aircraft.

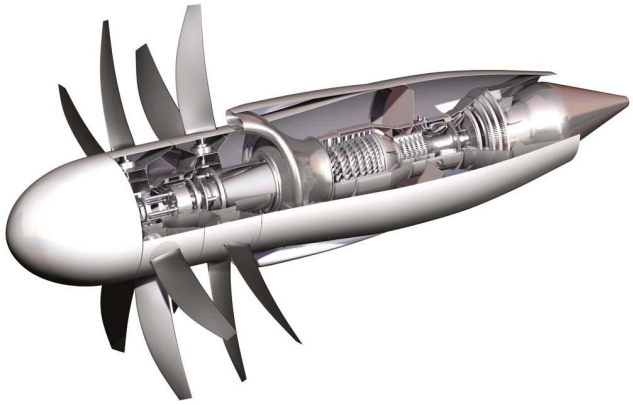

Figure 7.1: *Pulling counter-rotating open rotor engine concept RB3011 from Rolls Royce* [21]

7.2 Engine Sizing

CRPF's have not yet been build to the scale that is required to propel the aircraft that is presented in this report. It is therefore necessary to upscale the technology and to estimate the engine's characteristics in 2030.

Current studies on this technology do not consider very large CRPF's because the diameter of the engines gives integration issues. The RB3011 from Rolls Royce (see Figure 7.1) is intended for the use on an A320 sized aircraft. This implies a maximum take-off thrust around 33,000 lbf (148 kN) which current engines on this aircraft (e.g. V2533-A5 or CFM56-5B3) can produce as well. It was decided not to exceed this size too far because not being able to develop the engine introduces a high risk for the success of the entire aircraft, especially looking at the anticipated EIS 2030. For this reason, six engines will be mounted on the aircraft to keep them as small as possible.

For take-off, it was already determined in the design point calculation, that the engines need to produce 189,400 lbf (842.5 kN) of thrust in total which is 31,600 lbf (140.4 kN) per engine. The take-off thrust may, however, not be sizing for the flow path. Often, the top-of-climb (TOC) thrust determines the size of the engine because during this condition the highest corrected mass flows occur in the flow path. The thrust that is needed during this phase is approximated by equation 7.1 where k is a climb factor which is assumed to be 1.1 to allow for a positive climb rate at TOC such that the service ceiling of 40,000 ft can be reached. $ff = 0.97$ is the fuel fraction from take-off until TOC, $L/D = 17$ is at maximum climb condition and $n_{engines} = 6$ is the number of engines.

$$T_{TOC} = \frac{k \cdot D}{n_{engines}} = k \cdot \frac{L}{\frac{L}{D} \cdot n_{engines}} = k \cdot \frac{MTOW \cdot ff \cdot g}{\frac{L}{D} \cdot n_{engines}} = 1.1 \cdot \frac{988{,}000 \cdot 0.97 \cdot 32.174}{17 \cdot 6} = 10{,}300 \quad \text{lbf (46 kN)} \qquad (7.1)$$

From Henricks [27, 28] it can be concluded that the maximum thrust at TOC is approximately 18.5% of the sea-level static (SLS) thrust at ISA+27K for an open rotor engine at M=0.75 and 35,000 ft. This leads to a engine with a flow path which could theoretically produce 10,300 lbf/0.185=55,700 lbf (204.6 kN) at sea level static conditions. The engine is therefore flat-rated to a actual maximum thrust of 31,600 lbf (140.4) at SLS ISA+30K conditions that is required for take-off performance. This means that components like the gear and the shafts and the strength of the structures are still sized for take-off conditions where the highest thrust and the highest loads act on the machinery.

7.3 Engine Integration

The engines are mounted directly below the wings. As can be seen in Figure 7.1, there is some reasonable space behind the rotors and inside the nacelle. This space is used for the structural integration. This way, large amounts of the airflow from the propeller are blown over the wing, having positive effect on the lifting capabilities of the aircraft [29]. Three of

[21] URL: http://www.flugrevue.de/flugzeugbau/triebwerke/open-rotor-konzepte/527792?skip=1#1, [cited 19 Dec 2014]

the engines will be placed at different span fractions on each wing. The more inboard engines are shifted slightly forward. Together with the leading edge sweep this ensures that in a blade off event of one engine the rotors of the other engines are not directly damaged, hence increasing reliability. The installation below the wing allows easy access to the engine for maintenance purposes.

7.4 Engine Characteristics

Having defined the type and the thrust requirements on the engines, the detailed characteristics can be determined. In the following sections, fuel consumption, dimensions, weights and other performance characteristics will be discussed.

Dimensions The general dimensions of the engine have been scaled from reference engines. Assumptions that were used for this are summarized in the following list. Reference engines from Rolls Royce [30, 31] and NASA [27, 28] studies served as baseline. The dimensions were estimated by assuming that they scale with the square-root of the take off thrust. This assumption is based on the fact that the mass-flow of the engine scales squared with the diameter. With these assumptions, a rotor diameter of 18 ft (5 m), a maximum nacelle diameter of 8.4 ft (2.5 m) and a nacelle length of 27.2 ft (8.3 m) were obtained.

Weight The engine weight of this engine type is higher than for conventional turbofans due to the additional weight of the counter-rotating rotors and the additional gearbox [27]. As aircraft engines of the same type generally scale in weight with the static sea-level thrust, the same was done with the open rotor engine. Having a thrust to weight ratio for the reference engines of around 3, this results in a bare engine weight of 10,500 lbs (4750 kg) leading to an approximate installed engine weight of 15,500 lbs (7,000 kg).

SFC The thrust specific fuel consumption of the engine for cruise and take-off condition were estimated comparing numbers from NASA [27, 28] and Rolls Royce [31] concept studies as well as from Dallara [32]. The numbers for installed SFC were all found to be close to 0.44 lbs/hr/lbf for cruise at comparable conditions (approximately M0.75 and 35,000 ft) and 0.25 lbs/hr/lbf for take-off.

Table 7.1 summarizes the estimated engine characteristics.

Table 7.1: *Engine Characteristics*

Parameter	Value	Units
$T_{SLS,theoretical}$	46,000 (204.6)	[lbf] ([kN])
$T_{SLS,flatrated,ISA+30}$	31,600 (140.4)	[lbf] ([kN])
$T_{TOC,35{,}500ft,M0.75,ISA}$	10,300 (46)	[lbf] ([kN])
$W_{podded-engine}$	15,500 (7,000)	[lbs] ([kg])
SFC_{TO}	0.25 (6.88)	[lbs/h/lbf] ([g/s/kN])
SFC_{cruise}	0.44 (12.1)	[lbs/h/lbf] ([g/s/kN])
D_{fan}	18 (5)	[ft] ([m])
L_{engine}	27.2 (8.3)	[ft] ([m])
$D_{nacelle}$	8.4 (2.5)	[ft] ([m])

The engine thrust is dependent on both, altitude and Mach number. The thrust behavior, hence, had to be modeled to assess aircraft performance like climb rate at different flight phases. The altitude effect is described by Torenbeek [1] as a factor of σ^x. where sigma is the density ratio and x is an exponent that is typical for a certain type of engine. The Mach effect was afterwards modeled with a fit between the SLS thrust and the TOC thrust and implemented in Torenbeek's method. The resulting thrust as a function of Mach number and density ratio can be seen in Equation 7.2. This is a very rough method but it is assumed to be good enough at this stage of the design. Figure 7.2 shows the resulting thrust carpet.

$$T = T_{SLS} \cdot \sigma^{0.75} \cdot (1 - M)^{0.4} \tag{7.2}$$

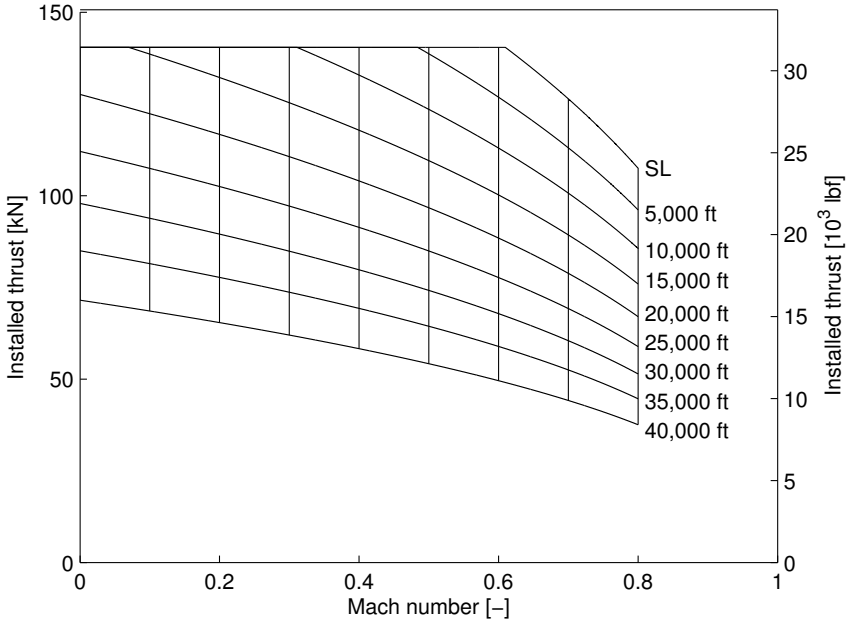

Figure 7.2: *Modeled engine thrust carpet*

8. Weights, Stability and Control

8.1 Class II Weight Estimation

After the concept selection a Class II weight estimation was done. The weights of various aircraft components were made using the Class I weight estimates and methods from Roskam [33] and Torenbeek [1]. The weights of the wing and fuselage were estimated by a linear regression using data from NASA [24]. The results of these calculations were then added to find a new OEW, which was again used to redo the calculation. This iterative process yielded the component weights as shown in Table 8.1.

Table 8.1: *Component weights*

Component	Weight [lbs] ([kg])
Wing	101600 (46100)
Fuselage	165000 (75000)
V-tail	26100 (11850)
Nose landing gear	5500 (2500)
Main landing gear	41700 (18900)
Fuel system	2400 (1100)
Propulsion system	6100 (2750)
Engines	92600 (42000)
Airframe Systems	35500 (16100)
Furnishing	3650 (1650)

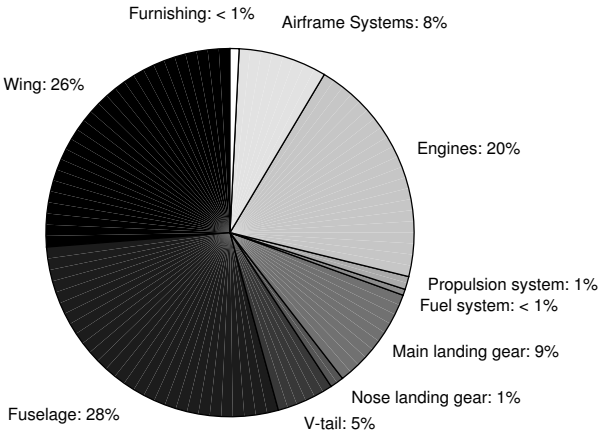

Figure 8.1: *Component weight fractions*

8.2 Empennage Design

The empennage for the aircraft consists of a fuselage mounted V-tail which is used for stability during the various flight stages. As compared to a T-tail or a conventional three-airfoil tail it consists of almost the same wetted area but less aerodynamic drag due to reduced interference between the fuselage and empennage.V-tails have an advantage in terms of effects of propwash on the horizontal tailplane which can be neglected. It also results in a smaller structural weight compared to a T-tail due to a smaller amount of parts and components. V-tails also provide advantages in terms of span loading due to a longer span of the empennage. However, pitch- and yaw controls are coupled and require a more complex

control system. Furthermore higher torsion loads act on the fuselage compared to a T-tail.

The V-tail was sized using methods for horizontal and vertical tail surfaces which were combined. The total surface area of the V-tail is equal to the sum of the surface areas for the horizontal and vertical tails. An adjustable horizontal tail was chosen to trim the aircraft.

8.2.1 Horizontal tail sizing

A horizontal tail is required to ensure longitudinal stability of the aircraft during any operating condition. The horizontal tail design was based on the stability with the stability margin of 4.1% and on controllability, which means pitching up until maximum lift coefficient at the most forward center of gravity position with full flaps deployed. The optimal horizontal tail area was determined using the center of gravity change and the stability and controllability requirements. The CG-range was determined with the use of loading diagrams. The OEW CG position, shift due to fuel burn and due to in-flight cargo dropping was taken into account. Overlapping of the plots for these two criteria was used to determine the optimal combination of horizontal tail surface and wing position that guarantees stability and control during any operational condition. These plots can be found in Figure 8.2a, 8.2b and 8.3.

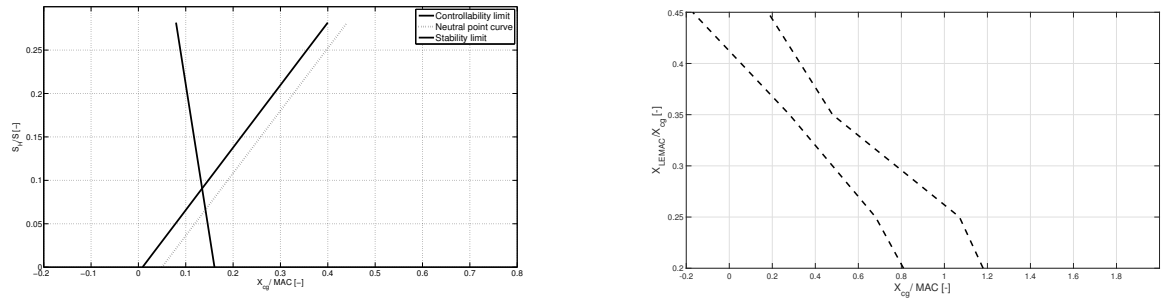

(a) *Allowed CG-range bound by stability and controllability curves.* **(b)** *CG-range determined from loading diagrams.*

Figure 8.2: *Scissor-plot and CG-range plots.*

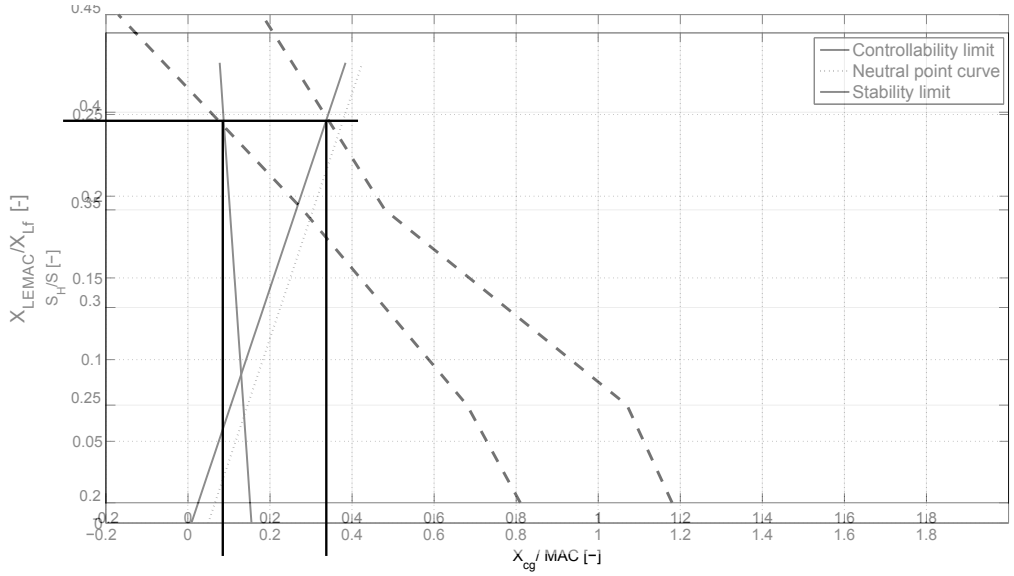

Figure 8.3: *Overlap of scissor plot and center of gravity plot*

The CG-range was determined to between 9% to 35% MAC from LEMAC. The wing position, x_{LEMAC}, was set at 39.5% fuselage length. Some important characteristics of horizontal tail can be found in Table 8.2.

Table 8.2: *Horizontal tail characteristics*

Parameter	Value	Units
Surface area ratio $\frac{S_H}{S}$	0.245	[-]
Surface area S_H	1873 (174)	[[ft^2] ([m^2]
Aspect ratio A_h	5.28	[-]
Horizontal tail volume coefficient H_v	1.1	[-]
Span b_h	99.4 (30.3)	[ft] ([m])
Sweep Λ_h	20	[deg]
Taper ratio λ_h	0.25	[-]

8.2.2 Vertical tail sizing

The vertical tail sizing was done using the method of Torenbeek [1]. Using this method the vertical tail was designed for three scenarios, namely control after engine failure, overall lateral stability of the aircraft and being able to control the aircraft during crosswind landings. The most critical of these scenarios determined the required surface area of the vertical tail. For the vertical tail a lift gradient of 2.7 rad^{-1} was assumed [34]. The effect of sidewash is neglected in the method because of two reasons; firstly calculating the sidewash is out of the scope of this project and secondly because the tail on this aircraft is a V-tail there is less interference between the empennage and the fuselage [35].The script was verified and validated with Boeing 747 and Galaxy C-5 data. The vertical tail characteristics can be found in table 8.3. The tail volume coefficient is comparable with aircraft of the same type [36].

Table 8.3: *Vertical characteristics*

Parameter	Value	Units
Surface area ratio $\frac{S_V}{S}$	0.16	[-]
Surface area S_V	1248.6 (116)	[[ft^2] ([m^2]
Aspect ratio A_v	2.2	[-]
Vertical tail volume coefficient V_v	0.07	[-]
Span b_v	52.4 (15.97)	[ft] ([m])
Sweep Λ_v	28	[deg]

8.2.3 V-tail

The V-tail is a combination of a horizontal and a vertical tail. The surface area of the V-tail is calculated with equation 8.1 and the dihedral angle of the V-tail is calculated with equation 8.2

$$S_{V-tail} = S_v + S_h \tag{8.1}$$

$$\Gamma_{V-tail} = tan^{-1}\frac{S_v}{S_h} \tag{8.2}$$

Due to losses caused by interference between the V-tail and the fuselage, a 10% increase in V-tail area was assumed. Important characteristics of the V-tail can be found in the Table 8.4.

Table 8.4: *V-tail characteristics*

Parameter	Value	Units
Surface area S_{V-tail}	3434 (319)	[[ft^2] ([m^2]
Dihedral angle Γ_{V-tail}	33.7	[deg]
Aspect ratio A_{V-tail}	5.32	[-]
Span b_{V-tail}	135.2 (41.2)	[ft] ([m])
Sweep Λ_{V-tail}	20	[deg]
Taper ratio λ_{V-tail}	0.25	[-]

8.3 Control Surfaces

This section covers the design of the control surfaces of the aircraft. The design of the control surfaces was done using the methods of Sadraey [37]. The control surfaces that were designed are ailerons, rudder and elevator. The ruddervator for the V-tail was the result of the combination of elevator and rudder for the horizontal and vertical tail, analogous to the design of the V-tail itself.

8.3.1 Aileron

The ailerons were designed such that the time to reach a required bank angle of 30° was lower than 2.5 seconds, when this requirement was reached the level 1 flying qualities described by Sadraey [37] were satisfied. The geometry of the ailerons can be seen in figure 5.4, and the characteristics of the aileron can be seen in table 8.5.

Table 8.5: *Aileron characteristics*

Parameter	Value	Units
Chord ratio $\frac{c_a}{c}$	0.3	[-]
Surface area ratio $\frac{S_a}{S_w}$	0.09	[-]
Span ratio $\frac{b_f}{b}$	0.23	[-]
Inboard span station η_i	0.7	[-]
Outboard span station η_o	0.93	[-]
Maximum deflection angle δ_a	20	[deg]

8.3.2 Elevator

The elevator was designed using the approach discussed by Sadraey in [37]. Since the main landing gear lies behind the center of gravity position, the take-off rotation and longitudinal trim requirements were employed to size the elevator. Important characteristics of the elevator can be found in Table 8.6.

Table 8.6: *Elevator characteristics*

Parameter	Value	Units
Chord ratio $\frac{C_E}{C_h}$	0.3	[-]
Surface area ratio $\frac{S_E}{S_H}$	0.3	[-]
Span ratio $\frac{b_e}{b_h}$	1	[-]
Maximum deflection angles δ_e	0 & -7	[deg]

The elevator deflections required to trim the aircraft longitudinally during cruise at sea level and at cruise altitude can be found in Figures 8.4b and 8.4a. These were generated using the most forward and aft CG-positions. Variation in the elevator deflections for different airspeed in order to maintain longitudinal trim is also known as the trim curve.

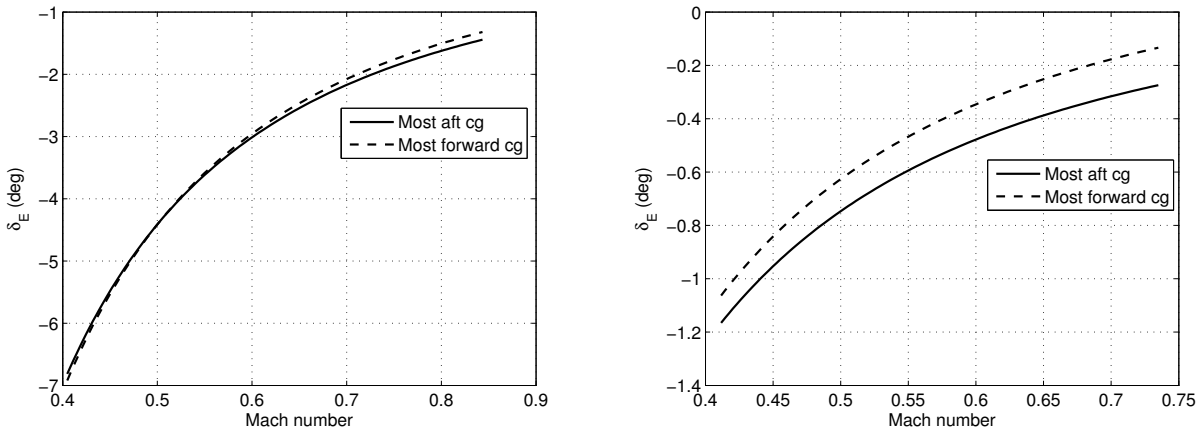

(a) *Elevator deflections at 35,000 feet.*

(b) *Elevator deflections at sea level.*

Figure 8.4: *Elevator deflections at cruise and sea level.*

8.3.3 Rudder

The rudder is designed to cope with the engine inoperative and the crosswind landing conditions. The most critical of these conditions turned out to be the engine inoperative condition. The maximum rudder angle was assumed to be 25

degrees and the rudder was designed to handle a maximum crosswind of 30 knots [37]. The characteristics of the rudder can be found in Table 8.7.

Table 8.7: *Rudder characteristics*

Parameter	Value	Units
Chord ratio $\frac{c_r}{c_v}$	0.3	[-]
Surface area ratio $\frac{S_r}{S_v}$	0.3	[-]
Span ratio $\frac{b_r}{b_v}$	1	[-]
Maximum deflection angles δ_r	+25 & -25	[deg]

8.3.4 Ruddervator

The ruddervator of the V-tail is a combination of an elevator and a rudder. In order to design it, a separate elevator and rudder design was made and the ruddervator is sized on the critical size and deflection of one of those two. In this case, maximum deflection angles from rudder are used as the maximum angles for ruddervator. Span ratio, chord ratio and surface area ratio for rudder are bigger than elevator so these are used in the design of the ruddervator. Some important characteristics of ruddervator can be found in Table 8.8

Table 8.8: *Ruddervator characteristics*

Parameter	Value	Units
Chord ratio $\frac{c_rv}{c_v-tail}$	0.3	[-]
Surface area ratio $\frac{S_{rv}}{S_v-tail}$	0.3	[-]
Span ratio $\frac{b_{rv}}{b_v-tail}$	1	[-]
Maximum deflection angles δ_{rv}	-25 & +25	[deg]

8.4 Eigenmotions

This section analyzes the eigenmotions of the aircraft. It is important to check the damping and time to half or double amplitude of these motions in order to asses the handling qualities. The aircraft should comply with level 1 handling qualities.

In order to analyze the eigenmotions of the aircraft, the stability- and control derivatives of the aircraft need to be determined. Volume 6 of the Roskam[17] series was used in combination with the Advanced Aircraft Analysis (AAA) software package, which uses the same equations. The calculated derivatives were compared in both sign and order of magnitude with data of the Boeing 747 [22] and other reference aircraft [38] in order to make sure they were correctly estimated. Table 8.9 shows the estimated stability- and control derivatives for the W.H.A.L.E.

[22]URL: `https://courses.cit.cornell.edu/mae5070/B747_Data.pdf` [cited 14 Jan 2015]

Table 8.9: *Estimation of stability- and control derivatives of the W.H.A.L.E.*

Derivative	Value	Derivative	Value	Derivative	Value
C_{Z_0}	-0.64	C_{Y_β}	-0.91	C_{m_u}	0.09
C_{Z_u}	-0.79	$C_{Y_{\dot{\beta}}}$	0	C_{m_α}	-2.74
C_{Z_α}	-6.80	C_{Y_p}	-0.07	$C_{m_{\dot{\alpha}}}$	-0.12
$C_{Z_{\dot{\alpha}}}$	-0.03	C_{Y_r}	0.67	C_{m_q}	-8.00
C_{Z_q}	0.31	$C_{Y_{\delta_a}}$	0	$C_{m_{\delta_e}}$	-1.28
$C_{Z_{\delta_e}}$	-0.32	$C_{Y_{\delta_r}}$	0.67		
C_{X_0}	0	C_{n_β}	0.31	C_{l_β}	-0.11
C_{X_u}	-0.065	$C_{n_{\dot{\beta}}}$	0	C_{l_p}	-0.14
C_{X_α}	-0.39	C_{n_p}	0	C_{l_r}	0.11
$C_{X_{\dot{\alpha}}}$	0	C_{n_r}	-0.35	$C_{l_{\delta_a}}$	-1.77
C_{X_q}	0	$C_{n_{\delta_a}}$	-0.01	$C_{l_{\delta_r}}$	0.034
$C_{X_{\delta_e}}$	-0.075	$C_{n_{\delta_r}}$	-0.15		

In order to estimate the mass moments of inertia the aircraft was modeled as several point-masses and summed using Equation 8.3 for I_{xx} and analogous equations for the other moments of inertia. Since the aircraft is symmetric over the x-axis, the cross products I_{xy} and I_{zy} are zero.

$$I_{xx} = \sum_{i=1}^{n} W(i) * ((y(i) - y_{cg})^2 + (z(i) - z_{cg})^2) \tag{8.3}$$

In Figures 8.5, 8.6a, 8.6b the graphs of the short period, phugoid and dutch roll are given respectively. The characteristics of these eigenmotions are given in table 8.10. In the table it can be seen that the damping ratio of the short period respects the level 1 handling qualities given by Sadraey [37]. However the damping ratio of the Phugoid and the Dutch Roll is not sufficient for level 1 handling qualities. That is why a yaw and pitch damper were designed to increase this damping.

Table 8.10: *Characteristics of the eigenmotions*

Maneuver	Period [s]	Half/Doubletime [s]	Dampingratio [-]
Short Period	3.64	1.00	0.37
Phugoid	57.20	166.40	0.038
Dutch roll	6.43	4.93	0.142
Aperiodic Roll	-	4.24	-
Spiral	-	119.78	-

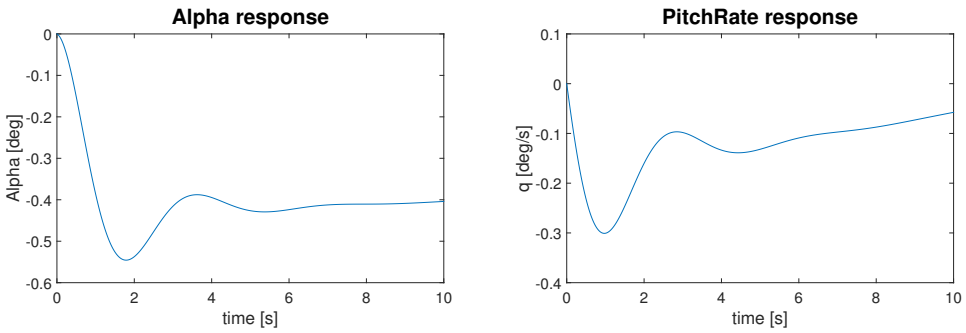

Figure 8.5: *Short period*

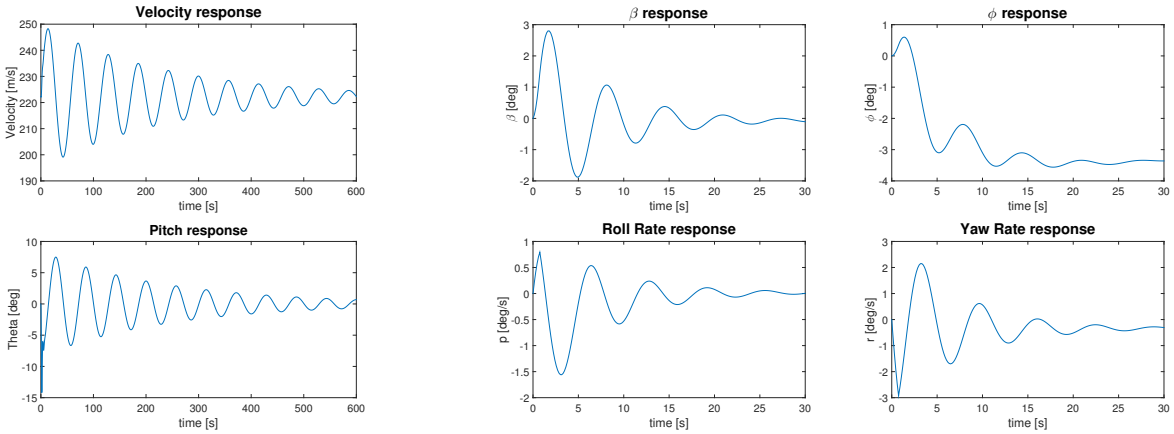

(a) *Phugoid 15° impulse in elevator*

(b) *Dutch Roll 10° impulse in elevator*

Figure 8.6: *Phugoid and Dutch Roll*

8.4.1 Yaw Damper

As it can be seen in Figure 8.6b, the dutch roll goes on for quite a long time, this means the damping ratio is to low.To overcome this problem a yaw damper was required to obtain sufficient damping. A schematic block diagram of the yaw damper can be found in Figure 8.7 .

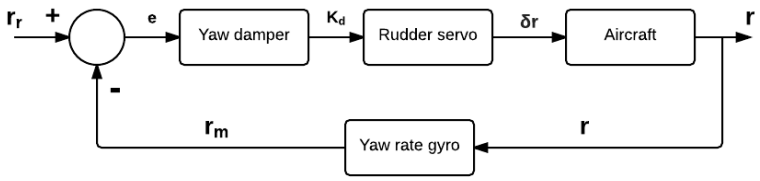

Figure 8.7: *Schematic block diagram for the yaw damper*

The yaw rate is measured with the help of a gyroscope which adds a certain input to the rudder input. As it can be seen in the figure, a rudder servo is added as well. As the actuator always lags behind the input signal, the rudder servo was required to overcome it. It is represented by the first order lag transfer function. The gain (K_d) of -0.71 was required to improve the damping ratio of the dutch roll from 0.142 to 0.3. A damping ratio of 0.3 is well within the level 1 flying qualities. A plot of dutch roll eigenmotions after implementation of the yaw damper can be seen in the Figure 8.8.

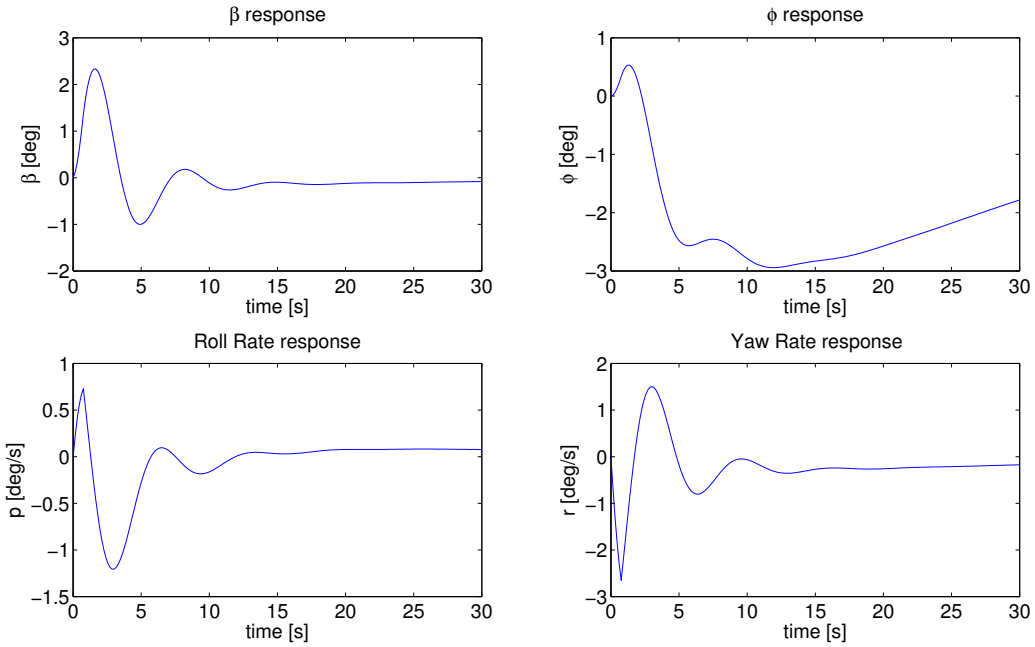

Figure 8.8: *Dutch roll after implementation of yaw damper*

8.4.2 Pitch damper

In Table 8.10, it can be seen that the damping ratio of the phugoid motion is less than the required level 1 flying qualities. A pitch damper was designed to improve the damping of phugoid which will result in decrease of oscillations in return. A schematic block diagram of pitch damper can be found in Figure 8.9

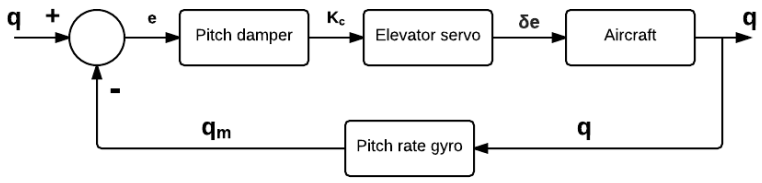

Figure 8.9: *Schematic block diagram for the pitch damper*

A gyroscope is used to measure the pitch rate in this case and a certain input is added to the pitch rate input. The elevator servo is added as well to make sure the actuator does not lag behind the input signal. It is represented by a first order lag function. A gain (K_c) of 0.014 was required to improve the damping ratio of the phugoid motion from 0.038 to 0.06. With this damping ratio, it is well within the level 1 flying qualities. A plot of the phugoid after implementation of the pitch damper can be found in Figure 8.10

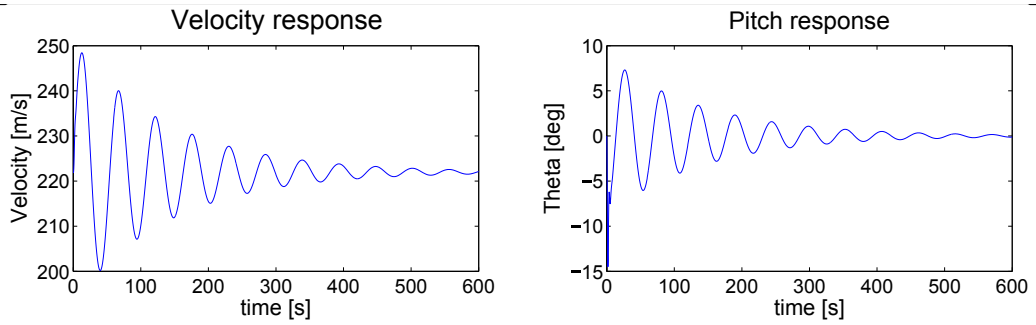

Figure 8.10: *Phugoid after implementation of pitch damper*

9. Subsystem Design

This chapter contains the design of subsystems for the W.H.A.L.E. This includes all major systems that are necessary to operate the aircraft like fuel, cargo, flight deck, hydraulics, electricity, furnishing and defense.

9.1 Communication and data handling

A communication flow diagram allows the designers of aircraft systems to see what kind of interaction their systems have with others. The communication flow diagram for the W.H.A.L.E. can be seen in Figure 9.1.

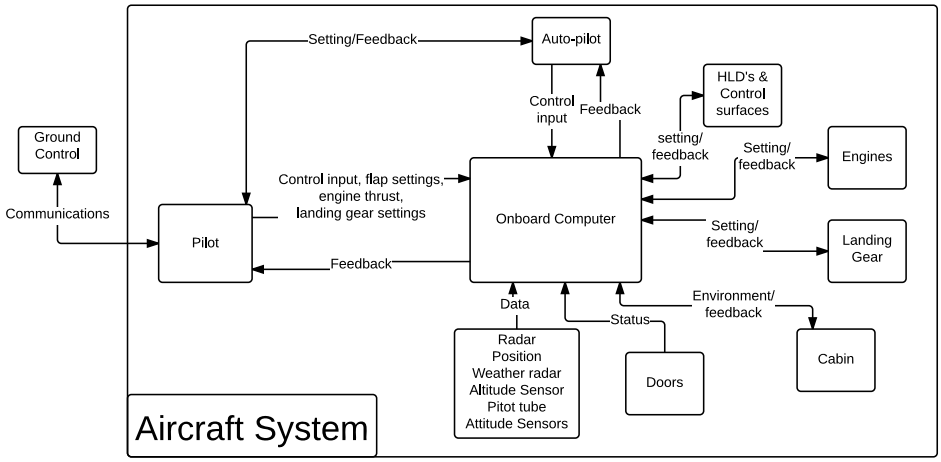

Figure 9.1: *Communication flow diagram*

9.2 Fuel System

9.2.1 Fuel Tanks

Figure 9.2 shows the layout of the fuel tanks and fuel system for the right wing. The left wing has the same layout. This fuel is divided over three wing fuel tanks and a fuel tank in the fuselage section of the wing. The wing fuel tanks use the

wing box as tank. The wing box is sealed so no separate bladder needs to be used. The fuel tanks start at 15% and end at 60% of the chord and runs from the root to 85% of the semispan. 15% is assumed useless due to cabling, pumps, ribs and stiffeners. Both wings together can hold a maximum of 374000lbs (170000kg) of fuel. The surge tank can hold 2500 kg per wing, so 5000 kg total.

While it is not required for fuel storage (all the required fuel fits inside the wing box), the empennage also contains fuel that is used to trim the aircraft. Mainly during take-off the center of gravity needs to be more to the back. Therefore a maximum of 45000lbs (20400kg) fuel can be transferred to the empennage tank. There are 9 fuel tanks in total. The ribs inside the wing tanks will contain holes (except at the fuel tank boundaries) to allow fuel to flow inside a tank. These ribs also limit sloshing since fuel cannot flow through the holes fast.

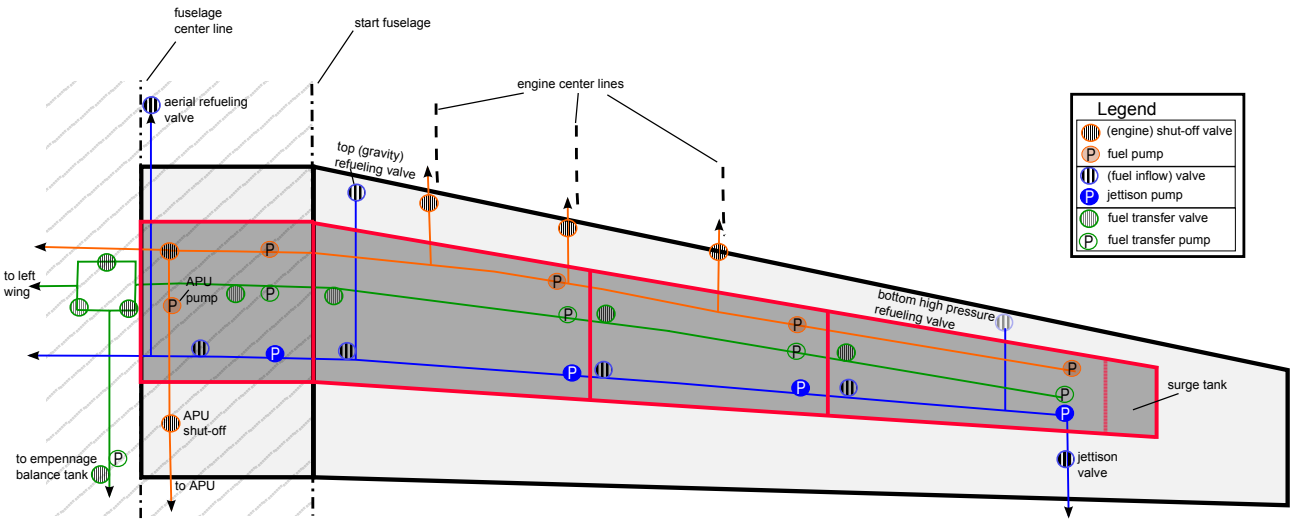

Figure 9.2: *Schematic overview of the fuel tank and fuel systems*

9.2.2 Fuel System Architecture

Figure 9.2 also shows the fuel control system. There are three separate systems: the system that delivers the fuel to the engines, the refueling system combined with the fuel jettison and the fuel transfer system.
The first system delivers the fuel from the tanks to the engines. Every engine has its own shut-off valve that can disconnect the engine from the fuel system. The APU has a separate pump. If the APU is used, the central valve will be closed and the APU pump is used to deliver fuel to the APU.

The refueling system shows three different refueling valves. The main valve is the bottom high pressure refueling valve. At airports with appropriate systems this will refuel the whole aircraft the fastest from one location. In case such system is not present, also the top refueling valve can be used. This one is located at the highest point of the wing near the fuselage. Since in this case mainly gravity distributes the fuel (the fuel truck pump might not be powerful enough for the other system), one might want to refuel at both sides of the aircraft at the same time if time is of the essence. The third refueling valve is located at the front of the aircraft and is used for aerial refueling. The valves attached to this system distribute the

incoming fuel over the different fuel tanks.

The pumps located in the tanks are used when fuel need to be dumped in case of an emergency landing while the current weight of the aircraft is above the maximum landing weight. In this case, the jettison valve will be opened and the pumps will dump enough fuel to make a safe landing.

The last system is the fuel transfer system. This system is used constantly throughout the flight to equalize the amount of fuel at both sides of the aircraft. Difference in engine performance can make fuel go faster at one side of the aircraft. This system allows the aircraft to be balanced with minimum use of the ailerons (and thus minimum drag).It is also the only system that connects the wing fuel tanks with the empennage balance tanks. This is done for maximum control over the amount of fuel in the balance tanks. If all fuel is required during flight, the fuel will be transferred to the main tanks when needed by the engines.

As can be seen, the valves are all closest to the fuselage while the pumps are closest to the wing tip in all three systems. This is because the wing has an anhedral so the wing tip is lower than the wing root. This way, the pumps are at the lowest point of the fuel tanks and the valves at the highest point.

9.3 Landing Gear

An important feature of the aircraft is the landing gear. To be able to land on normal airfields and even on compact desert grounds a tricycle configuration with 4 main gear struts was chosen. The nose gear has 4 tires and main gear 8 tires per strut to distribute the loads accordingly, as shown in Figure 9.3 The landing gear has been sized according to the Roskam[39] design methods. A safety factor of 1.5 was used in these calculations. The steel alloy AF1410 has been chosen as material for the landing gear. The maximum allowable stress was chosen to be 180 ksi (1241 MPa), such that the landing gear can handle at least 30,000 cycles[40].

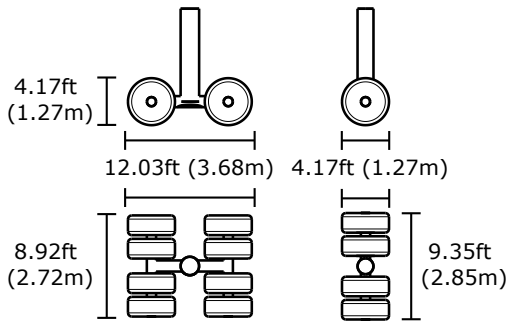

Figure 9.3: *Landing gear bogie dimensions*

9.3.1 Tire selection

The first step of sizing the landing gear is choosing the correct position. As stated in Section 4.1, the nose landing gear was positioned at 20% fuselage length from the nose and the main landing gear at 49% fuselage length from the nose. The tires are sized on the load carried per tire and the roll speed during landing and take-off. The number of tires is determined by the load which can be carried by the landing field pavement. In Table 9.1 the load per tire and the required tire dimensions are shown. The maximum rolling speed of the tires was found to be 143.4kts (73.76 m/s).

Table 9.1: *Tire data*

	Nose	Main
Load per tire	49240 lbs (22335 kg)	40160 lbs (18216 kg)
Tire width	1.75 ft (0.53 m)	
Tire outer diameter	4.17 ft (1.27 m)	
Tire load radius	1.68 ft (0.51 m)	
Rim outer diameter	1.67 ft (0.51 m)	
Tire weight	280 lbs (127 kg)	

The layout of the bogies is shown in Figure 9.3. The selected tire should allow the aircraft to land on hard packed sand, albeit at a reduced maximum landing or take-off weight of 700000 lbs (317500 kg).

9.3.2 Sizing the shock absorbers

The next step of designing the landing gear was determining the stroke and diameter of the shock absorbers. This was done by assuming all kinetic energy of the landing was to be absorbed by the main shock absorbers and the tires. For the nose shock absorber the energy to be absorbed was based on the maximum dynamic force on the nose landing gear. The sink speed of the aircraft was set to be 12 ft/s as stated by FAR25 regulations and the landing weight of the aircraft to be 90% of the MTOW. This high landing weight was based on the aircraft carrying maximum payload and with the maximum allowable dumping of fuel. The strokes and diameters of the nose and main gear found are given in Table 9.2

Table 9.2: *Shock absorber dimensions*

	Stroke ft (m)	diameter ft (m)
Nose shock absorber	0.542 (0.165)	1.426 (0.435)
Main shock absorber	1.071 (0.326)	1.454 (0.443)

The thickness of the shock absorbers was determined by the maximum pressure inside the absorber and the buckling and braking loads on the struts. The brakes are anti-skid carbon brakes which are capable of braking with an average of 0.5g and are located only in the main landing gear. The highest friction coefficient which can be obtained with these brakes is, according to Roskam [39], 0.7. With these values the brake forces and the bending moments caused by these forces on the landing gear can be obtained. For the pressure inside the shock absorber a zero deflection pressure of 210 psi was used. By assuming that P*V remained constant, the pressure at the maximum stroke could be determined. The stress caused by this pressure and the stresses due to bending and compression should be below the yield stress of the chosen material, in this case the AF1410 steel alloy. The thicknesses found are shown in Table 9.3. The selected material is also recyclable, fitting in the cradle to cradle design.

Table 9.3: *shock absorber dimensions*

	Thickness inch (cm)
Nose shock absorber	0.168 (1.44)
Main shock absorber	1.568 (3.98)

9.3.3 Minimum landing gear height

The next step was determining the required landing gear height. The height of the landing gear was sized on the required clearance angles. First the required rotation angle was determined. This angle was set to be equal to the angle during take-off. This was calculated to be 9 degrees. As a safety margin an extra inch of clearance was added and flat tires and compressed shock absorbers were assumed. This set the minimum landing gear length to be 7.2 ft (2.20 m). Next the minimum track width was determined. To be conservative, the angle between the most aft center of gravity of the aircraft when at MTOW and the line between the nose and main landing gear was set to be 57 degrees. This would be the worst case to still be able to satisfy the tip over requirement. The minimum track width was determined to be 30.61 ft (9.33 m), which fits inside the fuselage width of 39.37 ft (12 m). With this track width the roll clearance could be checked. The minimum angle between the landing gear and the bottom engines and the angle between the landing gear and the wing tip should be at least 5 degrees. With the calculated required landing gear height these angles were found to be 9.54 and 9.6 degrees respectively, thus the sizing requirement was the rotation angle at take-off. Last the turn over angle was determined. This angle should be larger than the rotation angle of the aircraft. With the landing gear height this angle was found to be 24.45 degrees. A summary of the clearance angles and landing gear height are shown in Table 9.4. In Figure 4.3 the lines and angles are shown.

Table 9.4: *Shock absorber dimensions*

	Value
Required landing gear height	7.2 ft (2.20 m)
Rotation angle	9 degrees
Lateral tip over angle	55 degrees
Engine clearance	9.54 degrees
Wing tip clearance	9.6 degrees
Turn over angle	24.45 degrees

In Figures 4.3 in Section 4.1 the clearance lines of the aircraft are shown.

An important feature of the landing gear is the so-called kneeling landing gear concept. This allows lowering of the aircraft while being loaded, making it easier to load cargo. To do so, the landing gear was designed to be one large shock absorber and by lowering the pressure the aircraft will be lowered. During the loading a computer monitors the height of the aircraft and increase the pressure as the load in the absorber increases to maintain the kneeled height by using a pump. This is done to avoid damage to the landing gear which would be too much compressed if the pressure inside was not increased with increasing aircraft weight.

The cylinder of the absorber was calculated to have a length of 55% of the combined required landing gear height and 50% of the bogie width for the part in the fuselage, minus the tire radius. The piston itself was assumed to be the same length as the cylinder plus one foot of piston which would be inside the cylinder at all times. For safety and internal

structures of the shock absorber, a minimum clearance inside the absorber of 0.4 ft was assumed. With these assumptions, the aircraft could be lowered from 7.2 ft during landing to 4.34 ft while being loaded/unloaded.

9.3.4 Bogie layout and storage

With the tire and shock absorber dimensions known, the bogie dimensions and storage dimensions can be calculated. Also the landing gear kinematics can be designed. Since the landing gear was designed to deal with the forces acting on it without side braces and drag struts, the only need for the side braces is to help retract the landing gear into the fuselage. Since the tires will expand during service life and due to centrifugal forces, a minimum clearance between the tires is required. This is set to be 10% of the diameter plus one inch in radial direction and 4% of the tire width plus one inch in width. The dimensions of the bogie are given in Table 9.5. The values are with the required clearances.

Table 9.5: *Bogie dimensions with clearance*

	length ft(m)	width ft(m)
Nose bogie	5.17 (1.58)	9.38 (2.86)
Main bogie	12.06 (3.68)	8.92 (2.72)

The landing gear will be stored inside the fuselage in the kneeled position, using a two way piston. The dimension of the total landing gear and its kinematics are shown in figure 9.4. It shows the side view of the nose landing gear (left) and the front view of the main landing gear (right).

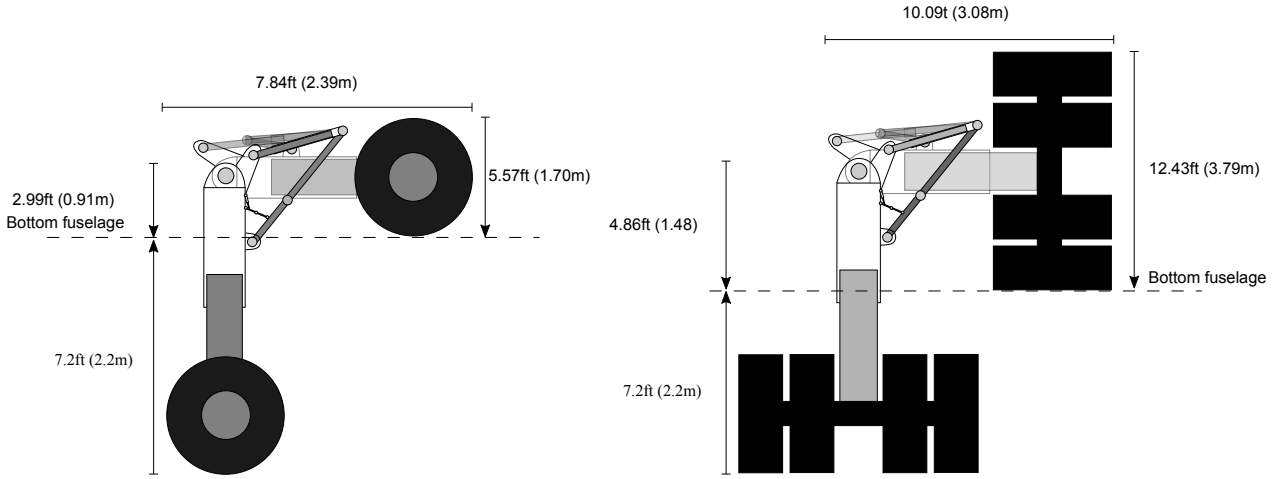

Figure 9.4: *Landing gear dimensions and kinematics of the nose (left) and main (right) gear*

Both landing gears will have a strut to retract the landing gear. This strut will have a lock mechanism to keep it in place during operation. Once the gear needs to be retracted, it will first shorten to kneeling length before storage. This was done to limit the space needed inside the fuselage. Also by fitting the landing gear inside the fuselage, no storage pods were needed. For the load to be equally distributed, the pistons will be connected through the pump system which will keep the pressure in the shock absorbers such that uneven loads are balanced out. This system is also applied in the main landing gear of the Boeing 747 [1] as shown in Figure 9.5.

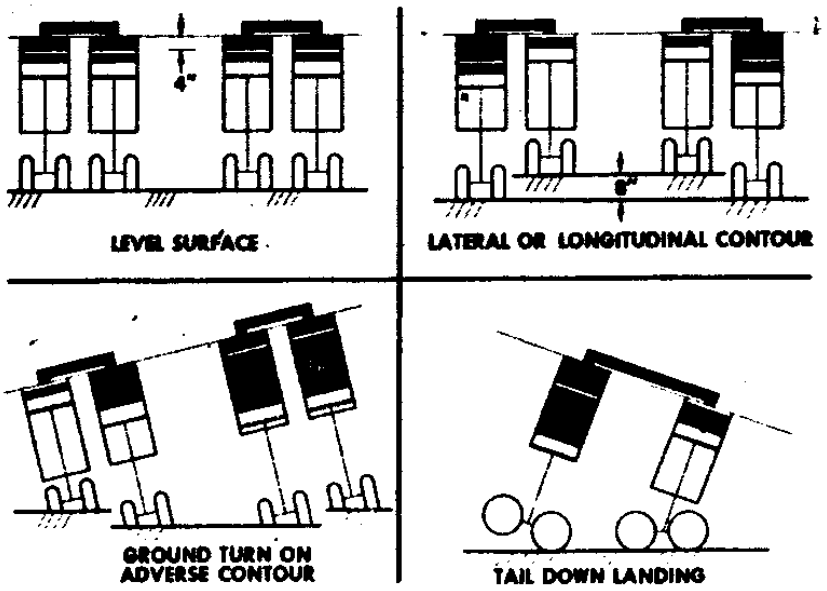

Figure 9.5: *Load distribution system of the 747 [1]*

9.4 Flight Deck

In designing the flight deck, close attention should be paid to requirements. Next to that, ergonomics of the human body should be taken into account. An important feature of the flight deck design is the pilot's Field of View (FOV). This FOV is defined from the reference eye point, see Figure 9.6. FAR 25 requirements for the FOV are shown in Figure 9.7. Here, the gray line represents the boundaries of the aircraft's windshield. A schematic sideview of the wind shield and pilot's seat, instruments and controls, including the forward FOV requirements is shown in Figure 9.6.

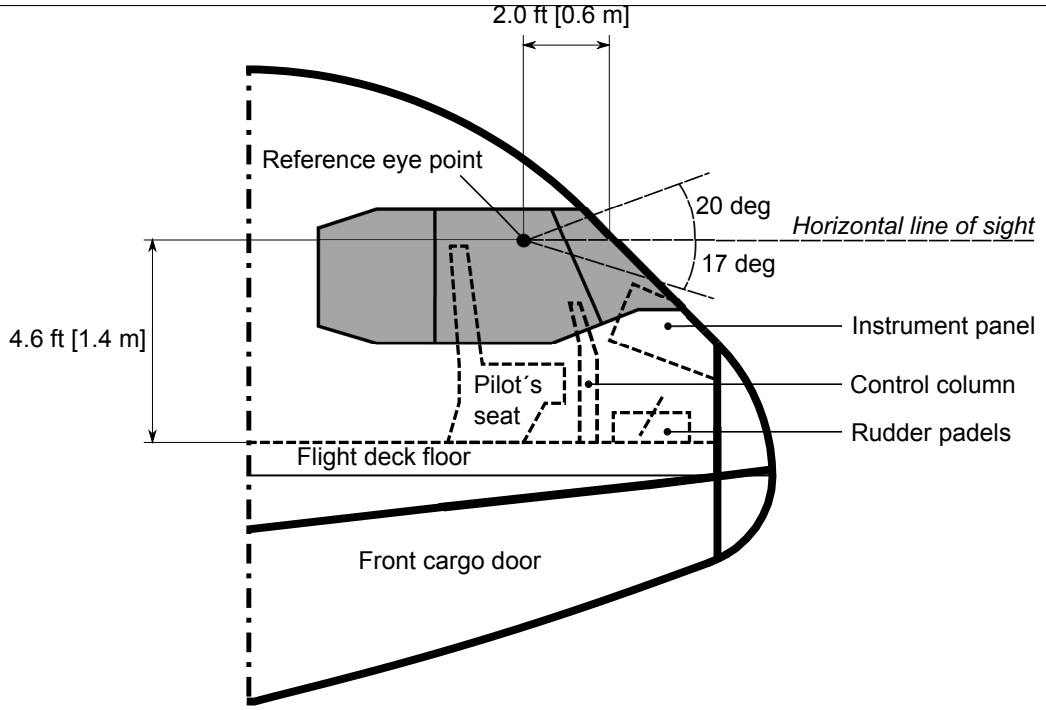

Figure 9.6: *Reference eye point and FOV shown in aircraft flight deck*

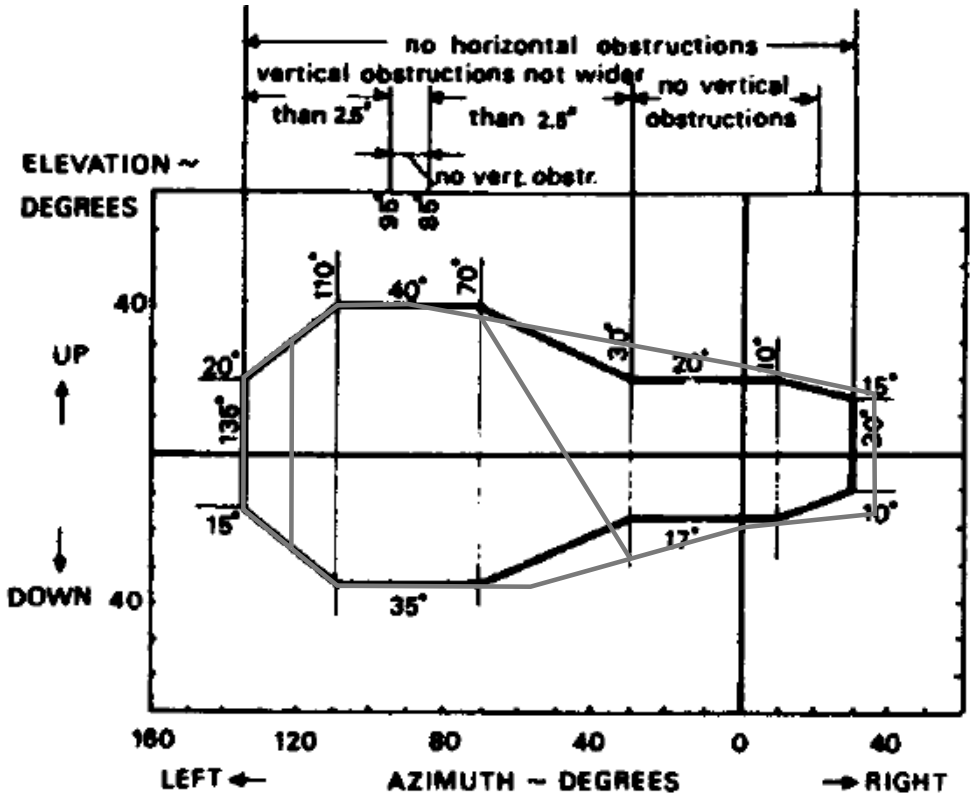

Figure 9.7: *Minimum required clear areas of vision and the aircraft's windshield boundaries shown in gray.*

Flight deck lay-out

Due to technological advancements over the past decades, flight deck lay-outs have changed significantly. Focus has shifted from analog to digital rendition of flight data, making the instrumentation more versatile. Also, the use of touch-

screens saves space in terms of user interface. Naturally, some analog instruments and interface should still be used for redundancy.

As an addition to electronic displays, a Heads-Up Display (HUD) is used to display flight information directly in the pilots field of view. This reduces pilot workload in IFR and VRF conditions [41] and enables pilots to read flight data while still keeping an eye on the flight path ahead.

Like the C-17, a centered control stick will be implemented in the flight deck of the aircraft. This is done because most US Air Force transport aircraft have a centered control column, meaning most USAF pilots are familiar with it. A control stick is favorable over a yoke, since it is less complex for fly-by-wire systems. The flight deck also features the loadmasters workspace, since close proximity will improve communication between crew. At last, tree jump seats are installed in the cockpit for the second crew.

In the upper deck of the plane some space is reserved for the crew to rest in case of long continuous flights. Also a lavatory, galley, some space for luggage and a stairwell have been included. Next to that there was still space to have 36 seats for personnel. A schematic layout of the upper deck is shown in Figure 9.8

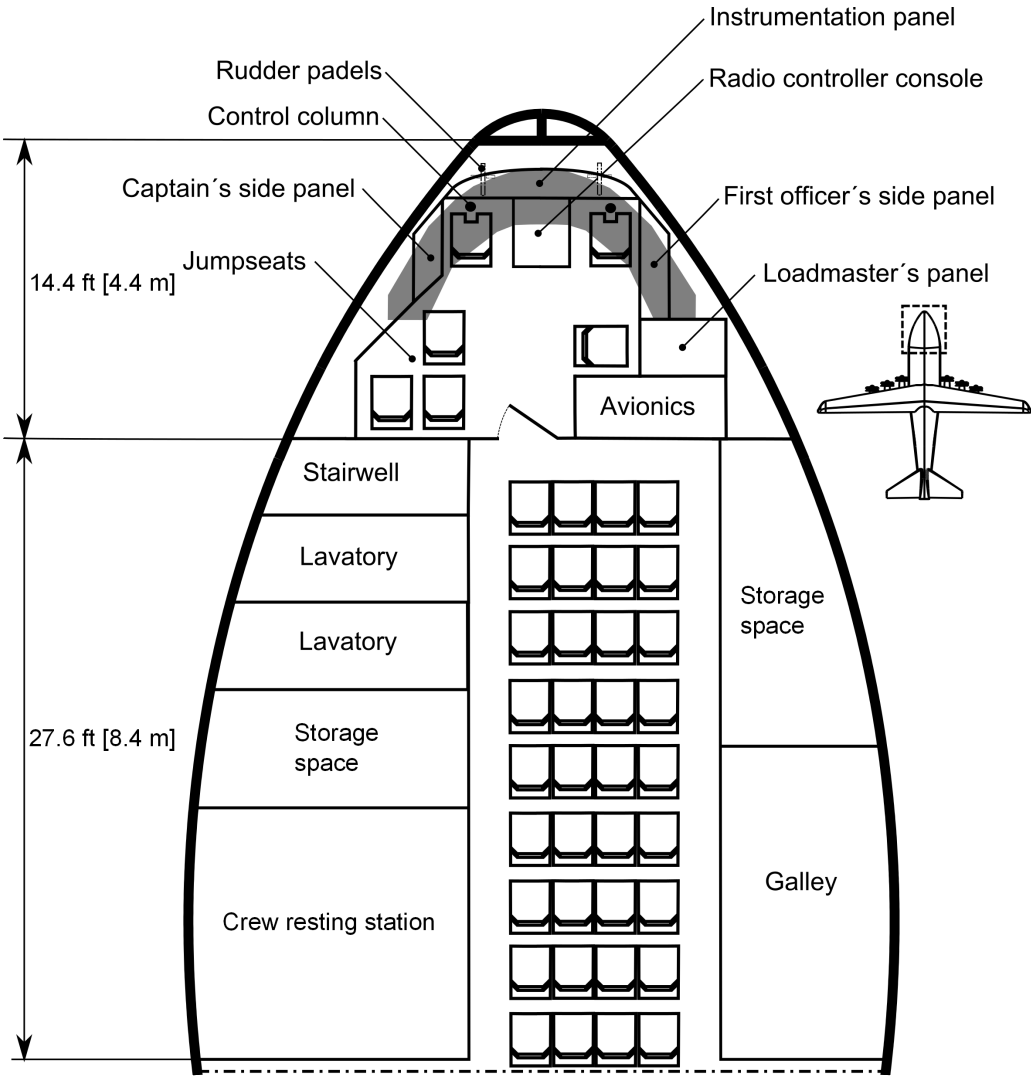

Figure 9.8: *Schematic layout of the aircraft upper deck*

9.5 Avionics

The aircraft's avionics system is located in a designated space on the flight deck, see also Figure 9.8 and under the flight deck floor for easy access. It will have the basic systems required on any transport aircraft accompanied with some specific military systems. All systems are listed and explained in Table 9.6.

Table 9.6: *Avionics systems and description*

System	**Function**
(Military) communications	Secure communication with other aircraft, ATC, US Air Force bases etc.
Navigation	Navigation using GPS.
Flight instruments	Measuring and display of flight data.
Collision-avoidance systems	Capable of locating other aircraft in nearby airspace to avoid collision.
Flight control systems	Autopilot and fly-by-wire system for (direct) control of the aircraft.
Weather radar	Measuring weather conditions in relevant airspace.
Flight data recorders	Records flight data and crew communication
Aircraft management systems	Tracks aircraft subsystem data to improve maintenance.
Military system	**Function**
Radar	For detecting and tracking hostile aircraft
Defensive Aid System (DAS)	Tracking incoming missiles and deploying flares.
Electro-optics	Heads-Up Display

9.6 Hydraulic System

This section will cover the hydraulic system of the aircraft. The system will be used to open and close the cargo doors, operate the control surfaces and control the pressure of the landing gear.

In figure 9.9 you can see the hydraulic system of the aircraft. Only half the system is shown, the other side has the same layout.

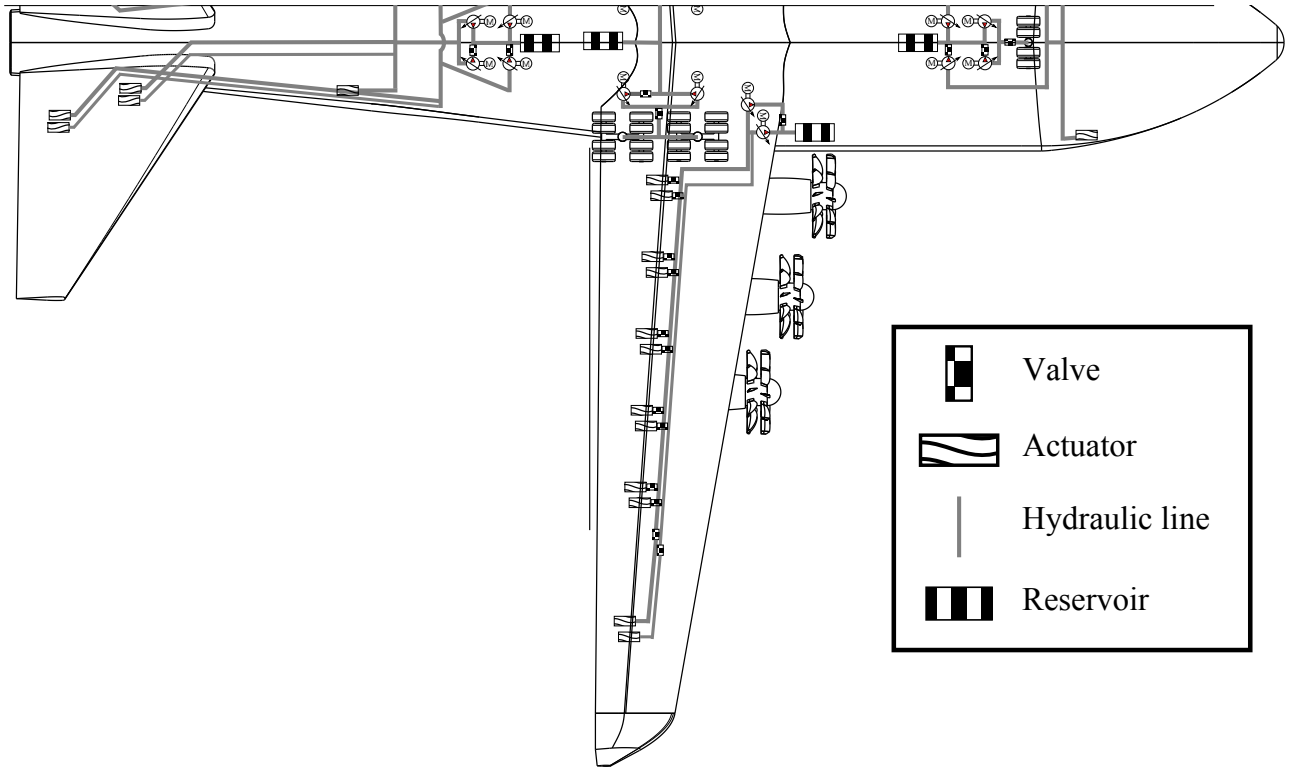

Figure 9.9: *Hydraulic system of the aircraft*

It consists of 5 reservoirs and each section consists of two pumps, of which one is a backup. Because there is no bleed system, the pumps are driven by electric engines and the backup pump can be used by opening a valve in the section. The main landing gear has its own section with reservoir, such that the kneeling of the aircraft and the weight distribution system do not cause too high loads on the sections when operated at the same time as the actuators of the flaps. The flaps and ailerons are operated from a separate section as can be seen in the figure. The nose landing gear is in the same section as the front cargo door, as the loads on it would not require it to have its own reservoir. The load distribution system of the landing gear can be set as a closed section by a valve. This is done to relieve high loads on the rest of the section. The rear cargo door is in the same section as the ruddervator of the V-tail and the actuator to move the tail itself. All actuators have a backup on a different line. This is to increase the reliability of the aircraft.

9.7 Electric System

Figure 9.10 shows the electrical block diagram of the aircraft. Power from the APU, battery, the engines and, in emergencies, the Ram Air Turbine. The power processor and Converter will manage the income of electricity and convert it to a standard (or multiple) voltages. Also, if needed, it will charge the battery.

The power distribution unit will distribute the available power to all the systems at their required voltages and also, if not enough power is available (for example in an emergency) limit or exclude the non essential systems from drawing power.

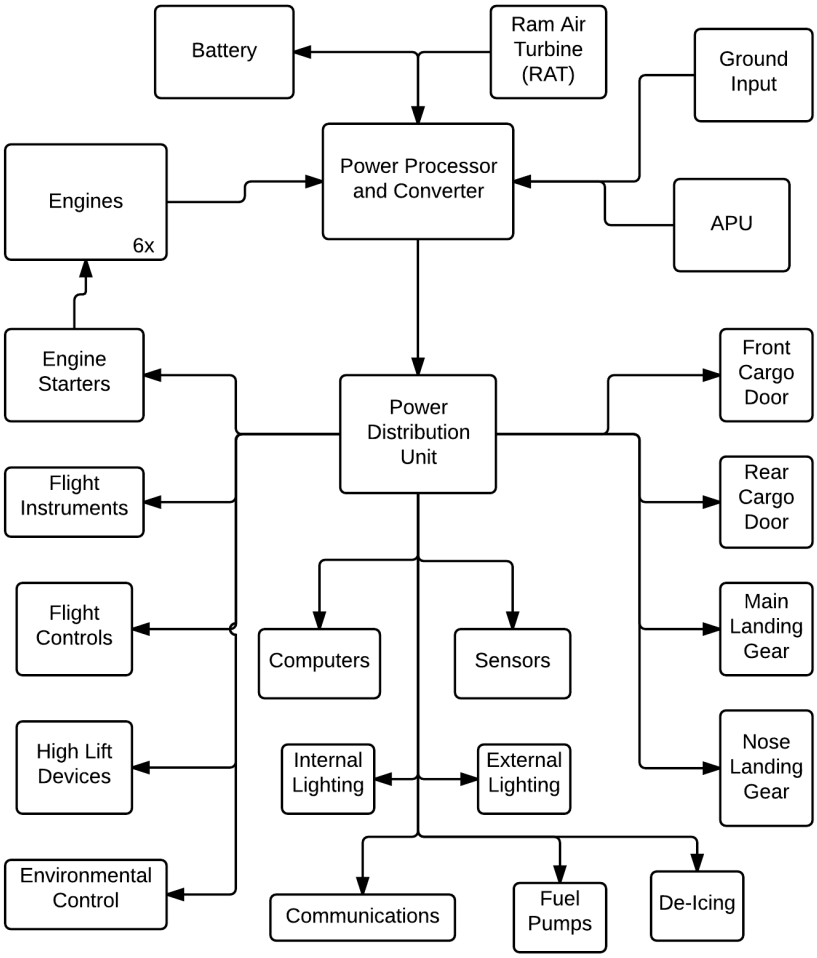

Figure 9.10: *Electrical Block Diagram*

9.8 Furnishing

In the aircraft space is made for a total of 72 passengers, divided between the upper deck, and the cargo bay. In Figure 6.4 the space for passengers available in the cargo bay can be seen. Along the fuselage hull, foldable seats are installed. More removable seats are put along the cargo floor. Both have a width of 39” [1.0 m], since no additional space is reserved for luggage. This arrangement gives room for 36 passengers in the cargo bay. The upper deck will house the other 36 seats, in rows of four with a seat pitch of 32” [0.8 m]. Along with these seats some luggage storage space is left to go with overhead storage bins.

As noted in Section 9.4 some space has been reserved for the crew to rest in case of long haul missions. Here, three beds are placed. Also a galley is embedded for storing and preparing food. Two lavatories are installed in the upper deck to service the total of 78 people (72 passengers and 6 crew) on board. Room is saved for a stairwell for upper deck access via a ladder. The general lay-out of the upper deck is shown in Figure 9.8.

9.9 Defense

Since this is a military transport aircraft, it will fly over active war zones. Next to the tactical approach, a missile warning system together with decoy flares are used as active defense mechanisms. Common, off the shelf, systems will be used as they have proven their effectiveness. Since such systems are continuously being developed and improved (to be able to defend against the latest threats), the exact system used will be determined at a later stage in the design. But since those systems have a lot of similarities (for example 360 degrees heat sensor coverage and space needed for decoy measures) this opposes no problem since space and power needed can be accounted for.

The sensor system will consist of multiple, spread out, heat sensors to provide a 360 degrees coverage around the aircraft. The missile warning system will monitor these sensors and alert the crew and/or take appropriate counter measures when a missile is detected. The flare deploy system will be integrated into the fuselage behind the landing gear.

9.10 Environmental Control System

The environmental control system (ECS) will be a completely electrical system. This means no bleed air from the engines is used to pressurize the fuselage. Normally, the de-icing system and hydraulic system use bleed air as well. These systems are electric or electric pump driven as well. The hydraulic system is already discussed in section 9.6.

On the fuselage, just in front of the wing, large inlets will allow ram air to enter the ECS. To allow more air to enter, a pump will provide under pressure when needed (for example when stationary and no ram air is available). The ECS will change the temperature and pressure to the current required values (which are depending on altitude, mission and cargo). This clean outside air is mixed with cleaned recycled air from the cabin. A mix of approximately 50 percent is used.

A same amount of air flowing into the cabin will also exit the cabin via outflow valves. These valves, together with the inlet pump, regulate the pressure inside the cabin. When needed, the pressure inside the fuselage can be dropped to match the outside pressure during flight. This allows the crew to gradually adapt to this pressure before opening the doors in flight for air drops. After closing, the pressure will be increased again, also gradually.

Next to the outflow valves, several over and under pressure valves are located at the bottom of the fuselage. Since the fuselage is only designed for over pressurization, under pressurization could damage the fuselage or the large cargo doors very quickly. These valves will open up if under pressure is detected. Over pressurization is also dangerous since this also might damage the fuselage or cargo doors. When the pressure difference becomes to large, the over pressure valves will open and let the air inside escape.

10. Performance Analysis

After the aircraft has been sized and the systems are designed, the performance characteristics of the vehicle can be assessed. Many of the requirements for this aircraft are related to performance metrics. Hence, this chapter will show whether the team succeeded in designing an aircraft that fulfills all requirements.

10.1 Take-Off and Landing Performance

Requirements 6,7 and 8 are related to runway performance. The runway performance was analyzed with the Bizjet method stated in Kundu [42]. Figure 10.1 shows the BFL for sea-level ISA+30K and hot and high (10,000ft, ISA+10K) conditions at different take-off weights and with N/2 engines off. Since the take-off requirement was sizing for the take-off thrust, the aircraft exactly needs 9000 ft of field length. The maximum increase in temperature for N/2 engines out for a 9000 ft field length therefore is 30 K and the the maximum increase in altitude to do the same was calculated to be 3,400 ft (1,036 m).

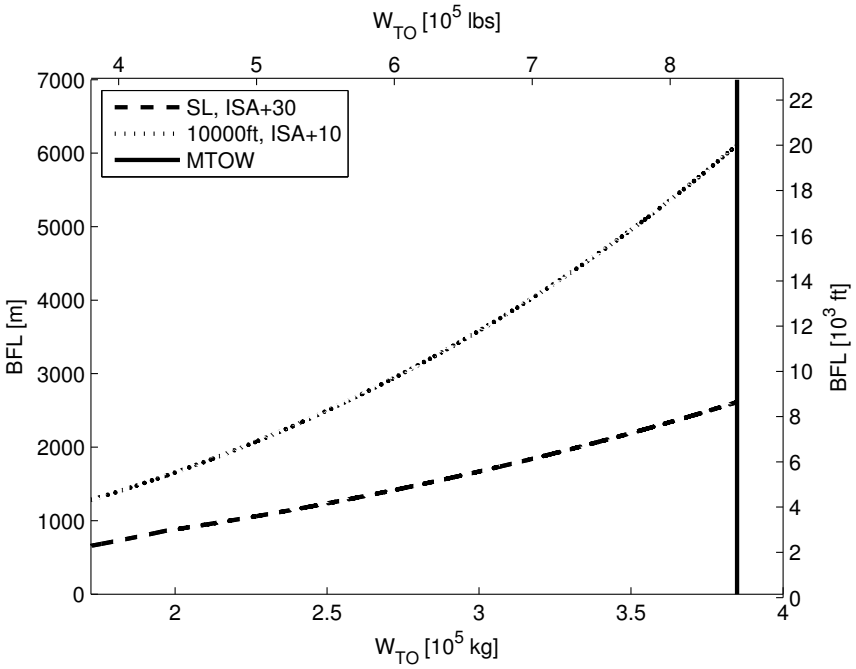

Figure 10.1: *Take-off performance at SL, ISA+30 and 10,000ft, ISA+10 conditions with N/2 engines off*

Figure 10.2 contains the landing field length versus landing weight according to the Bizjet method for both, sea-level

ISA+30K and 10,000ft, ISA+10 conditions.

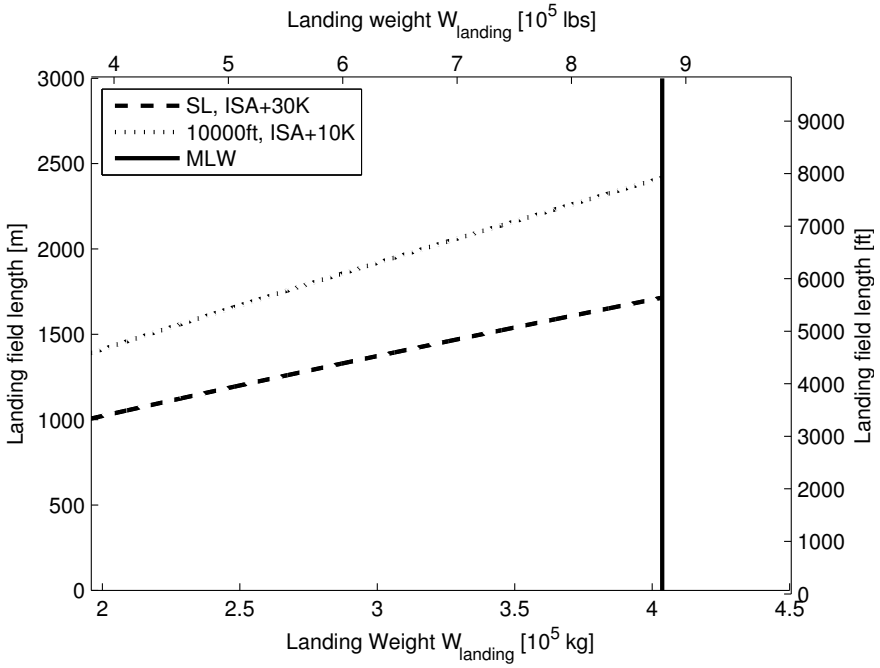

Figure 10.2: *Landing performance at SL, ISA+30 and 10,000ft, ISA+10 conditions*

Both, the landing and take-off requirements for SL, ISA+30K are met (required field length is less than 9000 ft) and the performance at hot and high conditions has been shown.

10.2 Climb and Descent Performance

As the runway performance the climb and descent performance has been analyzed with the Bizjet method [42]. Assumptions for this performance are the optimum climb condition of maximum $\frac{C_L^3}{C_D^2}$ (acc. to [43]) and a thrust setting of $T_{max,continuous} = 0.95 \cdot T_{max}$.

The climb performance has to meet requirement 5 which states that the time to climb to cruise altitude with a payload of 201,000 lbs shall not be higher than 20 minutes. As shown in Figure 10.3, this requirement is met with a climb time to cruise to 35,000ft of precisely 20 minutes with MTOW which reduces with decreasing aircraft weight. For the N/2 engines out condition, the analysis showed that the aircraft can still climb until 25,000 ft, hence being able to perform climb to pattern altitude and return to base (Requirement 8).

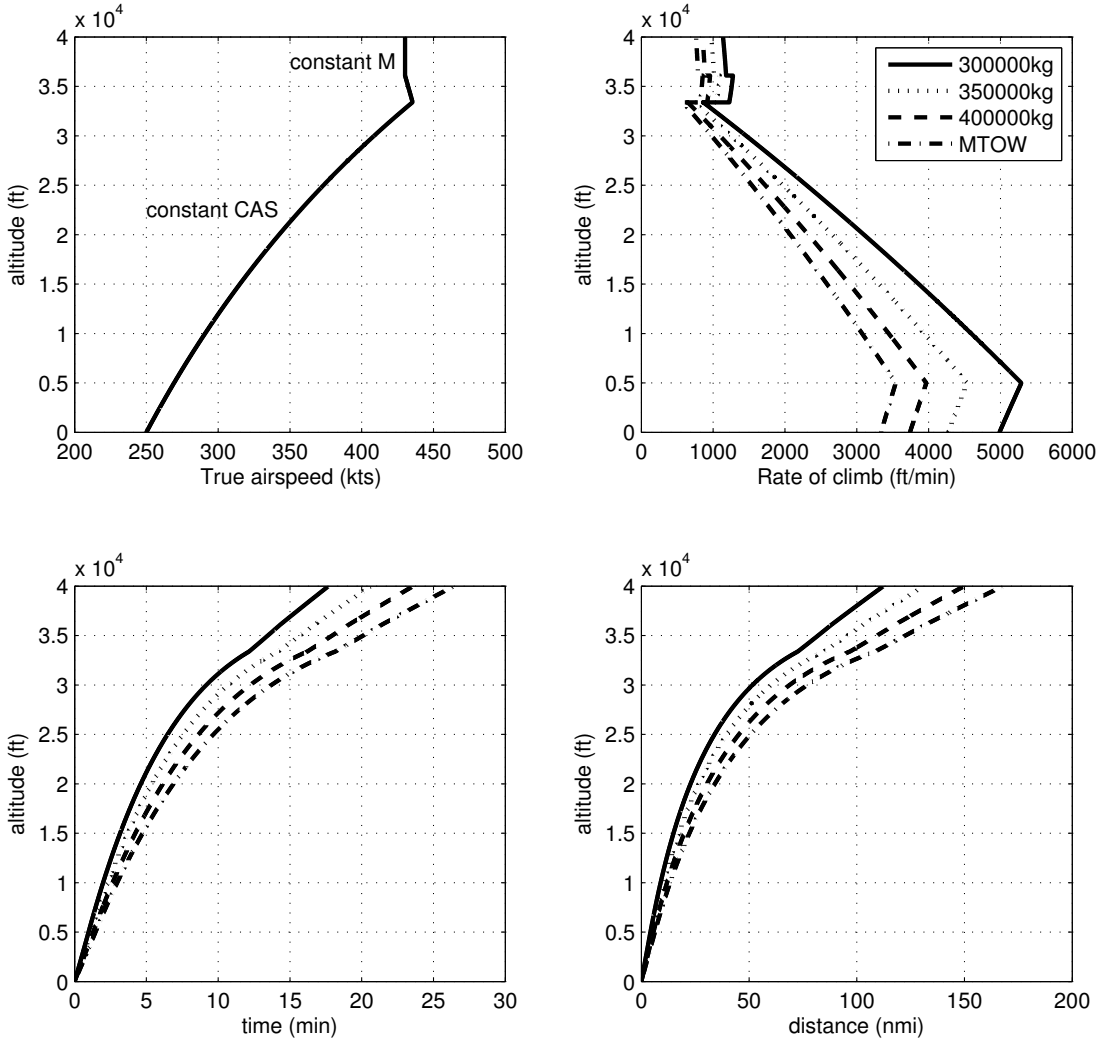

Figure 10.3: *Climb performance*

The descent performance of this aircraft is important because it shall be able to perform tactical approaches. Therefore, ground distance and time below 10,000 ft are to be minimized. In order to maximize the rate of descent, the drag needs to be maximized. This is done by using the spoilers to increase the drag created by the wing. From Mashud [44], it was found that the spoilers could increase the local drag coefficient by $\Delta C_d = 0.075$. It was assumed that this effects the overall drag by $\Delta C_D = \Delta C_d \cdot \frac{S_{wf}}{S}$ leading to a change of drag coefficient of 0.04. The L/D for descent becomes 3.5. The thrust is set to zero. The resulting performance can be found in Figure 10.4. The rate of descent is, however, also limited by the rate in pressure change for the human ear and the pressurization system on the aircraft. Having limits of rates of descent between 5,000 and 15,000 ft/min for comparable mission aircraft, it was assumed that a descent of 10,000 ft/min is a good first estimate. As a result, the aircraft can descent from cruise altitude with MLW in 5.5 minutes with a covered distance of 38 nautical miles.

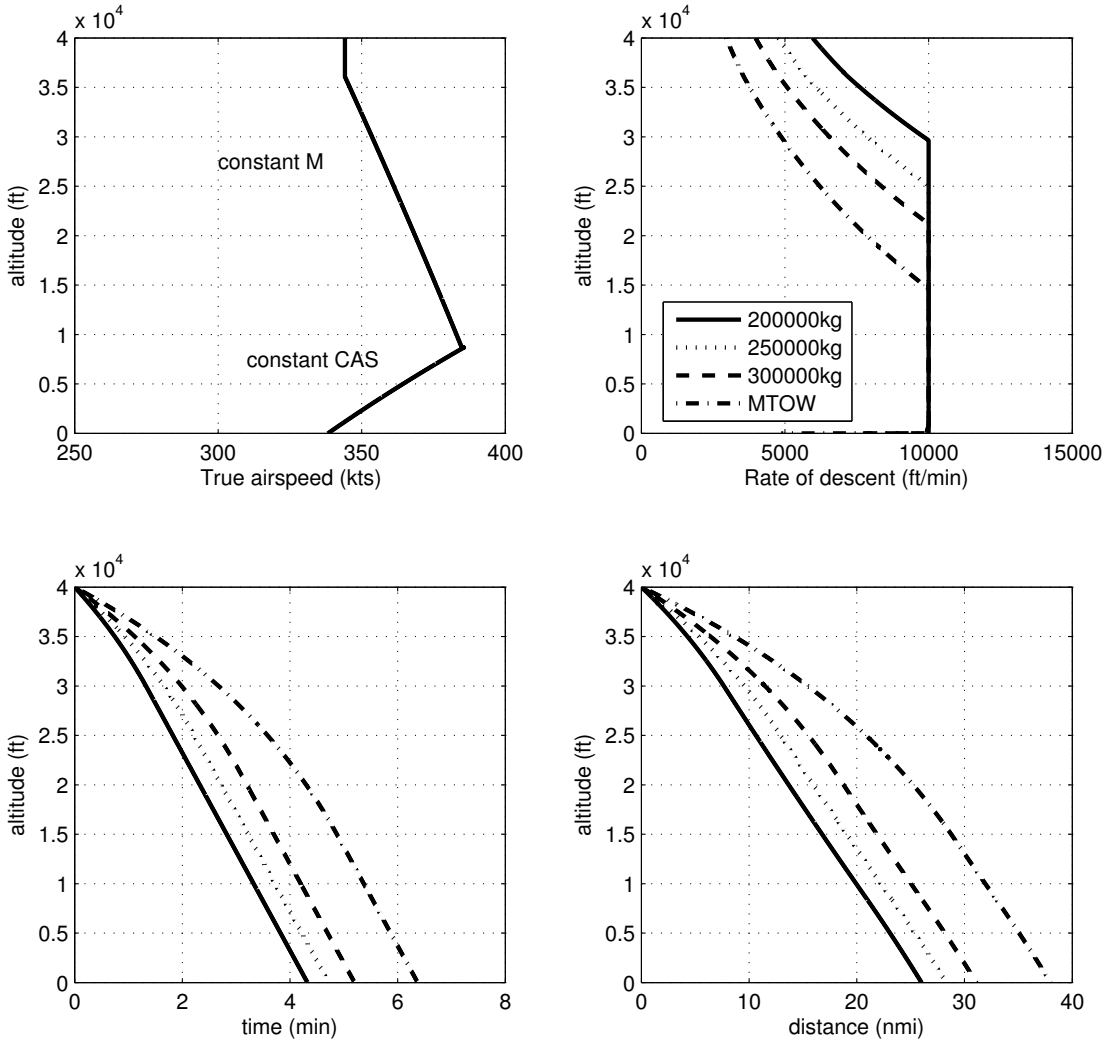

Figure 10.4: *Descent performance*

10.3 Maneuver Performance

For the maneuver performance, a distinction was made between the ground and air operations. On ground, the turning radius was determined while in flight, a V-n diagram shows the maneuver limitations. Figure 10.5 graphically shows that the radius of the landing gear during ground turn is 96.4 ft (30 m) while the tail rotational radius is 177 ft (54 m) and the wing turning radius in 210 ft (64 m).

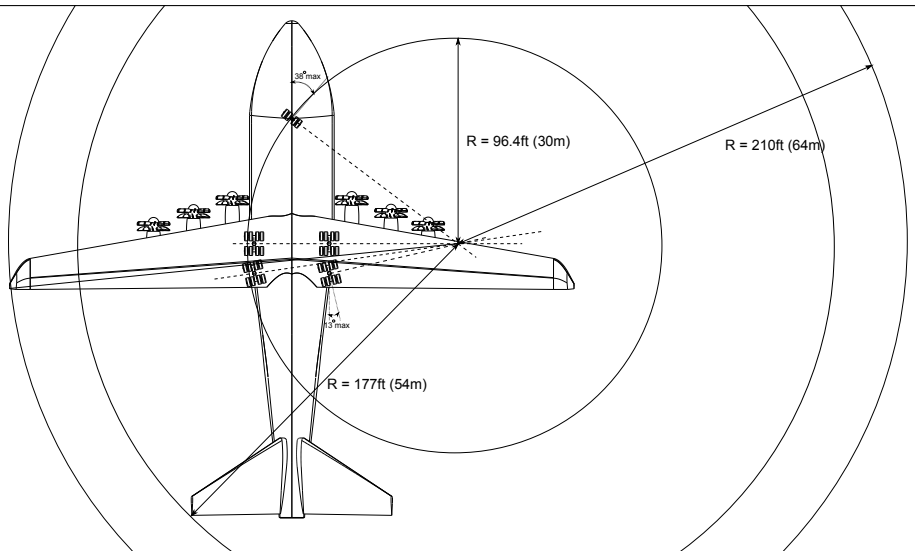

Figure 10.5: *Ground Turn Radius*

Figure 10.6 shows the v-n diagram for maneuver and gust loads. It was also used for the structural design of the aircraft.

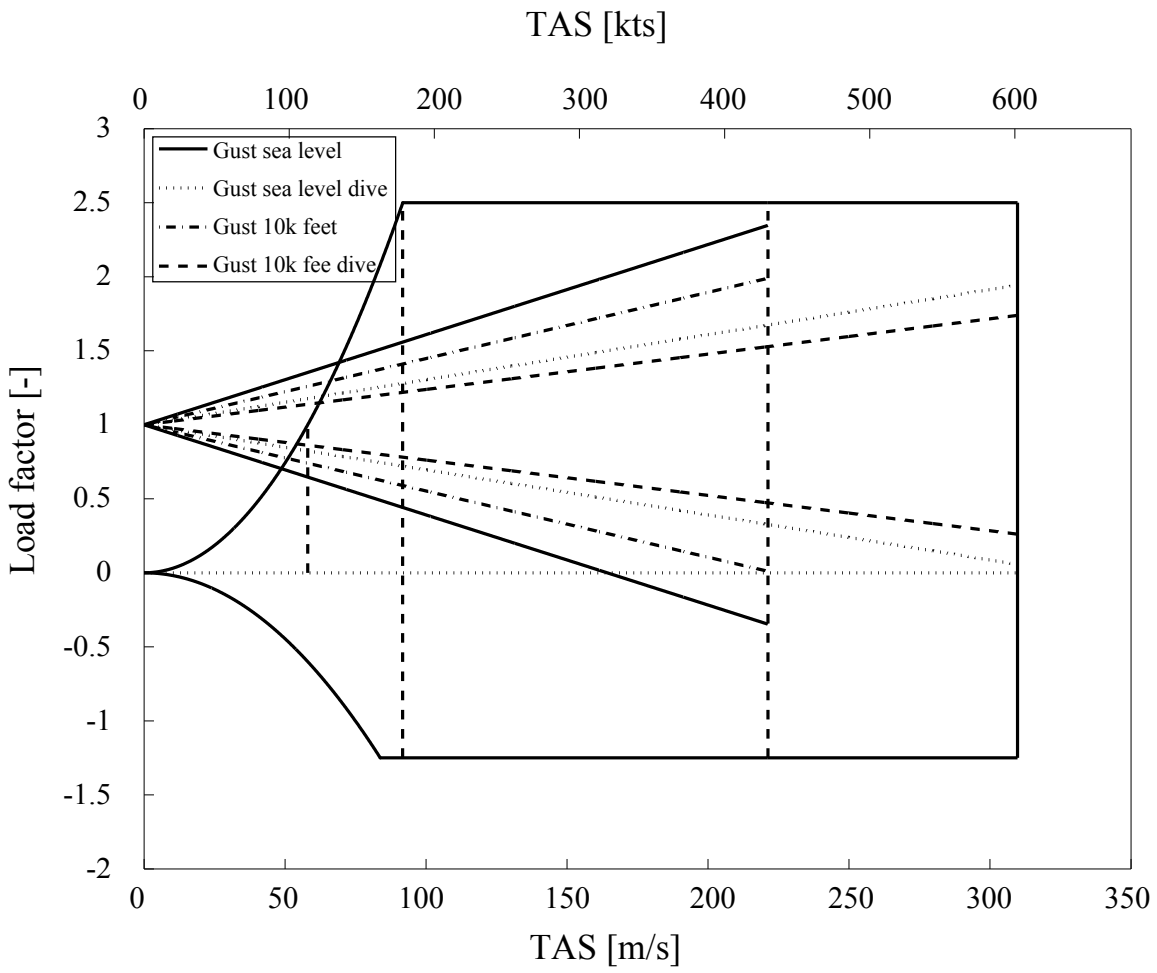

Figure 10.6: *v-n diagram*

10.4 Payload-Range Diagram

The payload-range diagram was constructed using the required maximum payload, the design load and design range. Additionally, the harmonic range was found to be maximum at 1867 nautical miles (3,457 km) where the tanks are filled up until the MTOW is reached. Figure 10.7 shows the payload-range diagram.

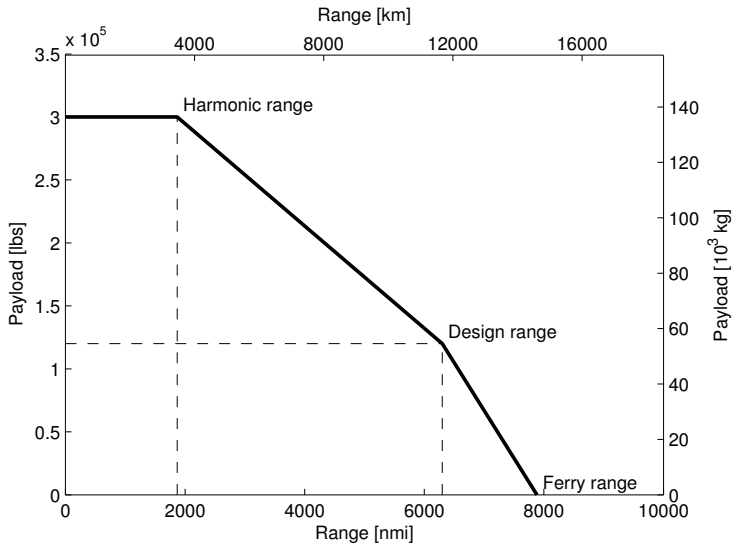

Figure 10.7: *Payload-range diagram*

Table 10.1 summarizes the important points of the payload-range diagram

Table 10.1: *Range*

Condition	Payload [lbs] ([kg])	Range [nmi] ([km])
Design range	120,000 (45,431)	6,300 (11,667)
Harmonic range	300,000 (136,078)	1,867 (3,457)
Ferry range	0	7,884 (14,601)

10.5 Flight Envelope

The flight envelope shows the speed and altitude combinations at which the aircraft can fly. It is bounded by maximum operating speed ($v_{MO} = 350$ kts) and Mach number ($M_{MO} = 0.8$), the service ceiling for which the fuselage is designed ($h_{MO} = 40,000$ ft) and the stall speed (acc. to Filippone [45]). Not taken into account at this stage are wing flutter and engine surge. These are to be determined at a later stage of the design. Figure 10.8 contains the flight envelope for the designed aircraft.

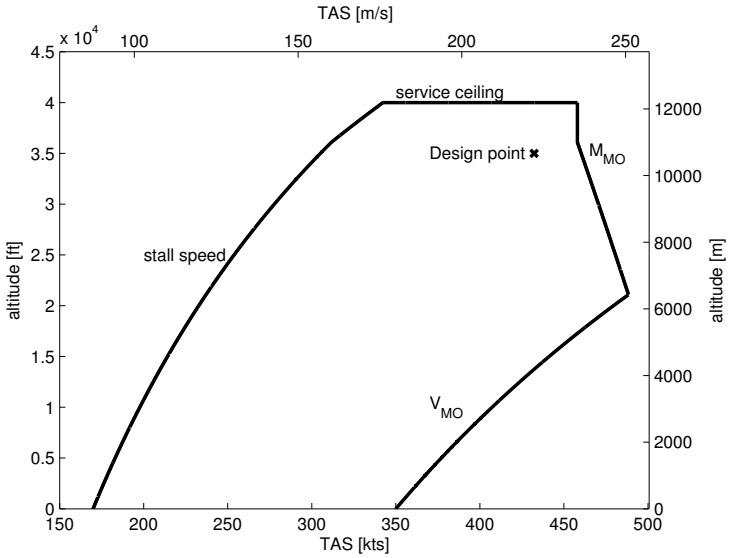

Figure 10.8: *Flight envelope*

11. Realization

11.1 Operations and Logistics

Because the W.H.A.L.E. carries as much as 300,000 lbs of payload weight it has a niche of its own within the military airlift. It carries more pallets than any other aircraft and it is able to lift outsized military hardware, such as the M104 Wolverine. In terms of logistics this aircraft is to be indispensable for the military.

11.1.1 Operations

The operation of such an aircraft is controlled by a central command center that controls all military airlifters and aerial refuelers. For the Whale the logistics flow diagram for typical transport missions is depicted in Figure 11.1.

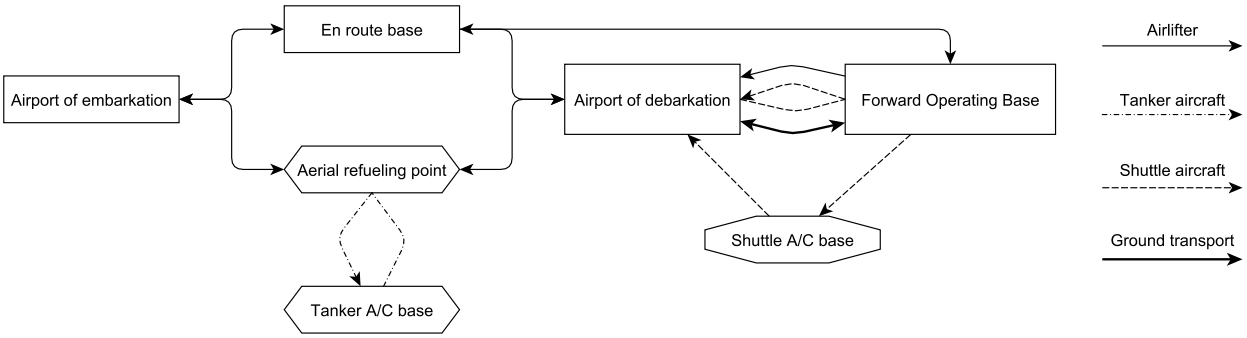

Figure 11.1: *Logistics flow diagram for typical missions for a large military airlifter*

When the aircraft is loaded it will fly towards its target airport, or airport of embarkation. The crew is allowed to operate the aircraft for at most 16 hours, after that they are assured 12 hours of rest. If the mission takes more than 16 hours another crew has to take over. This can be done by changing crew when the aircraft has landed on an en route base or changing mid air for the longer missions. The basic crew for the C-5 requires 2 pilots, 2 flight engineers and 2 loadmasters [23]. The Whale, being a modern aircraft, will not require any flight engineer due to a high level of automation of the on board computers. Additionally, taking only one loadmaster on board significantly reduces the operating cost of this aircraft. Usually the aircraft has to stop along the route on other airfields to load and unload (some of) the cargo and to refuel if

[23] URL: `http://www.globalsecurity.org/military/systems/aircraft/c-5-crew.htm` [cited 27 Nov 2014]

necessary, but it could also be that the aircraft has to make a direct flight to the final airfield where it unloads all cargo. During such a mission it might be required to refuel in air. The aircraft would rarely ever fly directly toward the Forward Operating Base (FOB). Instead all cargo is brought to a large airport that is not too far from the FOB and is well facilitated. The cargo that is dropped off will be further distributed by smaller aircraft or by ground. Aircraft such as the C-17 Globemaster are more appropriate for flying in an austere environment and to land on small airfields. Therefore this aircraft is well suited to fly as a shuttle between the airport on which the larger airlifter lands and the FOB.

After landing at the airport of debarkation the aircraft is refueled, a new crew is brought in, all systems are inspected and it is prepared for another flight. On the way back the aircraft can carry personnel, litter patients or parts that need repair. Preferably the cargo bay of the aircraft has to be as full as possible: either it is close to the maximum payload weight for the mission or there is no more available floor space. Stopping at en route bases might help to get the cargo bay as full as possible before the aircraft returns to home base. [46]

11.1.2 Maintenance

To make the aircraft as effective as possible, the down-time needs to be minimized. Key in achieving this is to maintain the aircraft as well as possible. Parts should be readily accessible, even when the aircraft is thousands of miles from its home base. Also professional repair crews need to be available that are trained to replace certain components. If a system of the aircraft fails en route, then it can be repaired at the next airfield where it lands. Based on an analysis by Ramey [47] on the operations of the C-5 Galaxy, a maintenance flow diagram was created, Figure 11.2.

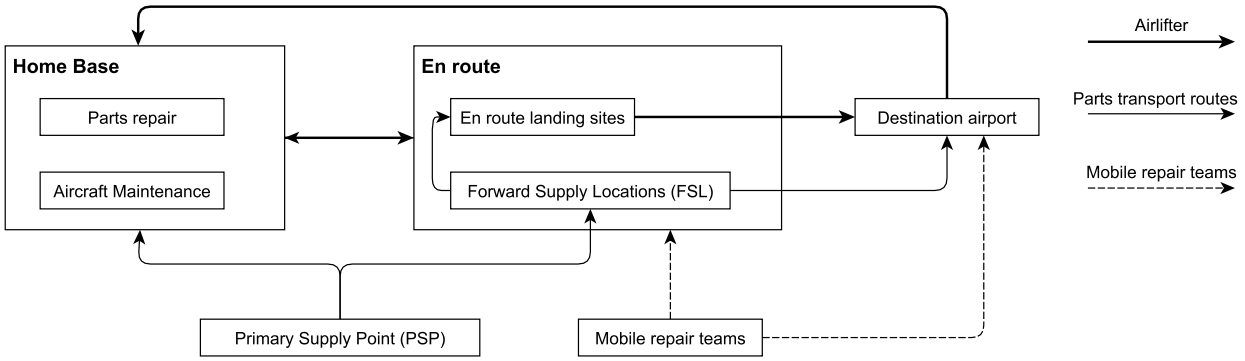

Figure 11.2: *Maintenance flow diagram for a large military airlifter*

Maintenance and thorough inspection of the aircraft takes place at the home base. Home bases are directly supplied by a Primary Supply Point (PSP) that delivers spare parts for the aircraft. The aircraft can however require maintenance when it is performing a mission on the other side of the world. About two-thirds of all the airports that the C-5 visited in 1992 were not a home base airport. In this case it takes too long to send a part from the PSP directly to the aircraft and it is impossible to fly the aircraft back home. Therefore a supply system is developed that makes use of Forward Supply

Locations (FSL). The FSLs are airports that are on tactical locations around the globe (for instance one on each continent) that is directly supplied by the PSP and has a small stock of spare parts for the aircraft. Each of these FSLs serves a number of airports in the vicinity. This could be one of the airports that is en route. In this way the part can be delivered to the aircraft in a relative short amount of time. Mobile repair teams can then be deployed to quickly replace the part or repair the damage on location. After completion of the mission the aircraft can fly back to home base for inspection or further repairs. [47]

11.1.3 Turnaround Time

An important selling point of this aircraft is the turnaround time. The turnaround time is the time the aircraft spends between landing and take-off and is used for unloading and loading.

The loading time is estimated using C-5 data[24], the C-5 takes about 90 minutes to load 36 463L master pallets. It is assumed that this is done by accessing the aircraft by two crews from two locations (nose and tail). So that gives a load time of 5 minutes per pallet. The W.H.A.L.E has place for 44 pallets, the layout of them can be seen in figure 4.1. The loading and unloading of the aircraft can be done by having three crews working simultaneously because the front section of the W.H.A.L.E. is four rows wide. Using the same time it takes to load a pallet as for the C-5 the total loading time is approximately 75 minutes, which is a reduction of 20%.

11.2 Production Plan

This section will handle the production plan of the aircraft, it will check if the designed aircraft is feasible to produce. The production plan will handle the procedure to produce the main parts of the aircraft and the assembly of the entire aircraft.

11.2.1 Fuselage

The fuselage will be made from aluminum 7075-T6 because of its high yield and low density properties, as well as good machining and forming properties. The fuselage will be split up in three main parts for assembly namely the front, middle and aft section.

The front section will be made in two parts, a bottom section including the floor panels and support and a top section including skin, stringers and stiffeners. This section is made from a skin with semicircular frames attached to it. The top and bottom half will be connected at the semicircular frames.

The middle section is divided into four parts. One part is the belly of the aircraft which consists of the floor and the bottom skin with the frames attached. The upper part is divided into three pieces; one in front of the wing intersection, one behind the wing intersection and one piece is the wing intersection itself. The two pieces in front of- and behind the wing intersection consist of the top skin with frames attached. The wing intersection part also consists of a skin with frames, but the frames are interrupted by the intersection with the wing box.

[24] URL: `http://www.fas.org/man/dod-101/sys/ac/c-5.htm` [Cited 23 Jan 2015]

The aft section consists of the upper half, which is made of tapered semicircular frames with a skin. The lower part is the frame of the cargo door which is made of frames and a skin. The cargo door itself is produced separately.

11.2.2 Wings and Strut

The wings will be made separately and are joined later by attaching them to the center wing box section. The wing production starts with the skin, which are shaved to the correct size and thickness. Then the skin sections are placed in a mold and baked in an autoclave to form them to the correct shape. The main spars, stringers and ribs separately manufactured. The stringers are attached to the skin sections and the spars and ribs are connected to form the skeleton. The skins, fuel lines and cables are then placed and finally the flaps, ailerons and spoilers will be installed. After that the wings are joined to the center wing box in the fuselage and to the strut.
The struts will be produced separately out of carbon fiber by means of extrusion and filament winding. It will be attached to the fuselage after the wing has been attached.

11.2.3 V-Tail

The production of the tail is essentially the same as of the main wing. Instead of ailerons the ruddervator is attached and no spoilers are present.

11.2.4 Landing Gear

The landing gear will be bought from an external supplier. The different landing gear components will be produced by various techniques, including casting, lathing and milling. Then all components will be assembled. The company will supply the landing gear as a finished product, ready to be installed on the aircraft.

11.2.5 Engines

The engines will be designed and manufactured by an external company. They will supply the engine as a finished product, ready to be installed on the aircraft.

11.2.6 Assembly

The assembly starts with joining the center wing box to the center fuselage section and then connecting the two wings to the center wing box. Then the struts are attached to the center fuselage section and the wings. Simultaneously the V-tail is attached to the aft fuselage section. Then the fuselage sections are joined. The landing gear will be attached and the engines will be installed using a front support with 3 bolts and an aft support with 4 bolts. In parallel, the cables, insulation, fuel lines and other systems inside the fuselage can be installed. Finally the interior is placed and the paint is applied.

11.3 Cost Analysis

This section presents the cost analysis of the W.H.A.L.E. The cost analysis was done using the AAA software which uses the Roskam book part VIII [48]. The cost is split up between research, development, test and evaluation cost, acquisition cost, operation cost and disposal cost. These cost categories together make the Life Cycle Cost (LCC) of the entire program. For the entire program a 10 % profit was assumed and the labor rates were extrapolated from 1989 data [48].

11.3.1 Research, Development, Test and Evaluation Cost

In estimating the research, development, test and evaluation (RDTE) cost some assumptions were made. These are listed below.

- The number of test airplanes is assumed to be two, one for static and one for dynamic testing.
- The difficulty judgment factor is assumed to be 1.1 because of the conventional layout with the advanced open rotor engines.

  The results from the RDTE cost analysis are presented in Table 11.1.

Table 11.1: *Cost overview for the RDTE-phase*

Category	Value	Unit
W_{AMPR}	72.5×10^3 (322×10^3)	lbf (N)
C_{RDTE}	$1,443 \times 10^6$	USD
$C_{pro_{RDTE}}$	144×10^6	USD

11.3.2 Acquisition Cost

The acquisition cost is the cost to manufacture and produce the aircraft. In this phase assumptions were made:

- A production life line of 8 years was assumed, 5 years for production with a 50 % safety margin for delays.
- An interior cost factor of 750 $^{USD}/_{pax}$ was estimated using a value in-between military and jet transport from Roskam.

These assumptions were implemented into the AAA cost estimation program and the results of the total costs for manufacturing and the price per aircraft can be seen in Table 11.2.

Table 11.2: *Cost overview for the Acquisition-phase*

Category	Value	Unit
C_{man}	$19,621 \times 10^6$	USD
$C_{acq_{TOT}}$	$21,580 \times 10^6$	USD
$C_{pro_{man}}$	$1,962 \times 10^6$	USD
$P_{ac_{est}}$	192×10^6	USD

11.3.3 Operation Cost

The cost of operating the aircraft is related to the fuel, oil and lubricants, the personnel cost and the consumable materials cost. The assumptions made here were:

- The fuel cost was estimated using average fuel prices of 1.52 $^{USD}/_{gal}$ (0.4 $^{USD}/_{l}$) from Index Mundi [25]. Also the cost for average fuel prices of 2.27 $^{USD}/_{gal}$ (0.6 $^{USD}/_{l}$) and 3.03 $^{USD}/_{gal}$ (0.8 $^{USD}/_{l}$) have been estimated. The cost for different subscripts are 40, 60 and 80 respectively.
- The average pay for the aircrew was estimated to be 84.000 USD [26].
- The annual hours the aircraft flies was estimated to be 1600.

The results of the operation cost estimation are presented in Table 11.3.

Table 11.3: *Cost overview for the Operation-phase*

Category	Value	Unit
$C_{fol_{prog}}$	$94,600 \times 10^6$	USD
$C_{ops_{TOT,40}}$	$194,000 \times 10^6$	USD
$C_{ops_{TOT,60}}$	$272,700 \times 10^6$	USD
$C_{ops_{TOT,80}}$	$351,500 \times 10^6$	USD
$C_{ops/_{hr},40}$	39,200	$^{USD}/_{hr}$
$C_{ops/_{hr},60}$	55,100	$^{USD}/_{hr}$
$C_{ops/_{hr},80}$	71,100	$^{USD}/_{hr}$

11.3.4 Life Cycle Cost

The life cycle cost is the sum of all the costs of the previous phases plus the disposal cost which is estimated to be 1 % of the life cycle cost. [48]

Table 11.4: *Overview of total cost of each phase and Life Cycle Cost*

Category	Value	Unit
C_{RDTE}	$1,500 \times 10^6$	USD
$C_{acq_{TOT}}$	$21,400 \times 10^6$	USD
$C_{ops_{TOT,40}}$	$194,000 \times 10^6$	USD
$C_{ops_{TOT,60}}$	$272,700 \times 10^6$	USD
$C_{ops_{TOT,80}}$	$351,500 \times 10^6$	USD
$C_{disp,40}$	$2,190 \times 10^6$	USD
$C_{disp,60}$	$2,990 \times 10^6$	USD
$C_{disp,80}$	$3,780 \times 10^6$	USD
LCC_{40}	$219,090 \times 10^6$	USD
LCC_{60}	$298,590 \times 10^6$	USD
LCC_{80}	$378,180 \times 10^6$	USD

[25] URL: `http://www.indexmundi.com/commodities/?commodity=jet-fuel`, [cited 19 Jan 2015]
[26] URL: `http://www.indeed.com/salary`, [cited 19 Jan 2015]

11.4 Market Analysis

The United States Air Force (USAF) is looking to modernize its strategic airlift fleet by acquiring 120 units of the new generation strategic airlift, the W.H.A.L.E. It is expected the USAF will be the only buyer of this aircraft. Therefore a production of 120 units has been assumed in the cost analysis in the previous section. In order to be competitive, the price of the W.H.A.L.E. should be comparable that of its predecessor, the C5-A Galaxy. The unit cost of a C5-A was $152.8 M in 1998 [27], equal to $221 M in 2014 [28]. Since the estimated unit price of the W.H.A.L.E. is $191 M, it will be very competitive on the market.

11.5 Sustainable Development Strategy

During the design of next generation airlift military support aircraft the development of sustainable systems and components was one of the driving aspects. Fulfilling the requirements for the aircraft are as important as making it sustainable as well.

Globally this means minimization of the noise, emissions and maximization of the fuel efficiency of the aircraft. The reduction of emissions and increase in fuel efficiency go hand in hand, as burning less fuel means fewer pollutants are released in the air. Open rotors were selected as the source of propulsion for the aircraft. Due to their better specific fuel consumption, open rotors save up to 14% of fuel weight as compared to turbofans. This means that less fuel is burned during flight which leads to 14% less emissions as well which is highly sustainable. This is valid for all segments of emissions as they are directly related to the fuel consumption. Comparison between propulsive efficiencies of various engines for cruise Mach numbers can be found in Figure 11.3.

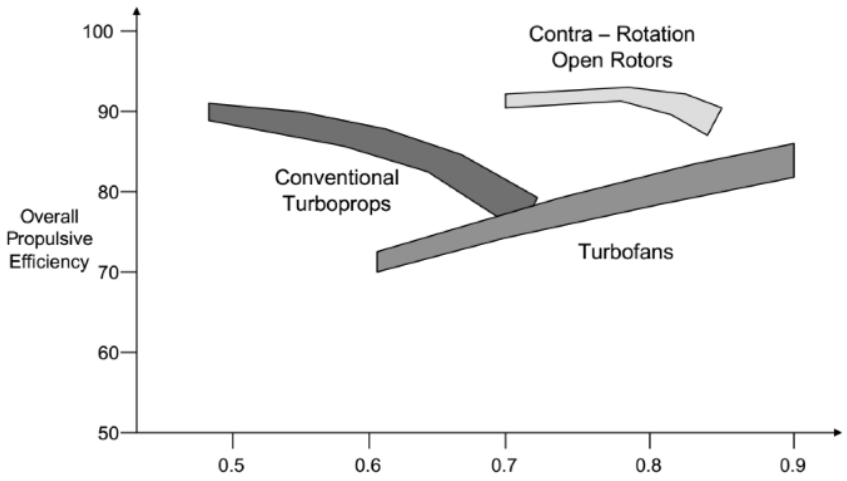

Figure 11.3: *Different engine efficiencies for cruise Mach numbers [30]*

[27] URL: http://www.bga-aeroweb.com/Defense/C-5-Galaxy.html [cited 25 Jan 2015]
[28] URL: http://www.in2013dollars.com/1998-dollars-in-2014?amount=152800000 [cited 25 Jan 2015]

Cradle to cradle design philosophy will be used for design of the aircraft. It essentially means that the aircraft has a built in plan when it reaches the end of its life cycle. The driving philosophy behind Cradle to Cradle is to re-use/recycle every single part of the aircraft after it has reached its end of life.

In the Cradle to Cradle design philosophy, there are five criteria on which the success of a design is graded[29,30]:

- Material Health: Chemical composition of the product. Amount of heavy metals and other hazardous materials need to be reported.
- Material re-utilization: Recycling and recovery at the end of life.
- Production energy: Amount of energy required to produce the product, at least 50% has to be renewable.
- Water usage: usage and discharge quality of product and production
- Social responsibility: Fair labor practices.

With respect to materials, sustainability comes from resistant against corrosion, recyclability and the production process. Enhancing these parameters of the materials that are used for aircraft the Eco-footprint can be reduced, resulting in less damaging aircraft for the Eco-system. All of the cradle to cradle characteristics mentioned will be incorporated during the production of the aircraft.

Aluminum AL-7075-T6 will be used as the primary material for the structural components. Aluminum AL-7075-T6 has been evaluated already against resistant for corrosion, exfoliation and stress-corrosion cracking as well for reference aircraft which give it an advantage over other untested materials.Corrosion is the atmospheric oxidation of materials which can have adverse effects on the environment so using AL7075-T6 makes design philosophy efficient in terms of sustainability. Materials used for the components need to be checked regularly for their fatigue limit as well.

Manufacturing processes for AL-7075-T6 are very well known as they are used for production of most of the aircraft components.This makes them easier ,cheaper as less labor is required and less energy intensive as compared to the manufacturing of other materials as they are faster to manufacture due to their repetitive manufacturing. It means less energy will be used during the manufacturing which is highly sustainable and the extra aluminum that is discarded during the manufacturing processes can be easily recycled as well.

At the aircraft end of life AL-7075-T6 is then recycled and used in the production of other products. This will lead to achieve the objective which was the optimization of recycling as well as valuation of the materials and eventually will lead to the minimization of the waste to be eliminated.

[29] URL: http://www.c2ccertified.org/resources/collection-page/cradle-to-cradle-certified-resources [cited 19 January 2015]

[30] URL: http://www.worldwatch.org/files/pdf/SOW08_chapter_3.pdf [cited 19 January 2015]

11.6 Compliance

Table 11.5: *Requirement compliance matrix*

Requirement	Description	Compliance	Section
Req1	Design range	✓	10.4
Req2	Warload	✓	10.4
Req3	Warload range	✓	10.4
Req4	Cruise speed	✓	5.1
Req5	Climb time to cruise	✓	10.2
Req6	Take-off, landing and balanced field length	✓	10.1
Req7	TO, climb and landing conditions	✓	10.1
Req8	N/2 engine out condition	✓	10.1 & 10.2
Req9	Tactical approach	✓	10.2
Req10	Cargo volume	✓	6.2
Req11	Loiter	✓	4.2
Req12	Fuel reserves	✓	4.2
Req13	Climb speed	✓	10.2
Req14	Passengers	✓	9.8
Req15	Airdrops	✓	6.2
Req16	Unpaved runways	✓	9.3
Req17	Airport types	✓	4.1
Req18	Aerial refueling	✓	9.2
Req19	Decoy flares	✓	9.9
Req20	Turn-around time	✓	6.2
Req21	Service ceiling	✓	10.5

11.7 Risk Assessment

In this chapter technical risks related to the design of the aircraft are analyzed. Risks for the aircraft can be divided into three groups namely design risks, operational risks and production risks.

Design risks

1. Struts on such a big aircraft has not been tested before which may lead to some uncertainties in terms of loads to be carried between struts and wing. Though it is straightforward to design, there can be some discrepancies in the wing weight as it has not been proven how much weight reduction can be achieved. Failure to carry design loads will eventually change in the geometry of the wing and all the calculation and analysis to be done again.

2. V-tail as well has not been used and tested on an aircraft as big as W.H.A.L.E which may lead to uncertainties in terms of stability and control and may force to change the geometry of the empennage in case of failure during testing.

3. Struts can also interfere with the exhaust from the engines which may lead to relocation of the engines and it can effect the design of other components affected by it.

Operational risks

4. Failure of flight instruments during flight is a risk that is always present. Consequences of it happening are always catastrophic whether it is during flight or taxing. During taxing it will mean that the aircraft can not continue to fly anymore.

5. Another failure that can occur during operational phase is due to the fatigue in metal structures. It can have very catastrophic consequences if it happens during flight. Structural components of the aircraft needs to be evaluated against resistant for corrosion, exfoliation and stress-corrosion cracking as well.

6. As mentioned earlier struts has not been used before on such a big aircraft and some unexpected events can cause the strut to fail which will eventually means failure of the whole wing.

Production risks

7. Basic production methods for W.H.A.L.E are comparable to conventional tube and wing aircraft except the struts and V-tail so very low risk of unexpected costs during production.

8. Production and assembly methods for struts and V-tails for a big aircraft are not very common which can cause some extra costs during production of the aircraft.

9. Production of struts and V-tail may take longer as they are a new concept for a big aircraft which may result in the delay of the assembly of the aircraft.

Risk map containing all the risks mentioned above along with their likelihood and consequences can be found in the Figure 11.4

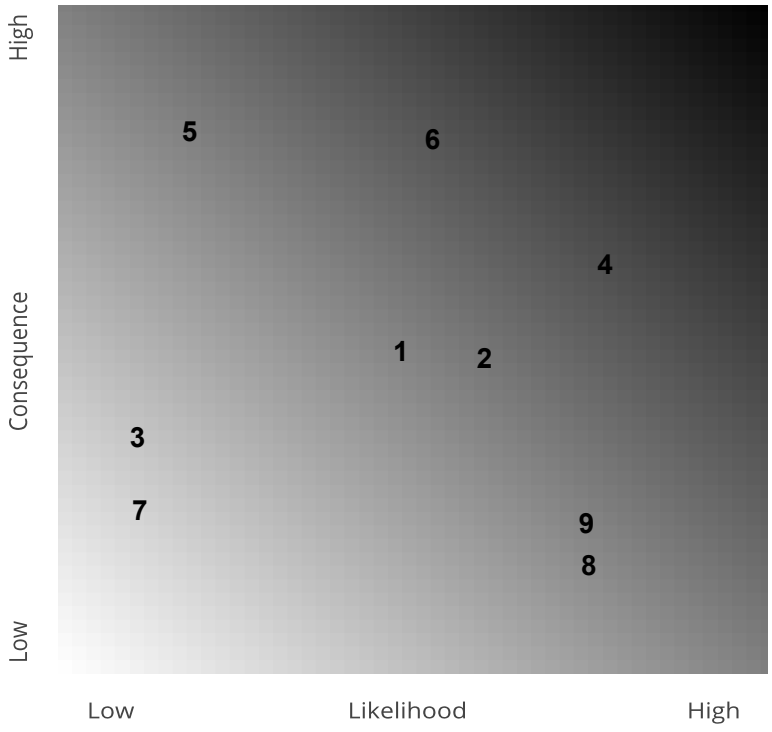

Figure 11.4: *Design risks along with their likelihood and consequences*

11.8 Resource Allocation

Allocation of resources and constraints during the design of the aircraft will be discussed in this section of the report. A design team of 9 members were supposed to design the aircraft within design time of 10 weeks. The design team was divided into different groups with their assigned technical tasks. This made it easier to get an overview of the progress as all of the groups were focused on their tasks and it enhanced the efficiency of the task completion as well. With no constraints on MTOW and budget, time was the only specified constraint during the design of this aircraft. Distribution of weights that adds up to the total operating empty weight of the aircraft can be found in Table 8.1.

Total cost of one aircraft was estimated to be around 190 million USD with propulsive units comprising 47 percent of the total cost. There was basically no constraint on the budget for the design of the aircraft. Budget mentioned here includes just the production costs for the aircraft. 6 counter rotating open rotors were used for the propulsion and the amount was fixed for the engines. As mentioned before these costs are solely based on the production of the aircraft. Some unforeseen circumstances that may lead to increase in production costs also needs to be kept in view. Other costs related to the design can be found in Section 11.3

Conclusion

The objective of this competition was to design the next generation transport aircraft for the US Air Force. Inherently, this meant coming up with a successor for the C-5 Galaxy. This proved not an easy task.

The design approach included a short turn-around time for efficient aircraft use. This was achieved by implementing two wide cargo doors for simultaneous loading and unloading of the cargo bay. Also a relatively narrow turn radius improved ground handling.

Increasing fuel efficiency was also one of the major design objectives. Drag was reduced by choosing a slender, strut braced wing with winglets resulting in a relatively high aspect ratio, which helped reduce induced drag. The strut counteracted the weight penalty which typically comes with slender wings. Parasitic drag was lowered by implementing a V-tail design empennage and integrating the main landing gear in the fuselage, thus not requiring external pods. The choice for highly efficient counter rotating propfans directly reduced fuel consumption.

A third design objective was to increase the versatility and the cargo capabilities of the aircraft. The W.H.A.L.E. is able to carry 44 463L Master Pallets, 2 M104 Wolverines and has additional space for 72 fully equipped troops at any time. The range it can fly with 120,000 lbs of payload is 6300 nm and the harmonic range is 1870 nm. It can land on hard packed dessert sand, perform high-velocity airdrops and make a tactical approach on airbases embedded in combat environments.

A cradle-to-cradle design philosophy was adopted where possible for the manufacturing and operations of the aircraft, thus reducing environmental impact of the W.H.A.L.E. At 191M USD, this aircraft will be very competitive in the market.

Recommendations

There are several recommendations that can be implemented for the design of W.H.A.L.E.

Structural Design The Von mises are calculated with the maximum of the found stresses on the cross-section locations. Von Mises should have been analysed with respect to every element on the aircraft, for which an extensive F.E.M. Analysis is required. The mass that is calculated is based on the assumption that using the length of the aircraft and using the largest cross-section is a good representation of compensation for all additional material that needs to be added for connections and cutouts. The floor is also over-designed with respect to flight loads, as the Von Mises for the floor is smaller than that of the skin.

The wing and strut combination was sized by optimizing for total structural mass, but other considerations such as aerodynamics were not taken into account. The struts might require to be swept in order to increase the critical Mach number. Also, the carry through structure of the winglet in the fuselage is now intersecting with the landing gear storage bay. Moving the root attachment of the strut more forward could solve both previously addressed issues. Also, the strut is not load carrying when the wing is bending down, but should be carrying when the wing is lifting. The mechanism that is required to make this work was not designed and could prove to be a bottleneck for the strut design.

Aerodynamics Detailed aerodynamic analysis should be performed to determine the exact performance of the dropped hinge flap. Also the propwash effects on the airfoil and high-lift devices should be looked into in more detail. Also, due to time contraints a value for wing twist was assumed based on literature instead of thoroughly analyzed. Aerodynamics analysis could provide with a more suitable wing twist.

Stability and control Analysis of propeller slipstream effects on the downwash can be done for more exact downwash gradient that can have an effect on the sizing of the horizontal tailplane. For a more accurate vertical tail area estimation an extensive analysis of the sidewash due to the interactions between the engine propwash, fuselage and tail needs to be done.Computational fluid dynamics analysis are required for it.

Yaw and pitch dampers were designed as for the separate elevator and rudder which can have conflicting impacts for ruddervator. As there is a V-tail for the empennage and a ruddervator for the control surface, more detailed analysis needs to be done on the gain sizing in case of damping requirement for both motions at the same time.

Landing gear The space the landing gear takes could be designed into more detail, as the landing gear retraction kine-

matics require a more thorough design as well.Also, the bending introduced when loading the aircraft should also be investigated, even though they are not critical for thickness when compared to the bending moments due to braking. Furthermore, the shock absorbers could be designed in more detail using a more refined method.

Bibliography

[1] E. Torenbeek, *Synthesis of Subsonic Aircraft Design*. Kluwer Academic Publishers, 1982.

[2] Mathworks, "MATLAB R2013 [computer software]." Mathworks, Natick, Massachusetts, 2013. retreived 2013, available from `https://nl.mathworks.com/products/matlab/`.

[3] D. Corporation, "Advanced Aircraft Analysis v3.6.2 [computer software]." Design, Analysis and Research Corporation, Lawrence, KS, 2015. retreived Jan 2015, available from `http://www.darcorp.com/Software/AAA/`.

[4] Dassault, "CATIA V5 [computer software]." Dassault Systèmes, Vélizy-Villacoublay, France, 1998. retreived Nov 2011, available from `http://www.3ds.com/products-services/catia/`.

[5] R. Vos, "AE-1201 Aerospace Design and Systems Engineering Elements I - Analysis of Aircraft Configurations." University Lecture, 2011.

[6] G. L. Rocca, "AE2101 Aerospace Design and Systems Engineering Elements II - Wing Design Part 2." Lecture slides, 2013.

[7] R. Jenkins, "NASA SC(2)-07 14 Airfoil Data Corrected for Sidewall Boundary Layer Effects in the Langley 0.3-Meter Transonic Cryogenic Tunnel." NASA Technical Paper 2890, 1989.

[8] M. Rivers and R. Wahls, "Comparison of Computational and Experimental Results for a Supercritical Airfoil." NASA Technical Memorandum 4601, 1994.

[9] T. Corke, *Design of Aircraft*. Pearson Education, Upper Saddle River, New Jersey, 2003.

[10] D. Howe, *Aircraft Conceptual Design Synthesis*. Professional Engineering Publishing Limited, London, UK, 2000.

[11] D. Raymer, *Aircraft Design: A Conceptual Approach*. The American Institution for Aeronautics and Astronautics, Inc., 1992.

[12] F. George, "Understanding Winglets Technology," 2010.

[13] E. Torenbeek, *Advanced Aircraft Design*. John Wiley and Sons, West Sussex, 2013.

[14] D. Berckmoes *et al.*, "DSE Baseline Report," internal publication, Delft University of Technology, nov 2014.

[15] H. Strber, "The Aerodynamic Design of the A350 XWB-900 High Lift System." ICAS 29th congress, 2014.

[16] M. Sadraey, *Aircraft Performance: Analysis*. VDM Verlag Dr. Mller, Saarbrcken, 2011.

[17] J. Roskam, *Airplane Design Part VI: Preliminary Calculation of Aerodynamic, Thrust and Power Characteristics*. DARcorporation, 2000.

[18] O. Gur, W. Mason, and J. Schetz, "Full Configuration Drag Estimation." 27th AIAA Applied Aerodynamics Conference, San Antonio, Texas, 2009.

[19] P. Tétrault, J. Schetz, and B. Grossman, "Numerical prediction of the interference drag of a streamlined strut intersecting a surface in transonic flow." 38th Aerospace Sciences Meeting and Exhibit, 2000.

[20] A. H. Naghshineh-Pour, "Structural Optimization and Design of a Strut-Braced Wing Aircraft." Virginia Polytechnic Institute and State University, 1998. Master thesis.

[21] "Metallic Materials and Elements for Aerospace Vehicle Structures." MIL-HDBK-5J Deparment Of Defence, Januari 2003.

[22] S.J. Lewis, "The use of carbon fibre composites on military aircraft," 1994.

[23] A. Elham, G. L. Rocca, and M. van Tooren, "Development and implementation of an advanced, design-sensitive method for wing weight estimation." Elsevier, 2013.

[24] M. D. Ardema *et al.*, "Analytical Fuselage and Wing Weight Estimation of Transport Aircraft." NASA Technical Memorandum 110392, 2007.

[25] "AC 25.491-1 Advisory Circular: Taxi, Take-off and Landing Roll Design Loads." Federal Aviation Aviation (FAA), November 2000.

[26] A. Elham and M. van Tooren, "Winglet multi-objective shape optimization." Elsevier, 2014.

[27] E. Hendricks and M. Tong, "Performance and Weight Estimates for an Advanced Open Rotor Engine." NASA, Technical Report NASA/TM-2012-217710, 2012.

[28] E. Hendricks, "Development of an Open Rotor Cycle Model in NPSS Using a Multi-Design Point Approach." NASA, Technical Report NASA/TM-2011-217225, 2011.

[29] D. Reckzeh, "Aerodynamic Design of the A400M High-Lift System." Airbus, Aerodynamics Domain, Bremen, Germany, ICAS 2008, 2008.

[30] J. Whurr, "Future Civil Aeroengine Architectures & Technologies." Technical Report, 2013.

[31] M. Taylor, "Open Rotor Engine Design and Validation." Rolls Royce plc, Presentation, 2008.

[32] E. Dallara, "Aircraft Design for Reduced Climate Impact." Stanford University Press, Stanford, California, 2011.

[33] J. Roskam, *Airplane Design Part V: Component Weight Estimation*. DARcorporation, 1997.

[34] G. L. Rocca, "AE3221-I - Systems Engineering and Aerospace Design Requirement Analysis and Design principles for A/C stability & control (addendum) ." Lecture slides, 2014.

[35] G. L. Rocca, "AE3221-I - Systems Engineering and Aerospace Design Requirement Analysis and Design Design of unconventional solutions for stability and control : V-Tail and Canard (Addendum 2) ." Lecture slides, 2014.

[36] G. L. Rocca, "Vertical Tailplane Data ." AE3221-Systems Engineering and Aerospace Design Requirement Analysis and Design, Word-document, 2009.

[37] M. Sadraey, *Aircraft Design: A Systems Engineering Approach*. John Wiley & Sons, 2012.

[38] J. Mulder *et al.*, "Flight Dynamics, Lecture Notes." TU Delft, Faculty of Aerospace Engineering. Internal publication.

[39] J. Roskam, *Airplane Design Part IV: Layout design of landing gear and systems*. DARcorporation, 1997.

[40] D. Rusk, A. Arocho, J. Pierce, and G. Abfalter, "Results of fatigue tests of bare AF1410 steel unnotched flat plates with surface corrosion damage," tech. rep., Naval Air Warfare Center Aircraft Division report, 05 2008.

[41] J. J. Schrager, "Heads-Up Displays: A literature review and analysis with an annotated bibliography," final report, U.S. Department of Transportation, apr 1978.

[42] A. Kundu, *Aircraft Design*. Cambridge University Press, 2010.

[43] G. Ruijgrok, *Elements of Airplane Performance*. VSSD, Delft, The Netherlands, 2009.

[44] M. Mashud *et al.*, "Effect Of Spoiler Position On Aerodynamic Characteristics Of An Airfoil." International Journal of Mechanical & Mechatronics Engineering IJMME-IJENS Vol:12 No:06, 2012.

[45] A. Filippone, *Flight Performance of Fixed and Rotary Wing Aircraft*. Elsevier Aerospace Engineering Series, Oxford, Unites Kingdom, 2006.

[46] S.F. Baker, D.P. Morton, R.E. Rosenthal, L.M. Williams, "Optimizing military airlift. operations research," 2002.

[47] T. Ramey, *Lean Logistics: high-velocity logistics infrastructure and the C-5 Galaxy*. RAND, 1999.

[48] J. Roskam, *Airplane Design Part VIII: Airplane Cost Estimation: Design, Development, Manufacturing and Operating*. DARcorporation, 1990.